The Analytical and Experimental Study on the Establishment of a Tidal Power Plant in South Africa

By

Namhla Faith Mtukushe

Student No: 21240801

A thesis submitted in fulfilment of the requirements for the Master of Engineering Degree in the Department of Electrical Power Engineering, Faculty of Engineering and the Built Environment

Durban University of Technology

Supervisor: Dr Evans Eshiemogie Ojo

February, 2021

Declaration

I hereby declare that this dissertation is my work, and each text has been correctly referenced or cited. Moreover, this work has not been previously published in portion or whole for another degree at any other University.

This research was duly supervised by Dr. Evans Eshiemogie Ojo at the Durban University of Technology.

Submitted by:

..... 26/04/2021

Namhla Faith Mtykushe Date

Student Number: 21240801

Approved for Final Submission by:

..... 28/04/2021

Supervisor: Dr. Evans Eshiemogie Ojo Date

Dedication

I dedicate this work to my family:
My mother Vuyokazi Mlata-Mtukushe
My sister Asanda Pinky Mtukushe
My brother Sinethemba David Mtukushe
My late father Dumisani Callman Mtukushe
My late daughter Lusanele Amyoli Mtukushe

Acknowledgements

Praise and thanks to God, the Almighty for his love, grace, and providence.

I would like to express my sincere gratitude to my supervisor Dr. Evans Eshiemogie Ojo for the continuous support, patience, and motivation. I appreciate the opportunity of working with him, the time and effort he contributed to my work. I could not have imagined having a better supervisor and mentor.

A special thanks to Mr. Sithembisa Nyawo, a Technician in the Department of Mechanical Engineering at the Durban University of Technology. No amount of words can ever express how grateful I am for your support.

I would also like to thank Prof. Derek Stretch and his team Mr. Ishaan Ramlakhan and Mr. Lingisprin Pillay at the University of KwaZulu-Natal for allowing me to utilise their facilities for the experiment.

Many thanks to the maintenance team at the Durban University of Technology; Denzyl Permall, Zikhali Phineas, and Biggs Makati.

I would like to thank express my deep and sincere appreciation to the following people: Malvern Makoni, Christoph Moma, Nandipha Madikizela, and Luyanda Zulu, for their academic, emotional, moral, and spiritual support throughout my studies.

Abstract

The majority of South Africa's electricity is generated from fossil-fuel plants that use mainly coal. In these power plants, the combustion of these fossil fuels liberates greenhouse gasses into the atmosphere that contribute to climate change. This problem coupled with the rapid depletion of fossil fuels has necessitated the need to explore the alternative form of energy such as renewable energy. Tidal energy is a form of ocean energy that can be considered as an alternative energy resource or renewable energy source. This form of energy has not been explored in South Africa, the only country in the world that is bounded by two oceans; the Indian and the Atlantic. Tidal energy can be harnessed from the movements of tides to generate electrical power. This study considered the possibility of harnessing tidal energy as the alternative energy source for power generation which can be used to mitigate the challenges associated with the energy crisis currently being experienced in the country.

For this study, an extensive literature review was carried out to understand the tidal phenomenon, the concept of energy conversion from tides, the different techniques or technologies that can be used to generated power from tides. There are two main technologies used for converting tidal energy to electrical energy and these are the tidal barrage and the tidal streams. Based on the inferences drawn from the literature reviews concerning the tides experienced around the South Africa coastal region, it was identified that the tidal stream technique is applicable. Harmonic analysis of the tidal resource for four identified sites was conducted, from these analyses, Esikhawini was selected as an optimum site. Tidal streams extract the kinetic energy of tides and the mode of operation of tidal stream plants is determined by the type of tidal turbine employed. Several turbine designs were reviewed, a helical cross-flow turbine was selected due to its self-starting capability and its ability to operate in reverse stream flows.

For this helical turbine, an analytical model using the blade element momentum theory (BEMT) was developed and was implemented on MATLAB environment. For the experimentation, a prototype was developed and tested in a laboratory concrete flume in the department of Civil Engineering at the University of KwaZulu-Natal. Based on the experimental results, an analysis of the unit turbine was done which was used to propose a conceptualized tidal power plant. Hence, the proposed tidal power plant was used to justify the reason for embarking on this study which is to ascertain the possibility of establishing a tidal power plant in South Africa.

Table of Content

List of Figures

List of Tables

Nomenclature

A_x : Amplitude of the x constituent

A_{us} : Surface area at the upstream

A_t : Surface area at the turbine

A_{ds} : Surface area at the downstream

a : Axial induction factor

a' : Angular induction factor

B : Number of blades

C_d : Drag coefficient

C_l : Lift coefficient

c : Chord length

C_P : Power coefficient

C_T : Torque coefficient

D : Diameter of the turbine

d : Distance between earth and celestial bodies

F_L : Lift Force

F_N : Thrust

F_T : Tangential force

F : Tidal Force

f_x : Frequency of the x constituent

G : Gravitational constant

g : Gravitational acceleration

H : Tidal Range

h_1 : High tides

h_2 : High tides

h : Turbine height

I : Moment of inertia

L : Angular momentum

l_0 : Sea level reference

M, m : Mass

P_{T1} : Upstream pressure

P_{T1} : Downstream pressure

R : Radius of the turbine

R_e : Reynolds number

V : Velocity of water currents

V_{us} : Surface area at the upstream

V_t : Surface area at the turbine

V_{ds} : Surface area at the downstream

V_{rel} : Relative Velocity

θ_x : Phase angle of the x constituent

ρ : Specific density of ocean water

σ : Solidity

λ : Tip speed ratio

μ : Viscosity of water

ω : Blade element angular velocity

Ω : Blade angular velocity

θ_p : Sectional pitch angle

ϕ : Angle of relative velocity

α : Angle of attack

Chapter One

Introduction

1.1 Background

Generally, an electrical power system is divided into generation, transmission, and distribution. The generation is usually used to convert all other sources of energy to mechanical energy and finally into electrical energy. The transmission lines are high voltage lines used to transport power from the generation station through a few to hundreds of kilometres to the distribution centres. Finally, the distribution centres then feed power to the loads. In South Africa, the role of generation and transmission is that of Eskom the country's power utility, and the municipality is tasked with the distribution of power to loads centres. These days the South Africa power systems are experiencing huge constraints. The challenges that have been experienced by the country's power system have to do with the increasing load demand which is higher than the supply from generation stations. Also, the environmental and health issues correlated to greenhouse gas emissions, and according to, as documented in references [1, 2], the capacity of fossil fuel is anticipated to decline in the future. The high electricity demand is due to the exponential increase in demand for electrical power from the country utility for domestic, commercial, and industrial purposes.

The majority of power generated in South Africa is mainly from coal-fire powered stations [3]. The use of such power stations means that a large amount of greenhouse emissions and will ultimately contribute to climate change due to the combustion of fossil fuel by these coal-fired powered stations. The depleting capacity of fossil fuel coupled with the concerning issue of climate change necessitates an exploration of alternative energy sources. Although the access to electricity in South Africa has increased, the challenge of providing affordable, adequate, and reliable supply is still an issue. The government working with Eskom is currently searching for alternative energy sources to mitigate the problems associated with the country's power system. This has prompted the need to consider the use of renewable energy sources such as solar, wind, ocean wave, tidal energy, biomass, and more for the establishment of power plants for purpose of production of electricity.

The ocean occupies over 70% of the earth's surface with a vast amount of energy stored in different forms [4, 5]. The emerging option of power generation is the exploitation of ocean energy that is renewable and abundant. Tidal energy is a form of ocean energy that is yet to

be explored in South Africa and it can be considered as an alternative energy resource or renewable energy source. The implementation of tidal technologies is expected to address the electricity crisis in the country and also minimizes the huge reliance on coal for power generation. This form of renewable energy has been implemented in France, South Korea, United Kingdom, Russia, China, and the Netherlands to generate electrical power. This has helped to mitigate greenhouse emissions and diversify the energy mix. Ironically, despite South Africa being bounded by two oceans the Indian and the Atlantic. Ironically, suffix to say, currently, there is no tidal plant in South Africa though placed with a huge reserve of energy. Due to its geographical location, the country has a high potential of establishing a tidal power plant. Thus, this research project is aimed at conducting a study on the feasibility of the establishment of a Tidal Power Plant in South Africa

1.2 The Potential of Tidal Energy

Tidal energy is often confused with ocean wave or marine current energy; the fundamental difference is that ocean wave and marine currents originate from wind-blown on the ocean surface [6] while tidal energy emanates from the interaction between the earth and celestial bodies such as the sun and the moon. Tidal energy is a form of ocean energy that can be harnessed from the movement of tides to generate electrical power. Both potential and kinetic energy can be extracted from the vertical and horizontal movement of the tides.

A number of techniques have been proposed, developed, and implemented throughout the globe for harnessing tidal energy. There are two basic forms of harnessing tidal energy namely; tidal barrages and tidal streams. They are dominant due to the promising potential for electrical power generation. Tidal barrages exploit potential energy from tidal ranges (vertical difference between high and low tides), while tidal streams harness kinetic energy similarly to wind turbines. The concept of harnessing tidal energy originated from the idea of tidal mills since the 11th century in France, England, and Spain [6, 7].

Table 1.1: The world's major tidal barrage site [8]

Location	Tidal Barrage Area (km-square)	Mean Tidal Range (m)	Potential Mean Tidal Power (MW)	Potential Annual Production (Gwh/year)
South America				
San Jose, Argentina	750	5.9	5 870	51 500
North America				
Bay of Fundy	83	6.4	765	6 710
Passamaquoddy	262	5.5	1 800	15 800
Cobscook	106	5.5	722	6 330
Minas-Cobequid	777	10.7	19 900	175 000
Amherst Point	10	10.7	256	2 250
Shepody	117	9.8	520	22 100
Cumberland	73	10.1	1 680	14 700
Petitcodiao	31	10.7	794	6 960
Memramcook	23	10.7	590	5 170
United Kingdom				
Severn	70	9.8	1 680	15 000
Mersey	7	6.5	130	1 300
Solway Firth	60	5.5	1 200	10 000
Thames	40	4.2	230	1 400
Europe				
Aber-Benoit	2.9	5.2	18	158
Aber-Wrac'h	1.1	5	6	53
Arguenon	28	8.4	446	3 910
Frenaye	12	7.4	148	1 300
La Rance	22	8.4	349	3 060
Rotheneuf	1.1	8	16	140
Mont St Michel	610	8.4	9 700	85 100
Somme	49	6.5	466	4 090
Strangford Lough	125	3.6	350	3 070
Eastern Europe-Northern Asia				
Kislaya	2	2.4	2	22
Lumbouski Bay	70	4.2	277	2 430
White Sea	2 000	5.65	14 400	126 000
Mezen Estuary	140	6.6	370	12 000
Australia				
Kimberley	600	6.4	630	5 600

The world's first tidal plant, LaRance was established in 1966 with an installed capacity of 240MW. Since the establishment of this plant, eight more plants throughout the globe have been constructed and are in operation. Currently, there are two tidal plants under construction in the United Kingdom and ten have been proposed in different parts of the world. There are many potential tidal sites worldwide, table 1.1 presents the world's major tidal barrage sites with their potential mean power in megawatts and an annual potential production in gigawatt-hour. From table 1.1 it is evident that there is limited or no research of these types of

technologies in the African continent specifically in South Africa. Considering that South Africa has an extensive 2800 km coastline [9, 10] and a region where the Atlantic and the Indian Ocean converge, there is a high probability of harnessing tidal energy.

1.3 Motivation

South Africa is currently facing a severe electricity crisis, and this is evident from the regular power cuts i.e. load shedding. This is as a result of insufficient power generation, poor plant maintenance, and breakdown of the plants as most of the power plants have reached their life span. Over 80% of the country's electrical power is generated from fossil-fuel plants as illustrated in Figure (1.1), this demonstrates the country's dependency on fossil fuel. Renewable energy sources are the alternative solution for the power crisis in South Africa.

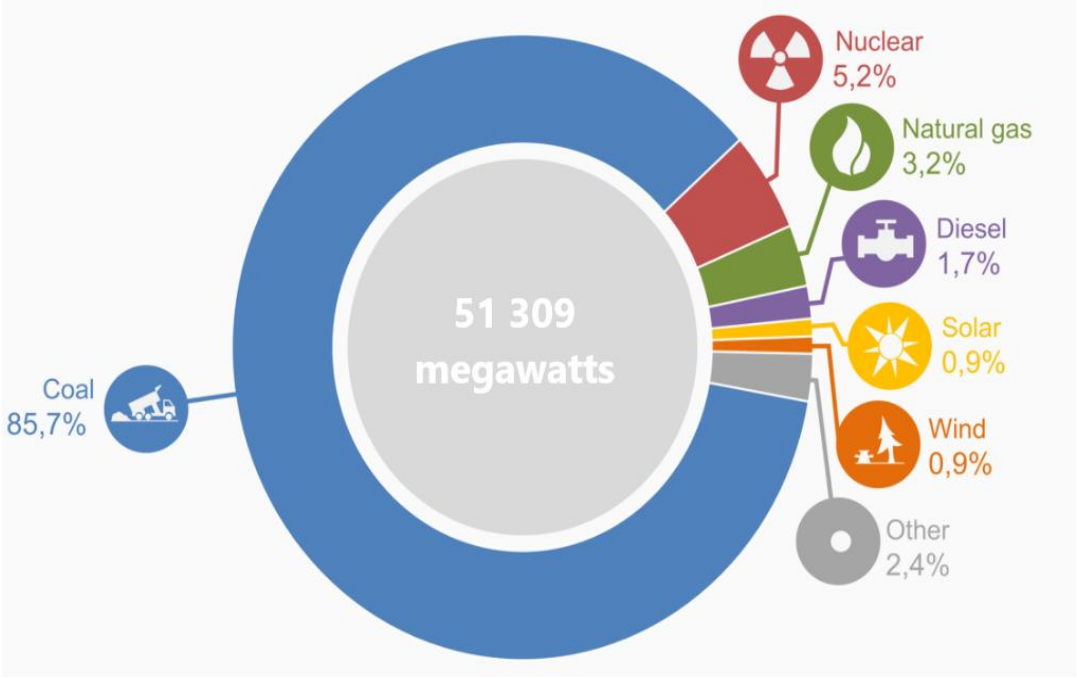

Figure 1.1: South Africa's electrical power generated capacity [11]

Energy from tides is renewable, clean, and can bring about environmental improvements. Tidal energy is highly predictable compared to wind and solar which are highly dependent on the weather conditions, hence tidal power is considered to be more reliable. Tidal plants have a long lifespan as the first tidal plant was established during the 1960s and it's still in operation. Based on the existing tidal plants, there are low maintenance costs and high efficiency of converting the energy from tides into electricity, thus the importance of this study.

1.4 Research Question

As highlighted in the previous sections, there is an enormous amount of tidal energy in our oceans, and South Africa is naturally blessed with this form of energy as it is bound by two oceans. Tidal technologies have been implemented in countries like Canada, France, and Russia that have established tidal plants. Thus, this is the answer to the question of whether the tides experienced around South Africa possessed enough or sufficient energy for power generation. There are several estuaries and bays in South Africa that can be evaluated for the purpose of harvesting tidal energy. As mentioned in [5] the first step towards employing tidal technologies is the characterisation and mapping of the ocean energy resources. If the technologies were to be implemented, the wide gap between the renewable energy policy statement and the actual implementation would be filled [12]. However, due to the geographical location of different countries, some countries can harvest more energy than others whereas in some countries it is impracticable.

Hence, this then raises the question that needs to be answered by the successful completion of this study:

"Do tides available on the South African coastlines possess sufficient energy for the establishment of a tidal power plant?"

1.5 Aims and Objectives

Based on the research question highlighted above, the following are the aims and objectives of the study:

- Investigate the tidal resource using the harmonic analysis of waves for the selection of an ideal site.
- Identify optimum characteristics for establishing a tidal plant and propose an energy conversion system that is suitable for South Africa.
- Develop the potential of continuous power generation from tidal currents.
- Develop an Analytical Model for a Power plant.
- Develop a realistic scenario of energy extraction for the site identified and ascertain its electrical power output capacity per unit.

As highlighted above with regards to the aims of this study, this study at its completion will be tasked to achieve the following objectives:

- Carry out a feasibility assessment for tidal power development in South Africa
- Determine the applicable tidal technology for energy conversion

- Select an appropriate tidal turbine for the proposed power plant
- Simulate on the basis of developed analytical model, design, and carry out a computer simulation of the tidal plant
- Construct a prototype development of the tidal power plant, to assess the amount of power that can be harnessed for the generation of electricity.

1.6 Benefits of the Study

Tidal power is an unexploited energy source in South Africa. This energy source which is abundant in South Africa has the capability to alleviate the issues related to the country's electricity crisis. It is a known fact that the siting of a tidal power plant is associated with high capital costs, despite this high initial costs, coupled with the fact it is a form of renewable energy and harnessing will go a long way in increasing the generation capacity of the country. Thus, the abundance of the energy source will ensure a continuous electrical power supply that is sustainable and affordable. A study conducted in 2005 as documented in [12] estimated that about 1.1% of the global greenhouse gas emissions were from South Africa. As mentioned in the previous section, most of the country's electricity is generated from thermal power plants that liberate greenhouse gas to the atmosphere; promoting renewable energy technologies could greatly reduce the emission intensity and the country's dependency upon fossil fuel.

Tidal energy offers increased power security as tides are highly predictable as compared to wind and solar energy, this means that the power that can be harnessed from tidal energy can be estimated in advance for easy integration to the national grid. In addition, due to its prediction and reliability, such plants can be designed to serve as baseload power plants. This study can be used as a baseline for further investigations and possibly establishments of tidal plants in the country.

1.7 Dissertation Outline

Chapter 1, has already been discussed, this chapter introduced the general background of the study and the potential of tidal energy in South Africa. Also discussed, was the motivation and the research question to be answered on the completion of this study. Also, discussed in chapter 1 were the aims and objectives for carrying out this research study and the benefits of the study. Chapter 2 focuses on reviewing the literature pertaining to the analysis of ocean tides, the two dominant tidal conversion systems, tidal stream technologies, and the types of electrical generators suitable for this application.

Chapter 3 outlines the design consideration of the tidal plant components and the development of the analytical model used in this study.

Chapter 4 was developed on the analysis of the experimental and analytical model results to verify the accuracy of the model developed in the chapter.

Chapter 5 summarises the study by drawing appropriate conclusions based on the aim of the study, the objectives, analytical and experimental results. Necessary recommendations are provided based on the finding for future work.

Chapter Two

Literature Review

2.1 Tidal Wave Fundamentals

The force interaction between the sun, moon, and earth causes the sea level to rise and fall. The rise and fall of large bodies of ocean waters owing to the gravitational and centrifugal forces between the sun, moon, and earth, cause tides. As the moon orbits around the earth, a centripetal force known as gravitational force keeps the moon in its orbital. The gravitational force exerted by the moon on the earth creates a bulge on the earth's surface in the direction of the moon. According to Newton's third law of motion, for every force exerted on an object, there is always an equal and opposite force. A resultant centrifugal force that acts in the opposite direction of the gravitational force, creates another bulge on the opposite side of the earth's surface. The latter is true for the interaction between the sun and earth. The interaction between the sun, moon, and earth is illustrated in Figure (2.1).

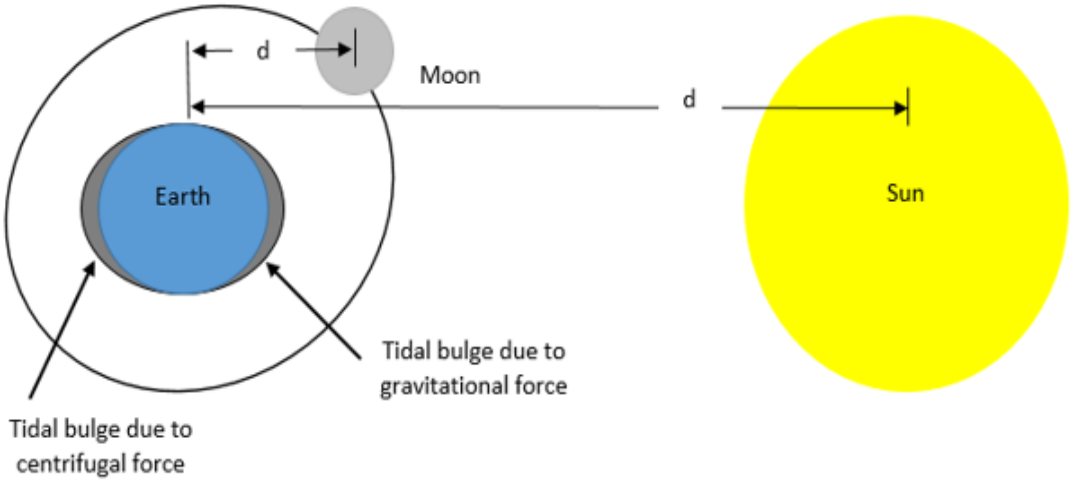

Figure 2.1: Sun, moon, and earth interaction [13]

The bulges are accompanied by high and low tides where the magnitude of tides is a function of the distance and position of the moon and sun with respect to the earth. The tide generating forces vary inversely to the cube of the distance between the earth and the celestial bodies as expressed in equation (2.1).

$$F = \frac{-4GMmR}{d^3} \tag{2.1}$$

Where G is the gravitational constant, M , m and R are the masses, radii of the two objects and d is the distance between the earth and the celestial bodies. Thus, the tides generated as a

result of the interaction between the sun and earth are smaller compared to those generated by the moon due to the distance between sun-earth and moon-earth. When the sun and the moon are aligned, the tides generated are greater than the average called spring tides [1, 2]. The orthogonal position between the sun and moon with respect to the earth results in tides, lower than the average known as neap tides. The position of the sun and the moon with respect to the earth during spring and neap tides are illustrated in Figure (2.2).

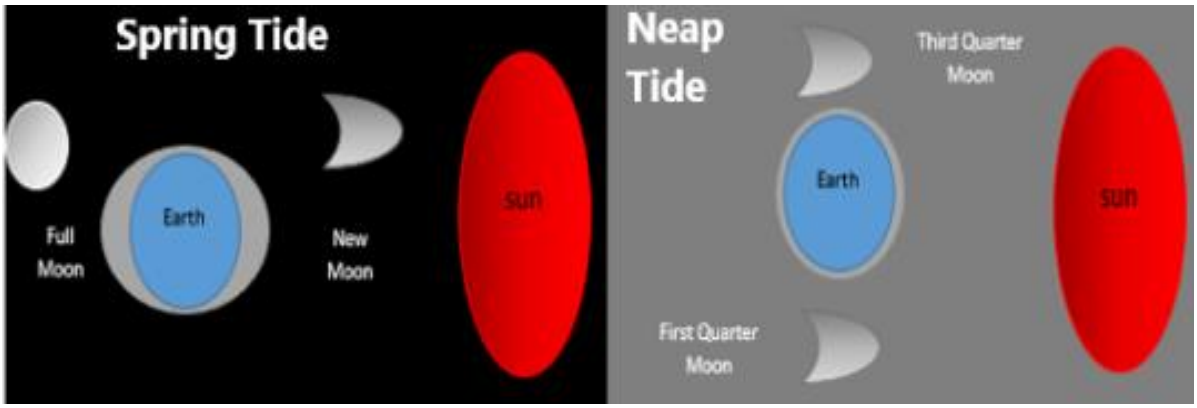

Figure 2.2: The spring and neap tides [14, 15]

There are three types of tidal patterns namely the diurnal, semidiurnal, and mixed-semidiurnal tides as shown in Figure (2.3). Diurnal tides consist of one high and one low water level during a period of a lunar day of 24 hours and 50 minutes. Semidiurnal tides comprise two high and two low water levels during a lunar day of 12 hours and 25 minutes and the mixed semidiurnal tides embody two unequal high and two unequal low water levels during a period of 12 hours and 25 minutes [16].

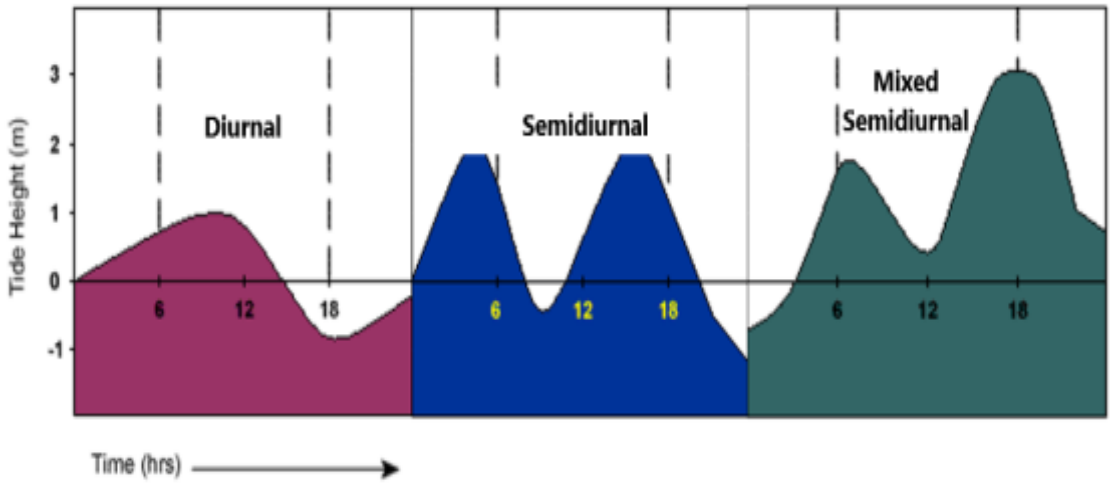

Figure 2.3: Types of tidal patterns

South African coastal areas experience semidiurnal tides whereas some places such as Klabat bay in Indonesia experience a combination of diurnal and semidiurnal tides [17]. A tidal form number is used to determine the type of tidal patterns experienced at a location. Semidiurnal

tides occur in locations where the tidal form number is below 0.25, between 0.25 and 3 are mixed tides, and above 3 are diurnal tides [18, 19]. The tidal form number can be evaluated by:

$$Form\ Number = \frac{K_1 + O_1}{M_2 + S_2} \tag{2.2}$$

Where K_1, O_1, M_2 and S_2 are the four tidal constituents that are determined for a particular location.

2.2 Tidal Wave Characteristics

In physics, a water wave can be described as a manifestation of forces acting on the fluid, hence the size of any wave depends on the magnitude of the forces acting on it [20]. The longest known water waves are tides which are classified as mechanical waves as they require a medium for energy transportation. Thus, tidal waves are referred to as energy transporters that possess both potential and kinetic energy from the point where the tide is manifested, as they travel towards the coast, the wave characteristics change due to refraction, diffraction, and frictional dissipation [21] to the point where all energy is completely transformed to other forms of energy. For optimum site selection and the estimation of tidal power for a specific site, the wave characteristics have to be known. The amplitude (A), frequency (f), velocity (V), period (T), height (h) and wavelength (λ) as indicated in Figure (2.4) are the characteristics that are used to describe a wave. These characteristics are used in predicting the motion of tides.

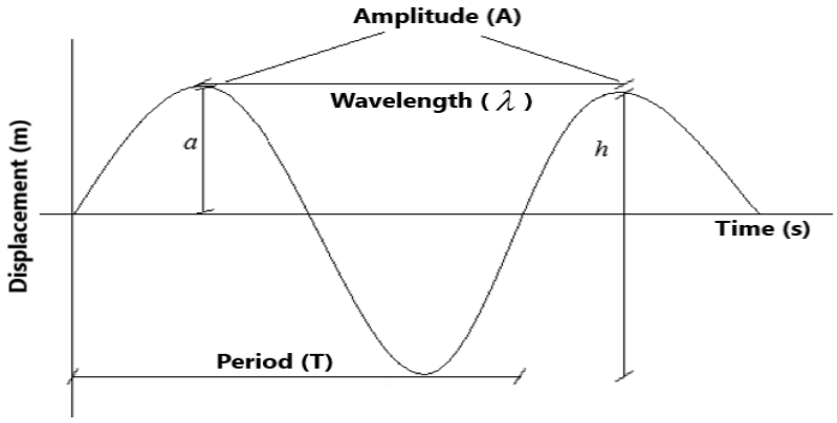

Figure 2.4: The wave characteristics

A tidal energy conversion system is selected based on the tide level or high tidal stream velocities at a specific site. Both the tide level and stream velocity are predicted by a summation of major tidal constituents [22]. Each tidal constituent comprises an amplitude,

frequency, and phase angle that varies based on the interaction between the sun, moon, and earth. Equations (2.3) and (2.4) are used to determine the tide levels and stream velocities, respectively.

$$t_l(t) = l_0 + \sum A_x \cdot \cos(2\pi f_x t - \theta_x) \tag{2.3}$$

$$v(t) = \sum A_x \cdot \sin(2\pi f_x t + \theta_x) \tag{2.4}$$

Where l_0 is the sea level reference, A_x is the amplitude, f_x is the frequency, and θ_x is the phase angle of the x constituent.

2.3 Tidal Power

Amongst all ocean energies, harnessing tidal energy is one of the oldest techniques [23]. The concept originated from the idea of tidal mills which had been used from the 11th century in France, England, and Spain [6, 24, 25]. Tidal energy is often confused with the wave or marine current energy; the fundamental difference is that wave and marine currents originate from wind-blown on the ocean surface [26] while tidal energy emanates from the interaction between the earth and celestial bodies. Both potential and kinetic energy can be extracted from the vertical and horizontal movement of tides. Several techniques have been proposed throughout the globe to harness tidal energy; tidal barrages and tidal streams are the dominant techniques being used due to their promising potential for electrical power generation. Tidal barrages exploit potential energy from tidal ranges (vertical difference between high and low tides), while tidal streams harness kinetic energy similar to the wind turbines. From literature; sites with tidal ranges of 5 m [27] and above were used for tidal barrage plants and sites that experience strong tidal currents with a stream velocity of 1 m/s were used for the tidal stream plants.

2.3.1 Tidal Barrage

Tidal barrages are dam-like structures [28] built across the entrance of an estuary, the barrage separates the ocean from the estuary as illustrated in Figure (2.5). Turbines are installed on the barrage wall and on either side of the turbines are sluice gates. The sluice gates are used to create a head difference between the basin (dam) and the ocean water levels by controlling the incoming and the outgoing tide through engaging and disengaging sluice gates. This process is automated but for the purpose of maintenance, the gates are manually operated to completely block off large bodies of water [29]. Tidal barrages generate electricity similar to hydro dams [30] as both systems exploit the kinetic energy from the fluid flow. When an adequate difference in the water elevation on either side of the barrage is developed, the

sluice gates are disengaged and the hydrostatic head causes water to flow through the turbines, allowing electric generators to generate electricity. Electrical power generation can be conceived from the water flowing into the basin and the water reflected out of the basin [31].

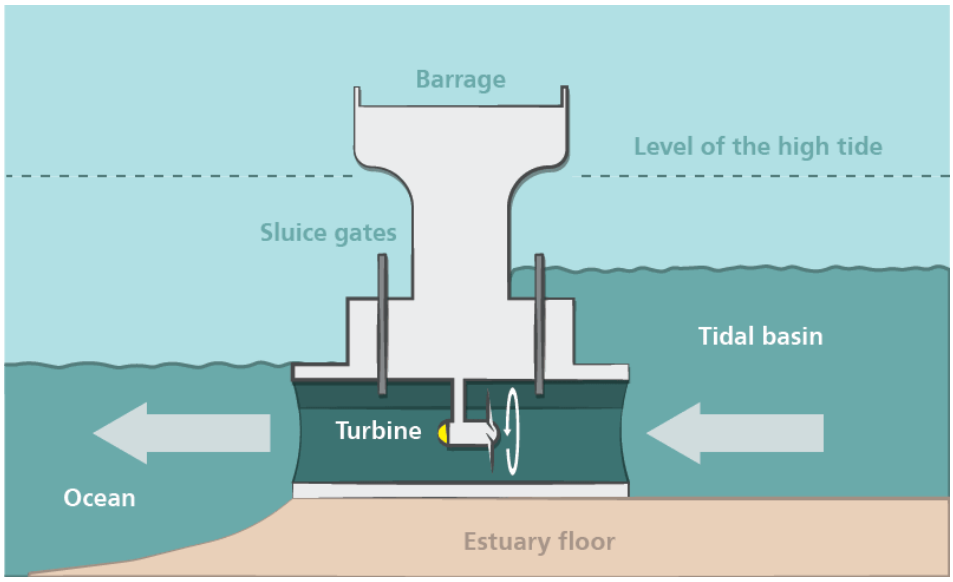

Figure 2.5: Tidal barrage [32]

For areas that experience semidiurnal tidal patterns, there are four tides in each lunar day. Two high tides and two low tides and occur at intervals of 6 hours and 13 minutes. Thus, tidal barrage plants generate power for a duration of 12 hours with no electricity being generated in the 1st and 3rd quarters [33]. There are two types of tidal barrage plants, a single-basin, and a double basin plant. The tidal barrage shown in Figure (2.5) is a single-basin plant, two double basin systems are shown in Figure (2.6). Double basin schemes consist of two adjacent basins, Figure (2.6 (a)) is a non-communicating double-basin whereas Figure (2.6 (b)) is a communicating double-basin system. The operation of non-communicating basins is similar to that of a single basin, the difference is that one basin operates with an ebb generation mode while the other basin operates with a flood generation. The communicating double basin system consists of a primary basin one that extracts the energy directly from the incoming tide (flood tide). When there is a low demand for electricity, the power generated from the main basin is used to pump water into the secondary basin, which acts as a storage element. The water is then released when demand on the system is high (peak period), thus allowing the tidal plant to function with some of the characteristics of a pumped-storage hydroelectric facility.

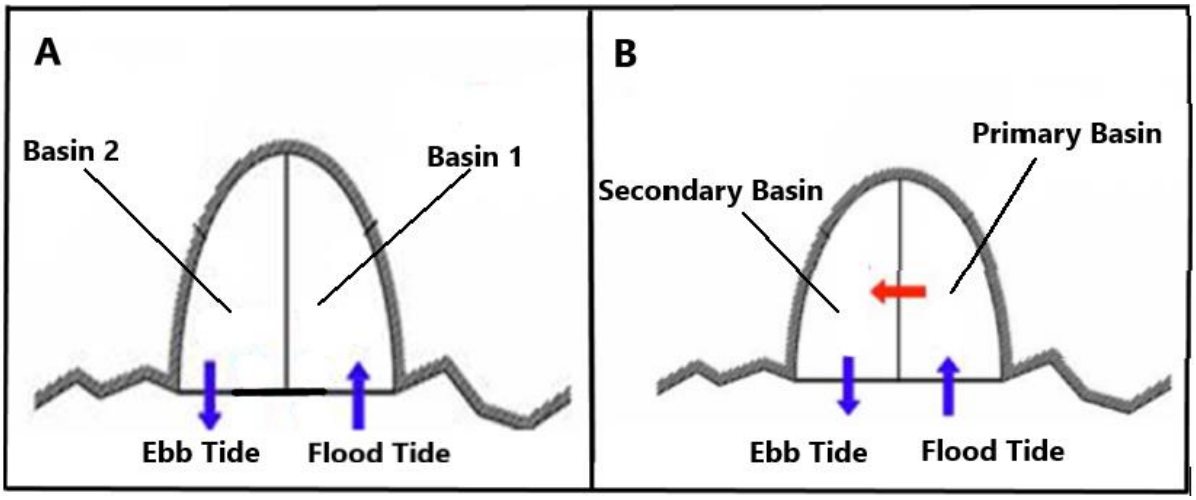

Figure 2.6: (a) Non-communicating (b) Communicating double-basin system [17]

There are three modes of operation that tidal barrages can operate in and these are the ebb, the flood, and the two-way generation.

2.3.1.1 Ebb Generation

The ebb mode of generation generates electricity with an outgoing tide. During high tides the sluice gates are disengaged to allow the tide from the ocean into the basin, elevating the water levels inside the basin. When the desired water level has been reached in the basin, as indicated at point A as shown in Figure (2.7), the sluice gates are engaged allowing the ocean water levels to drop. As the ocean levels continue to drop, a head difference is created between the two large bodies of water. When the sluice gates are disengaged, allowing a flow of tide through the turbines and electricity is generated and this will occur between points B and C. Turbines cease operation at point C and the same process begins at point D. An ebb generation is considered efficient and cost-effective as compared to flood generation which will be discussed in the next section [6].

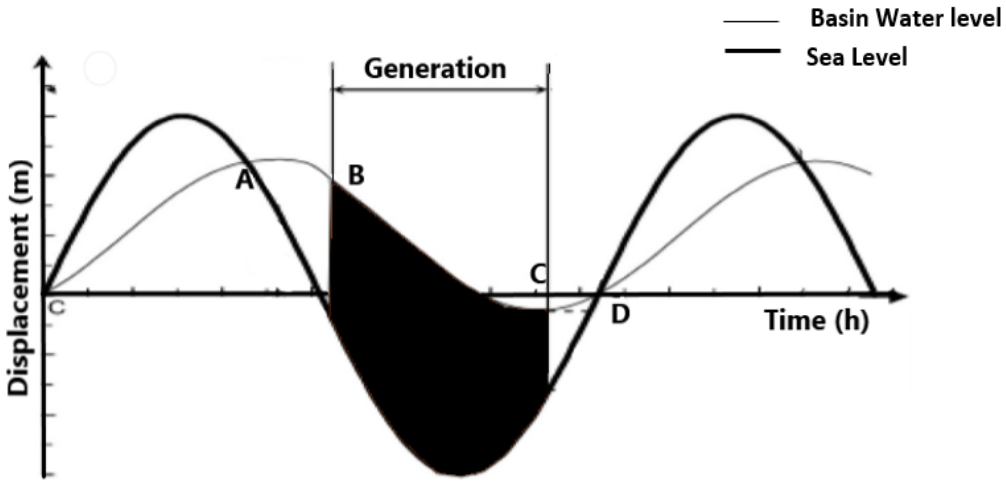

Figure 2.7: The wave diagram for an ebb generation [34]

2.3.1.2 Flood Generation

The flood generation mode, also known as the overflow generation makes use of the incoming tide. During low tides, the sluice gates are unlocked to maintain very low water levels in the basin. In the course of high tides, the sluice gates are closed resulting in low water levels in the basin while the tide reaches the desired head height. When the desired head is reached the sluice gates are unlocked, the water flows into the basin through the turbine, thus, generating electrical power. This mode employs low-speed turbines [35] which has the advantage of not harming marine life but has the disadvantage of harvesting small amounts of electricity. As shown in Figure (2.8), power generation occurs between points A and B.

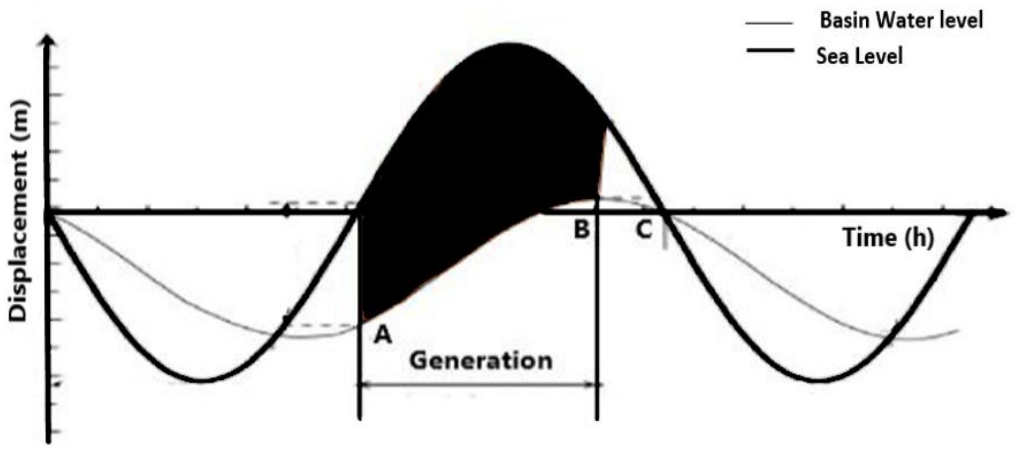

Figure 2.8: The wave diagram for flood generation [34]

2.3.1.3 Two-way Generation

The two-way generation method utilises both incoming and outgoing tides [31, 36]. The non-generation time is reduced as compared to the two other modes of operation. The world's first tidal plant, LaRance in France operates on a two-way generation. During high tides the sluice gates are closed (see point A in Figure (2.9)), the water fills the basin until a hydrostatic head is reached. When the desired head is achieved, the sluice gates are opened allowing the tide in through a tidal turbine, thus, generating electricity. As the ocean levels (point B) begin to drop, maximum water levels are achieved and the sluice gates are locked. Ocean levels continue to drop until a sufficient head is built, thereby generating power from point C to D. This method has a low maintenance cost.

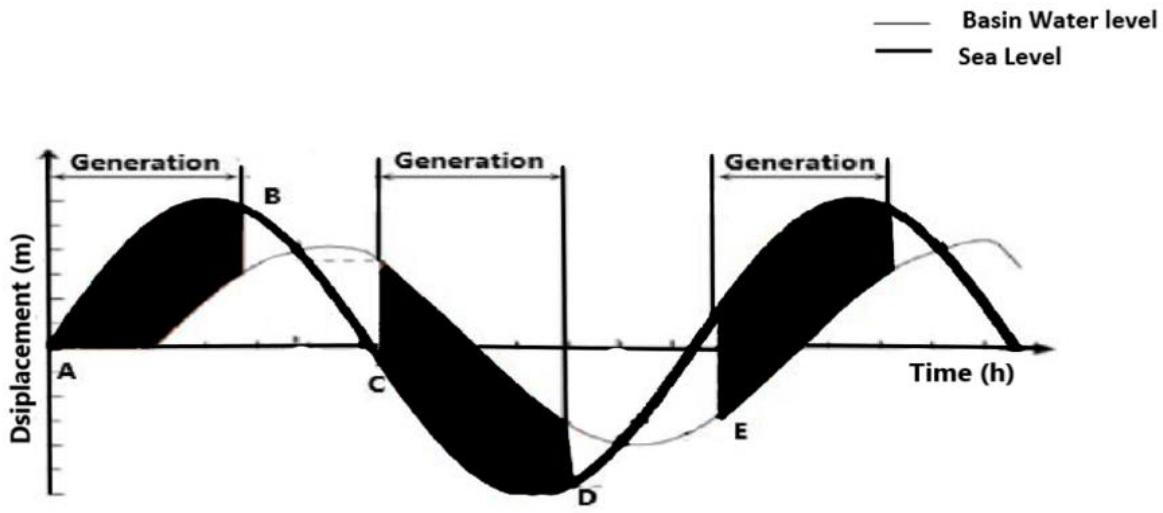

Figure 2.9: Two-way generation [34]

2.3.2 Tidal Stream

The enormous energy available from tidal streams can be exploited by placing large underwater turbines [37] in areas that experience strong currents. When two or more units of the large turbines are deployed and interconnected they form a tidal farm that extracts energy from the horizontal movement of tides [38] as shown in Figure (2.10). The concept of energy extraction is akin to that of wind farms as both techniques harness energy from a moving fluid. The advantage of tidal energy in comparison to the wind is that; tides are highly predictable with a water density that is 823 times denser than air [39]. The same amount of power can be generated with the same size turbine despite the low tidal velocities [40-42]. The energy flux contained in the fluid [43] is directly proportional to the density of the fluid, turbine swept area, and the velocity cube. The fluid exerts a force on the turbine blades due to the fluid's rate of change in momentum, generating mechanical power which is then converted into electrical power

Figure 2.10: A typical tidal farm [44]

The configuration refers to the axes of rotation of the turbine which is distinguished from the turbine shaft orientation. Placement defines the plant layout, a tidal stream plant can be fixed or floating. A fixed placement is achieved with the monopile or gravity-based installation whereas a floating placement requires mooring or anchors to keep it in place. Ducting refers to the placing of a turbine rotor in a duct as shown in Figure (2.11). According to Bernoulli's principle, when a fluid is in motion the pressure of the fluid is relatively low. This low pressure is accompanied by high velocities, hence, the stream flow entering the duct is at high velocities. This flow enhancement results in high power being generated as compared to a turbine placed in an open stream flow.

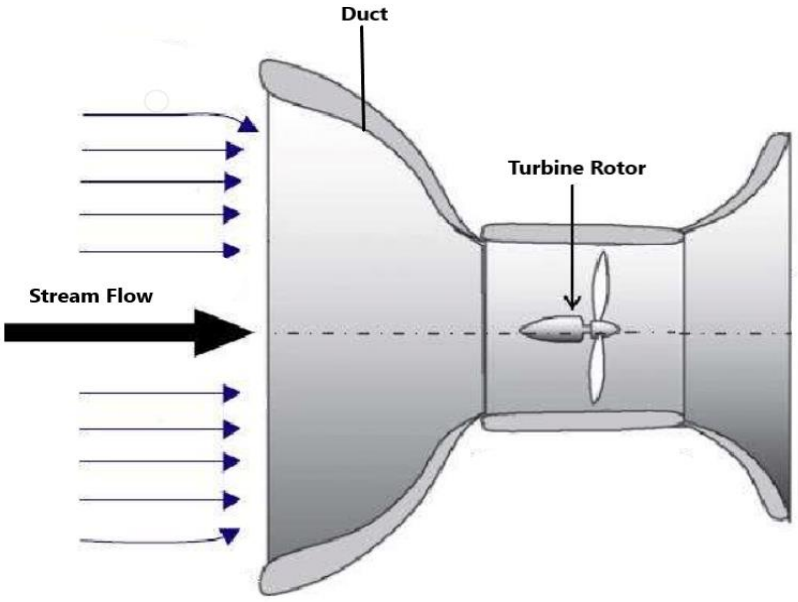

Figure 2.11: Ducted turbine [45]

2.4 Tidal Steam Technology

Tidal stream technologies are slowly improving on their competitiveness with the increased research and new design adaptations. To date a number of tidal turbines have emerged, a few have been deployed and some are at the prototype stage. Tidal stream technologies comprise four major components presented in Figure (2.12). The turbine rotor extracts power from the stream flow, the low stream velocities result in low turbine speeds. The turbine shaft is coupled to a gearbox which increases the rotational speed by means of gears. The other end of the gear train is coupled to an electric generator that converts the mechanical power into electrical. The above three components form a unit that is mounted and secured in place by either a monopile, gravity-based, or a floating structure that is anchored on the seabed.

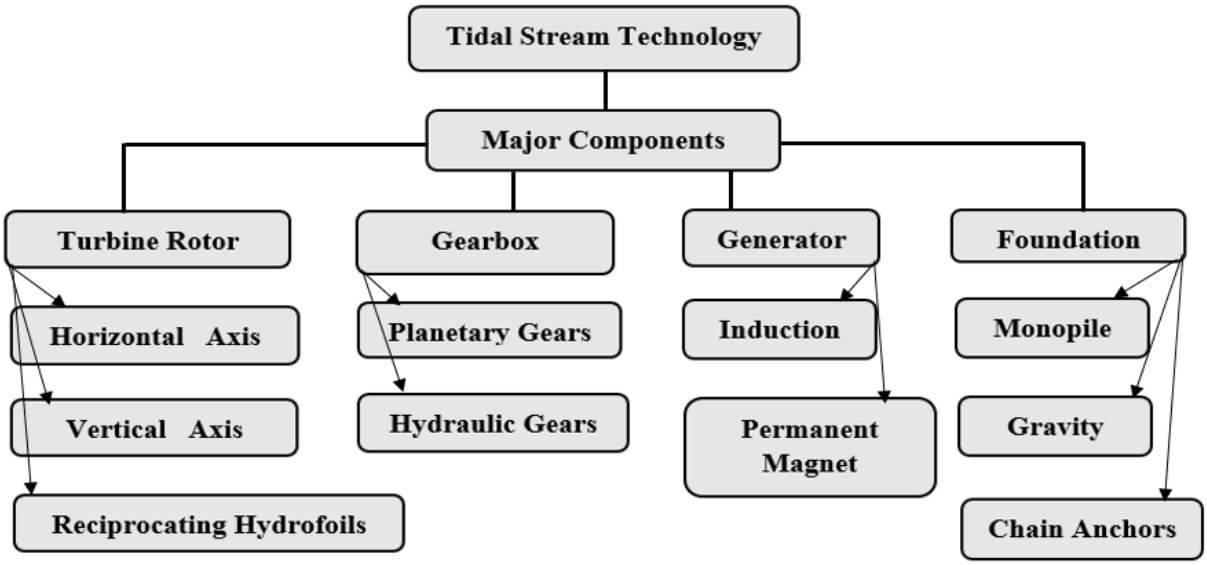

Figure 2.12: The major components of tidal stream technologies

2.4.1 Turbine Rotor Configuration

Three turbine configurations can be considered for tidal stream technologies, horizontal axis, vertical axis, and reciprocating hydrofoils as illustrated in Figure (2.13). The two major turbine configurations mostly used are the horizontal and vertical axis [46]. Both horizontal and vertical axis turbines exploit the horizontal movement of tidal streams with the difference being in the shaft configuration. For horizontal turbines, the turbine runner rotates through a horizontal shaft while in vertical axis turbines, the shaft is vertical and perpendicular to the flow of the tidal stream. Horizontal turbines have the advantage of high peak efficiency. Reciprocating hydrofoils do not rotate but move up and down repeatedly [47]. They have a great advantage of being able to sweep a larger area in more shallow waters. This section provides a literature survey on the two dominant technologies.

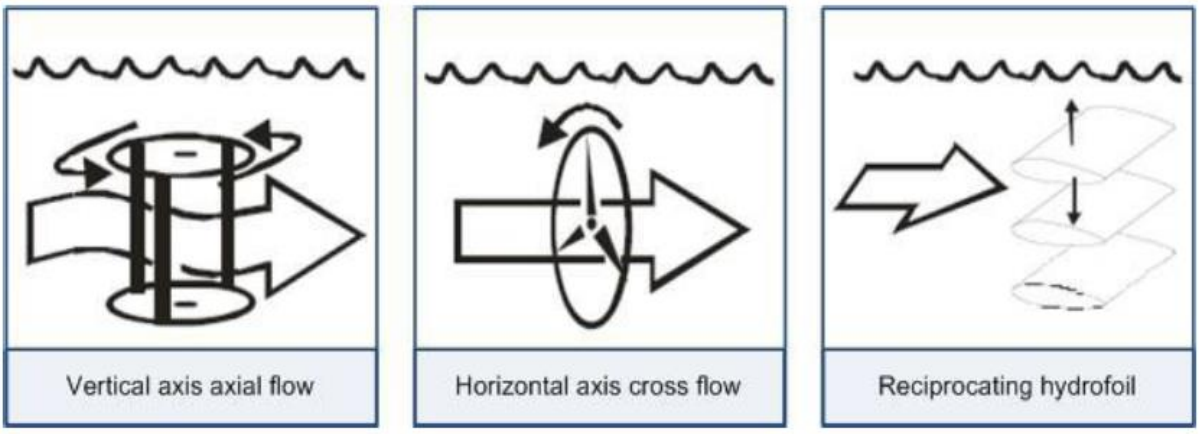

Figure 2.13 Different tidal stream turbine configurations [17]

2.4.1.1 Horizontal Axis Water Turbines

Horizontal axis turbines are also known as axial flow water turbines (AFWT), they are the simplest and most popular configuration used for tidal streams. They are defined by the axis in which they rotate in i.e. the horizontal axis. These turbines consist of two or more rotor blades that are coupled to the rotor hub. AFWTs are suitable for large-scale tidal applications where yawing and pitch control mechanisms are required. Recent tidal turbine designs have been developed in order to increase the efficiency of harnessing energy in the future. The following are tidal stream devices that can be used to harvest tidal energy, they are discussed as follows:

(a) Rotech Tidal Turbine

Rotech Tidal Turbine (RTT) is a type of bi-directional horizontal axis turbine. This turbine comprises a gravity-based support structure and has a ducted rotor as illustrated in figure 2.14. The ducted symmetrical rotor makes use of the venturi effect which optimizes the angle of attack by directing the tidal flow through the turbine. The advantages of ducting include; the increased energy capture per unit of rotor area, the insensitivity to off-axis flow, and the potential for supporting rotor blades at their tips, leading to the greater load resistance. These features eliminate the need for the yawing mechanism that is complicated and expensive [48]. This design allows the turbine cassette to be removed and maintained or replaced completely as shown on the right-hand side of Figure (2.14).

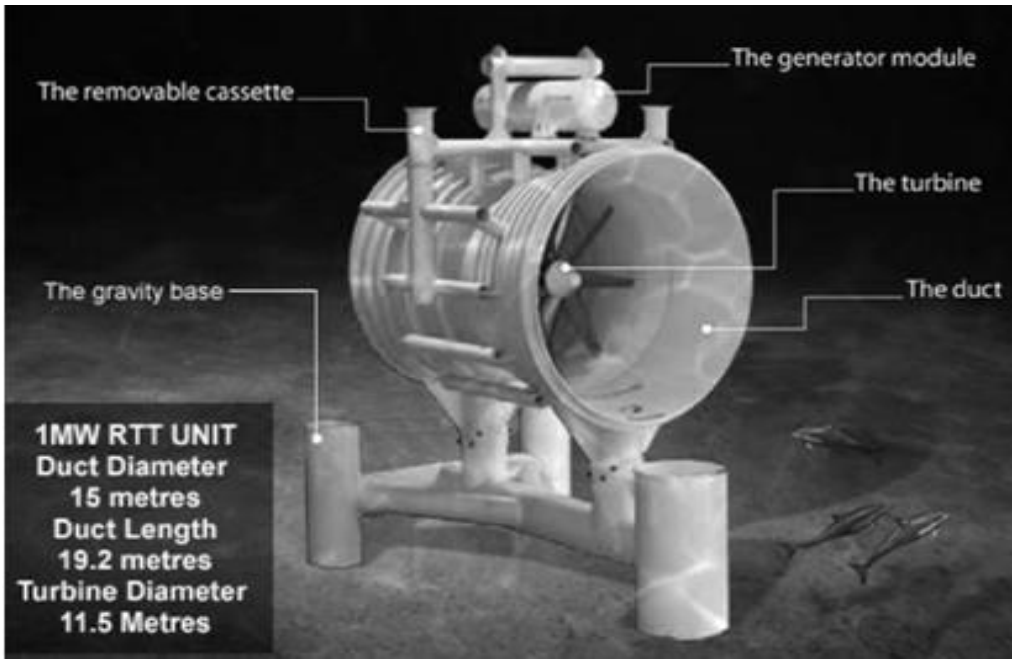

Figure 2.14: Rotech tidal turbine [49]

(b) SeaGen

SeaGen is a twin-bladed axial flow turbine. The rotor blades are mounted on a monopile support structure that enables the rotor to move up and down the monopile [50] to the ocean surface for the purpose of maintenance. Figure (2.15) shows a 16-meter rotor SeaGen with an installed capacity of 1.2MW, the turbine was tested and connected to the grid at Strangford Narrows in the UK since 2008 [51]. This was the world's first tidal stream device to generate electrical power and integrated into the grid.

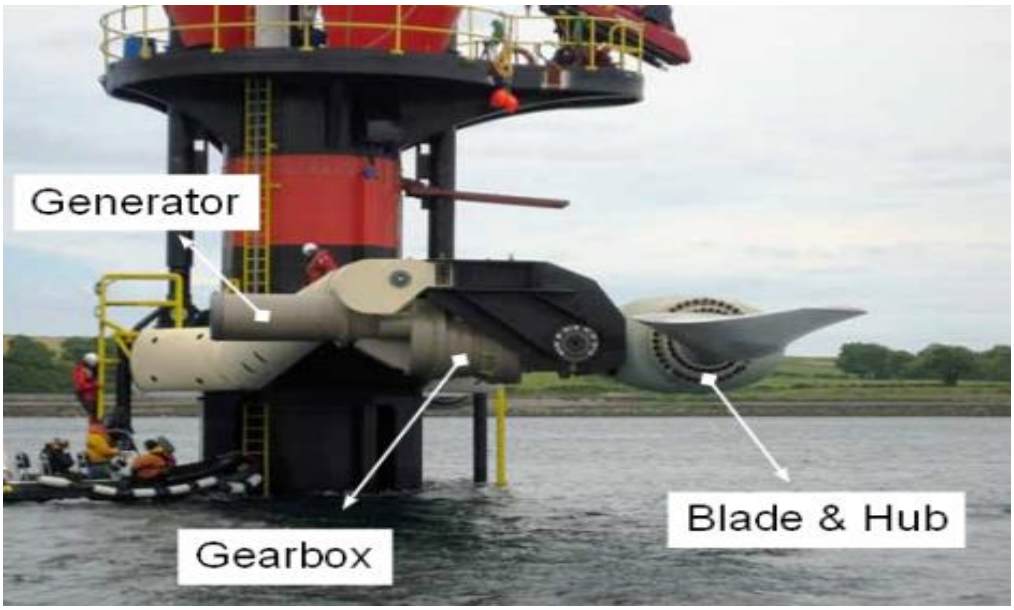

Figure 2.15: The SeaGen [50]

2.4.1.2 Vertical Axis Water Turbines

Vertical axis turbines are also known as the cross-flow water turbines (CFWT) operate as a lift-based generation system with the axis of rotation perpendicular to the stream flow. The CFWT design makes them very efficient in extracting useful power from the horizontal movement of tides as they are independent of the stream direction. The major advantage of these devices include; less environmental impact as their installation requires minimum land use [52] and they have the ability to provide unidirectional rotation in reversible fluid flow [53, 54]. Crossflow turbines do not require a pitch control and yawing mechanism.

(a) Darrieus Turbine

A French inventor, G. J. M. Darrieus developed and patented the conceptual design of Darrieus turbines in 1926 and 1931 [55-57], respectively. Darrieus turbines are lift-driven devices that consist of two or more rotor blades. Two types of Darrieus turbines are

characterised by their rotor blades, a troposkein and straight-bladed as shown in Figure (2.16). The troposkein-bladed has curved rotor blades that are mounted on the shaft turbine, this shape allows the turbine to be stressed in high tensions during high rotational speeds. The straight-bladed turbine has straight rotor blades that are connected by horizontal structures to the turbine shaft. These turbines are subjected to the varying angle of attack which can be optimised by redesigning the shape of the turbine rotor. They offer a high operating tip speed ratio as compared to the axial flow turbines. Due to the varying angle of attack, in some instances, the angle is either too low or even negative which results in a very low starting torque [58] hence, there is the issue of self-starting.

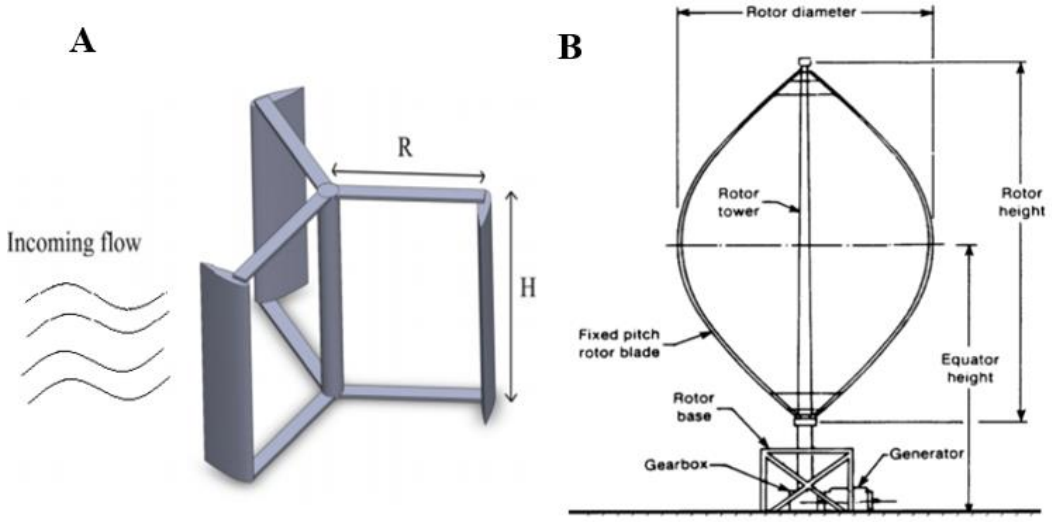

Figure 2.16: A. Straight-bladed, B. Troposkein-bladed [59]

(b) Savonius Turbine

The Savonius turbine developed by S.J. Savonius in the 1920s is a drag-driven turbine with an S-shaped rotor [60]. The S-shaped rotor blades are mounted on two end plates as illustrated in Figure (2.17). As the tidal stream flows through the structure and comes in contact with the opposite facing surfaces, lift and drag forces are exerted on the two surfaces. The basic working principle is based on the difference in the drag force between the convex and the concave parts of the rotor blades when they rotate around a vertical shaft [61]. The angular velocity of the drag-driven turbine is always less than the stream velocity, which means that the tip speed ratio is equal to 1 or smaller [62, 63]. The design and performance of Savonius turbines have been tested and optimised by several researchers, the highest efficiency based on tests on this device is 30% [64].

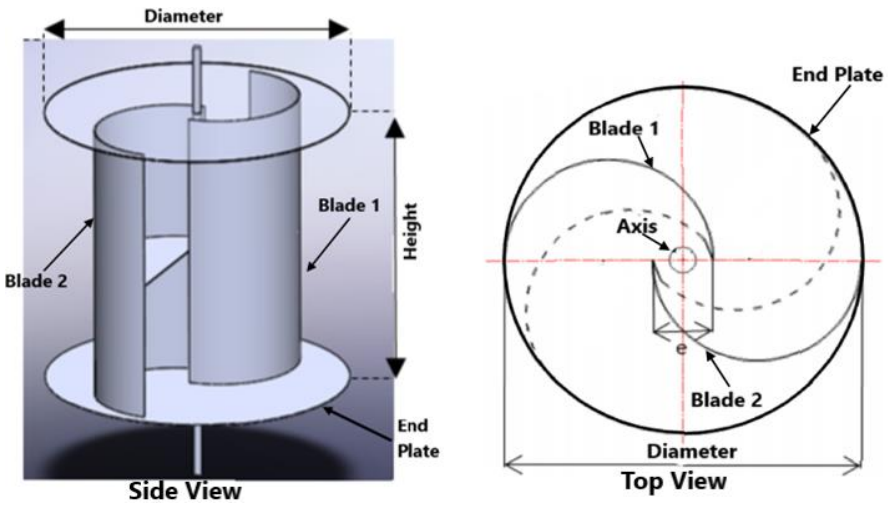

Figure 2.17: Two different views of the servonius turbine [65]

(c) Gorlov Helical Turbine

The Gorlov helical turbine is a self-starting cross-flow turbine that was designed by Professor Alexander Gorlov during 1994-1995. The concept originated from the idea of improving the performance of the Darrieus turbines. The helical turbine blades regulate the periodical unsteady torque characteristics produced by the straight-bladed turbines [66]. The Gorlov turbine possesses all the advantages of Darrieus turbines without the disadvantages [54]. This improved performance is due to the shape of the blades which have a hydrofoil profile with a helix path. Gorlov turbines can be designed with a vertical or horizontal shaft, with two or more rotor blades. Figure (2.18) shows two types of triple-helix Gorlov turbines with different support structures for the blades.

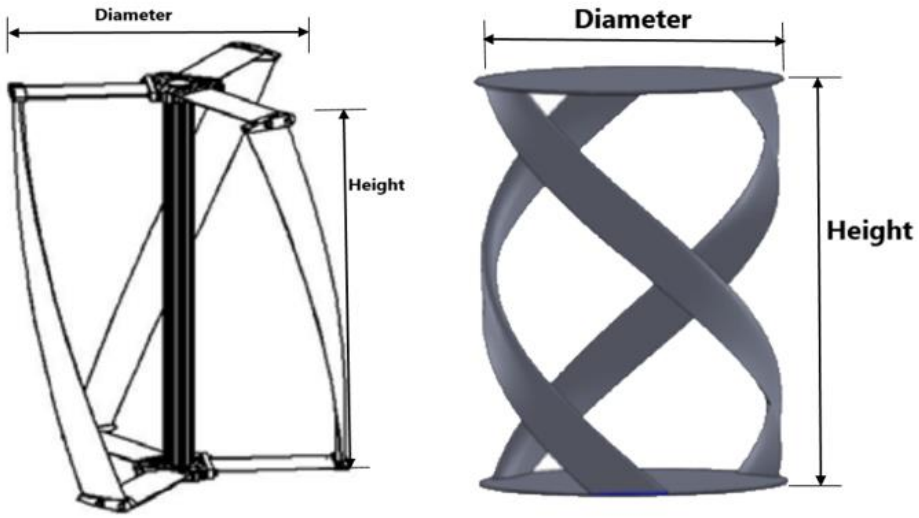

Figure 2.18: Gorlov triple-helix turbines [67]

In the mid-1990s, an experimental test was conducted on the triple helix turbines with different dimensions for the rotor blades as shown in the above figure. Although the designs are slightly different, both turbines demonstrated an efficiency of 35% with no vibration observed [54]. A decrease in the turbine diameter can be compensated for with an increase in the turbine height with no power losses. The turbine can be as long as desired, also there is the option of mounting more than one turbine on a common shaft. An example of multiple turbines mounted on a common shaft is illustrated in Figure (2.19).

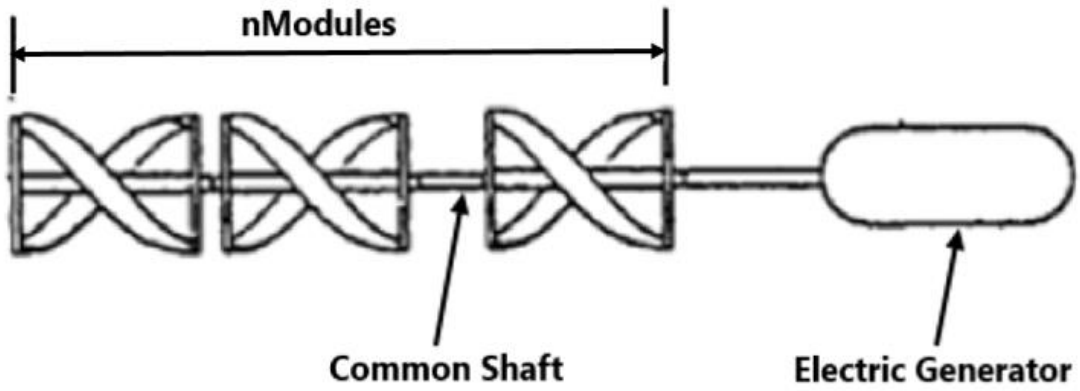

Figure 2.19: An option of assembling the helical turbines [54]

The turbine blades are always at an optimal angle of attack, this provides a reaction thrust that can rotate the turbine faster than the water flow, and a nearly constant torque is developed which subsequently can produce a near constant electrical power.

2.4.2 Gearbox

A group of components that are responsible for transmitting power are known as drive trains. The drive train used in a tidal turbine generator system consists of the blade pitch mechanism, rotor blades that are mounted on a turbine hub, turbine shaft, and a gearbox [68]. As mentioned in the above sections, tidal turbines often rotate at a slower speed than the maximum efficiency of the generator [58, 69]. To increase the slow rotational speed of the turbine shaft means of gears to the desire higher speed, a gearbox is installed with one end coupled to the turbine shaft. The gearbox is also coupled to the shaft of the generator to convert the torque and rotational speed of the turbine output shaft to the torque and rotational speed of the generator input shaft. Figure (2.20) show a typical planetary gearbox that is commonly employed in both wind and tidal application.

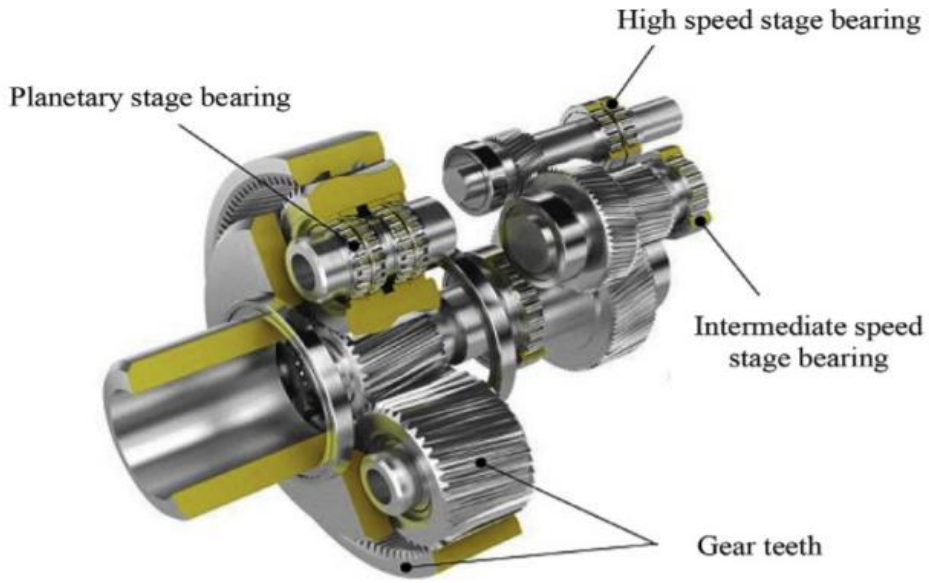

Figure 2.20: A typical planetary gearbox [70]

There are several types of gears that may be used in a gearbox such as spur gears, bevel gears, or helical gears. The above gearbox employs helical gears which can achieve a gear ratio of approximately 10:1 [71]. It is essential to a generator that requires a minimal gear ratio to maintain high efficiency.

2.4.3 Electric Generators

An electric generator converts mechanical power from the gearbox (or turbine) into electrical power. The power generated can either be direct current (DC) or alternating current (AC). Both DC and AC generators are further classified as synchronous and asynchronous. In synchronous generators, a DC is applied to the rotor winding of the generator producing a rotor magnetic field [72]. The rotor which is coupled to a prime mover is rotated by the prime mover, generating a rotating magnetic field. The output voltage is synchronised with the rotor speed. The asynchronous generator produces electrical power by mechanically rotating the generator rotor faster than the synchronous speed. The choice of generator is a function of the desired output and prime mover.

There are two generators that are suitable for tidal plants, a doubly-fed induction generator (DFIG) and a permanent magnet synchronous generator (PMSG). The stator and rotor of a DFIG are connected directly and via power electronic converters to the grid. An AC signal is fed to the rotor, inducing an ac current in the rotor windings. The turbine exerts a mechanical force on the rotor generator, thus a rotating magnetic field. An AC current is induced in the stator windings from the rotating magnetic field. The power converter that regulates the active and reactive power is called the rotor-side converter that is connected directly to the

rotor. The grid-side converter maintains the dc-link voltage [53]. The main advantage of the DFIG is the reduced cost of the converter and generator [73]. A schematic diagram of a DFIG-based tidal generation system is given in Figure (2.21).

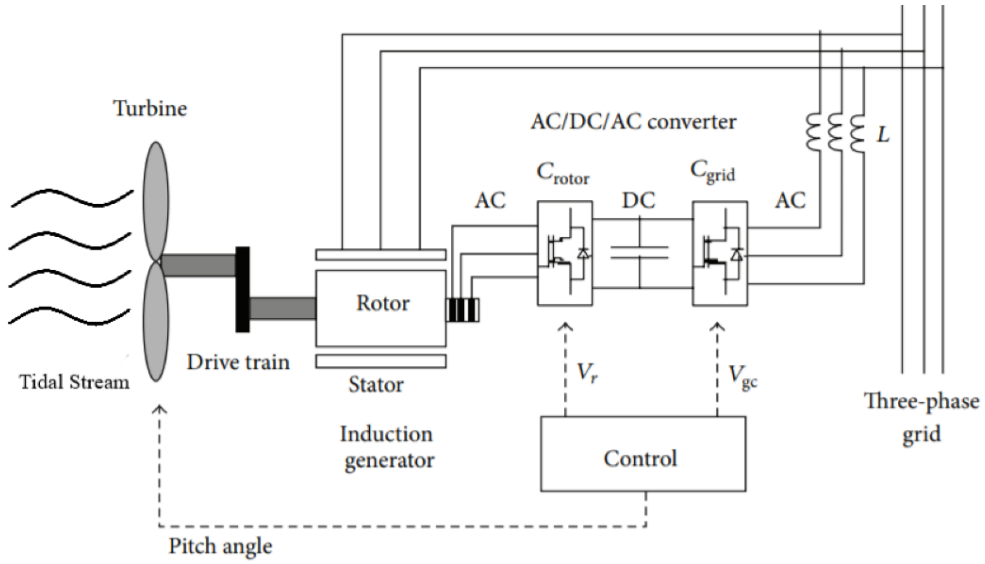

Figure 2.21: Schematic diagram of a DFIG -based generation system [74]

A PMSG can be connected directly through a mechanical coupling or via a gearbox to the turbine. The generator stator is connected to the grid via an AC-AC power converter as shown in Figure (2.22). The excitation field of this machine is provided by the permanent magnets. A high number of pole pairs enables the machine to be directly driven by the turbine, eliminating power losses associated with the gearbox. The advantages of employing PMSG are the low starting torque and rotational speed in direct drive, high constant efficiency over a range of operating speeds [58], and no external excitation circuit are required for the magnetic field.

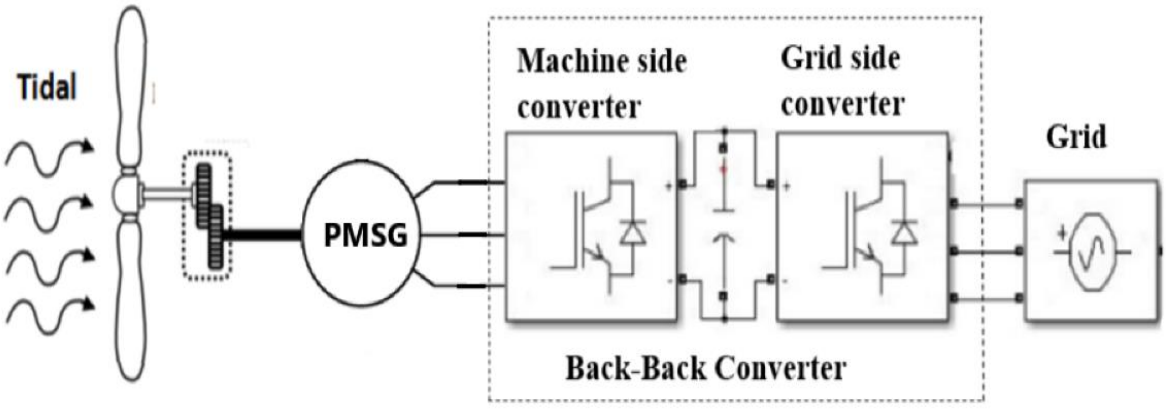

Figure 2.22: Schematic diagram of a PMSG-based generation system [75]

2.5 Theoretical Estimation of Tidal Power

2.5.1 Potential Tidal Power

The amount of power generated from the tidal barrage system as shown in Figure (2.23) can be determined from the following expression:

$$P = \frac{1}{2} A \rho g H^2 \tag{2.5}$$

Where A is the surface area of the barrage, ρ is the specific density of ocean water, g is the gravitational acceleration, and H is the tidal range at the site

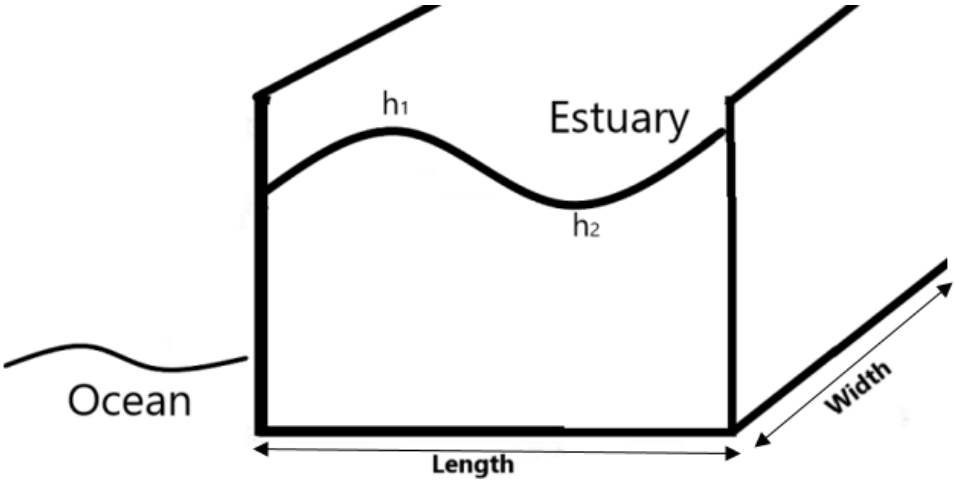

Figure 2.23: Theoretical tidal barrage

The surface area is given by:

$$A = LW \tag{2.6}$$

Where L and W are the length and width of the tidal plant, respectively. The tidal range can be determined using equation (2.7).

$$H = h_1 - h_2 \tag{2.7}$$

Where h_1 and h_2 are the high and low tides at the site. For a tidal plant situated in a geographical location that experiences semidiurnal tide (two high and two low tides), the potential energy per day is given by:

$$P_t = P \times 2 \,(high\,tide) \tag{2.8}$$

Considering the power conversion efficiency, the total power generated can be evaluated as:

$$P_T = \eta P_t \tag{2.9}$$

2.5.2 Kinetic Tidal Power

The amount of power generated is a function of the available tidal power and the turbine performance coefficient of the turbine. It is known that not all the available power in the free stream can be extracted and converted to rotation motion in the turbine, the amount of possible extractable power from tides is given by:

$$P = \frac{1}{2}\rho A V^3 \tag{2.10}$$

Where ρ is the sea water density in kilograms per cubic meter A is the turbine swept area in square meters, and V is the tidal current velocity in meters per second. The swept area depends on the type of turbine employed. The cross-sectional area of flow swept by an axial flow turbine can be determined from the equation

$$A = 2\pi r \tag{2.11}$$

Where r is the rotor radius. Considering the conversion efficiency, the total power generated can be determined from the following expression:

$$P = \frac{1}{2}\eta\rho A V^3 \tag{2.12}$$

2.6 Existing Tidal Plants

As part of a wide-ranging review of the South African tidal energy potential, this study is tasked with evaluating a series of scenarios of the various aspects of tidal power. This study will analyse the tidal resource, the status of the technology, and its potential environmental impacts. This section is used to discuss the existing tidal power plants around the world. The LaRance was the world's large-scale tidal power plant [76], the first ever tidal plant established between 1961 and 1966 in France which is still in operation. It employs 24 identical 10MW bulb turbine units with an installed capacity of 240MW and an estimated average annual output of 540GWh [77, 78]. Before the establishment of Sihwa Lake tidal plant, LaRance was the largest tidal plant. Sihwa Lake tidal plant in South Korea has an installed capacity of 254MW with 10 25.4MW bulb-type turbines [60]. The other tidal plants have small installed capacity such as Kislaya Guba in Russia with 1.7MW, Jiangxia in China with 3.2MW, Udlomok in South Korea with 1.5MW, and lastly Eastern Scheldt in the Netherlands with 1.25MW. Though all these tidal plants have different capacities, they all went through the same establishment phases with the first being the most important, which is the analysis and understanding of the type of tides experienced by the particular site. Table 2.1 documents the list of a few proposed tidal projects currently being investigated

throughout the globe for possible siting of tidal plants. Ironically, South Africa with an enormous amount of potential of tidal energy was not recorded in this project.

Table 2.1: Proposed tidal plant projects [79]

Tidal Range (m)	Area (km^2)	Theoretical Power (MW)	Actual Power (MW)	Station Name
2.1	947	583.24	200	New Zealand
4.7	100	308.5	480	Carolina, South Korea
5.2	5.5	20.76	33	Conwy, Britain
5.3	170	666.9	900	Kutch, India
6	20.5	103.06	87	Penzlinslenby
6.5	61	359.9	700	Marsely, British
6.8	1970	1272.67	7000	Cambay, India
7.8	450	3823.5	8640	Servern, British
9.1	2300	26599.34	19200	Mezen, Russia
10	115	1606.04	1800	Shepody, Canada
10.9	90	1493.33	1400	Cumberland, Canada
12.4	240	5153.65	5338	Cobequid, Canada

Chapter Three

Analytical Analysis and Computer Simulation

3.1 Tidal Stream

In this chapter, the concept of the tidal stream was analysed followed by a computer simulation. The concept of tidal streams was chosen in this research study because tidal current experienced in South Africa are tidal streams. In addition, tidal stream technologies for generating electrical power are better as compared to tidal barrages. Tidal stream turbines are less intrusive to the local environment, and it is in contrast to the tidal barrage, they can be installed incrementally in a location. Tidal stream technologies are at their developmental stages with a promising future to develop a tidal stream plant in South Africa. For the analysis of tides, it is necessary to have adequate knowledge of the tidal stream velocity. An investigation of the potential sites in South Africa was conducted to determine the viability of a tidal plant that can be used for either tidal barrage or the tidal stream i.e. the two dominant tidal energy conversion techniques. A study conducted in [52] measured tidal ranges at the mouth of twenty South African estuaries, and the highest tidal range recorded was 4.50 m at Richards Bay. Based on the available tidal range data, there is no potential site for the establishment of a tidal barrage plant in South Africa. Sites that are considered feasible for a tidal barrage must experience tidal ranges of about 5 m and above. Hence, the potential sites in South Africa can only be evaluated for tidal stream technologies.

As will be discussed in detail in various sections in this chapter, a tidal energy resource assessment was conducted by analyzing, modeling, and simulating the tidal velocity, and the extractable tidal energy was done at four sites around the South African coastal lines. From the resource assessment, an optimum site was then selected. Based on the tidal velocity of the selected site, the use of a helical tidal turbine was proposed. This with respect to the tidal velocity profile, the design process of a cross-flow helical turbine was done in order to determine the amount of electrical power that can be obtained. Prior to the turbine design, the analysis of the cross-flow turbines was done, a comparative analysis of two dominant cross-flow turbines was also carried out. The turbine that demonstrated a higher performance for the tidal stream was chosen and this was the helical cross-flow turbine. This turbine was modelled using the blade element momentum theory (BEMT). The diagram used to illustrate the generation of electrical power from the kinetic motion of the tidal stream with the use of the helical cross-flow turbine is shown in Figure (3.1).

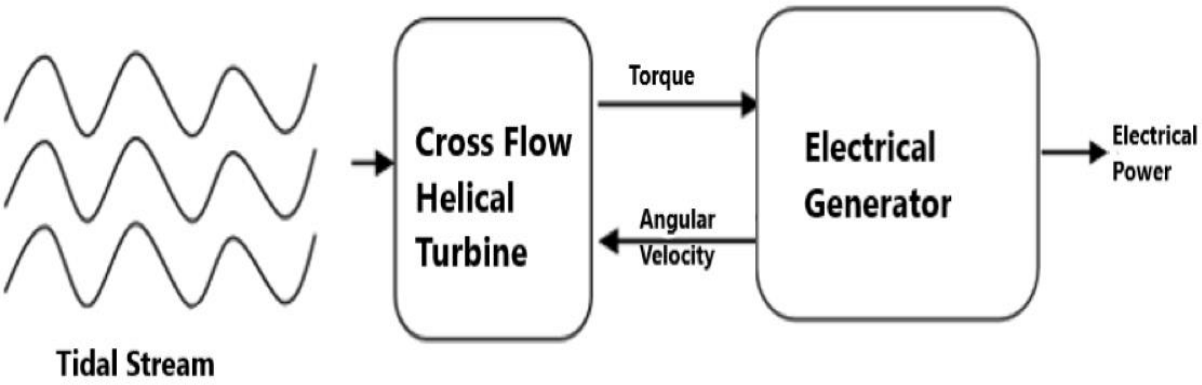

Figure 3.1: Tidal stream energy conversion system

As shown in the diagram, the cross-flow helical turbine converts the kinetic energy from the tidal stream into mechanical power which is given as a function of the torque and the angular velocity. The turbine shaft is coupled to the electrical generator that converts the mechanical power into electrical power.

3.2 Analysis of Tides in South Africa

The amount of tidal power obtained from tides is a result of the function of the cube of tidal stream (current) velocity. Thus, the analysis and prediction of the stream velocity are essential for estimating the amount of electrical power that can be generated from a site. The amount of power available from a tidal site can be assessed using a tidal velocity profile. An evaluation of potential sites was conducted based on their geographical location. South Africa possesses the world's second-fastest current with an average velocity of 1.3 m/s and a surface velocity of 2 m/s [19] called the Agulhas current. The current flows along the east coast of South Africa as shown in Figure (3.2) and the sites in this region can be considered for the establishment of a tidal farm site. An economical site for establishing a tidal farm is one with a stream velocity of at least 1 m/s.

Mosselbaai, Knysna, Ballitoville, and Esikhawini were identified as potential sites based on the tidal data available from the South African Navy Hydrographic Office (SANHO). The major constituents in the above locations as defined in equation (2.2) are the principal lunar semidiurnal constituent (M2), principle solar semidiurnal constituent (S2), lunisolar semidiurnal constituent (K1), and lunar-solar semidiurnal (O1). The other constituents are extremely small and can be neglected [80] for the purpose of simulation. The tidal constituent data in this study was estimated based on previous studies carried out as documented in [9, 81].

Figure 3.2: The Agulhas current system [82]

The data was collected using Acoustic Doppler Current Profilers (ADCP) which measured the velocity, depth, and frequency of each constituent. The ADCPs were placed 153 to 230 kilometers from the shoreline in water depths of about 10 to 24 meters below the ocean surface. The tidal constituent data is presented in table 3.1.

Table 3.1: Tidal constituent data

MOSSELBAAI			
Tidal Constituent	**Amplitude (m)**	**Phase (rad)**	**Frequency**
M2	**0.95**	**0.89884**	**0.0807**
S2	**0.20**	**0.89921**	**0.0834**
K1	**0.21**	**1.60221**	**0.0418**
O1	**0.15**	**3.55174**	**0.0389**
ESIKHAWINI			
M2	**0.96**	**0.81088**	**0.0818**
S2	**0.21**	**0.91738**	**0.0835**
K1	**0.22**	**1.93033**	**0.0418**
O1	**0.16**	**2.73151**	**0.0374**
BALLITOVILLE			
M2	**0.66**	**0.5411**	**0.0805**
S2	**0.31**	**0.9162**	**0.0833**
K1	**0.38**	**0.3577**	**0.0418**
O1	**0.27**	**3.8048**	**0.0389**
KNYSNA			
M2	**0.57**	**0.5411**	**0.0816**
S2	**0.47**	**0.9226**	**0.0844**
K1	**0.31**	**0.8978**	**0.0429**
O1	**0.26**	**4.2428**	**0.0398**

From the above information no firm conclusion can be drawn on the tidal resource in each location, in the proceeding section, a numerical model was used to evaluate the tidal resource.

3.3 Numerical Simulation of Tidal Stream

A harmonic equation was used to model the sinusoids movement of the tidal stream. This model assumes that tidal elevation is a summation of harmonic components with each component representing a tidal constituent. Each tidal constituent consists of a unique amplitude, frequency, and phase angle which can be simulated individually as a sinusoidal function as illustrated in Figure (3.3). Equations (3.1a) to (3.1d) can be used to predict the sinusoidal movement of each tidal constituent, where v_{M2}, v_{S2}, v_{K1}, v_{O1} are the velocities of each harmonic constituent, θ, f and A are the phase angle, frequency, and amplitude of the harmonic constituent respectively.

$$v_{M2} = A_{M2}\sin(2\pi f_{M2} + \theta_{M2}), \quad (3.1a)$$

$$v_{S2} = A_{S2}\sin(2\pi f_{S2} + \theta_{S2}), \quad (3.1b)$$

$$v_{K1} = A_{K1}\sin(2\pi f_{K1} + \theta_{K1}) \quad (3.1c)$$

$$v_{O1} = A_{O1}\sin(2\pi f_{O1} + \theta_{O1}) \quad (3.1d)$$

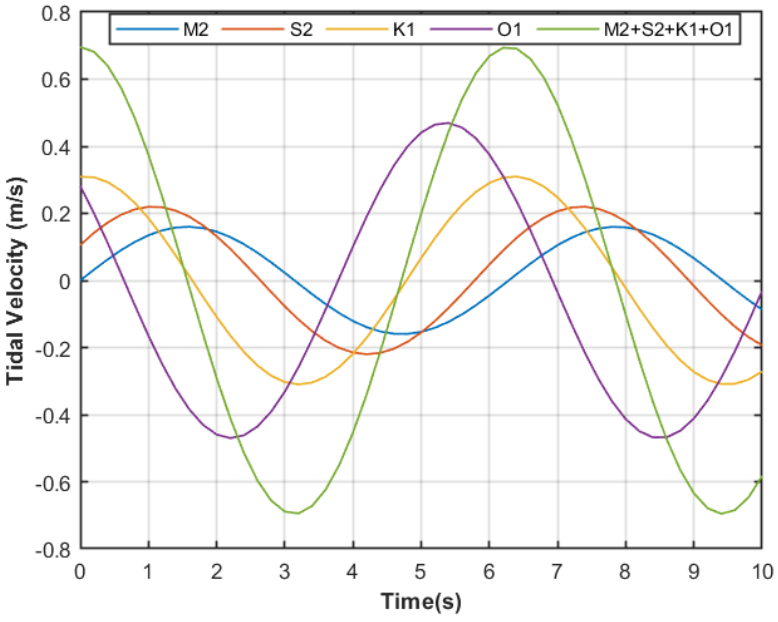

Figure 3.3: Tidal constituent

The exact tidal speed that can be observed at a location can be determined from equation (3.2).

$$v(t) = v_{M2} + v_{S2} + v_{K1} + v_{O1} \quad (3.1)$$

A generic tidal velocity function as presented in equation (3.3) can be used for modelling the tidal current velocity profile at a location with different tidal constituents.

$$v(t) = \sum_{n=1}^{\infty} A_n \sin(2\pi f_n t + \theta_n) \tag{3.2}$$

Where $v(t)$ is the tidal current velocity with respect to time, θ_n, f_n and A_n which are the phase angle, frequency, and amplitude of the harmonic constituent respectively. This equation was implemented on MATLAB/SIMULINK environment and the simulation model is shown in Figure (3.4). In this model, each function block represents a tidal constituent as provided in table 3.1, and the summation block adds up the output of the four tidal constituents.

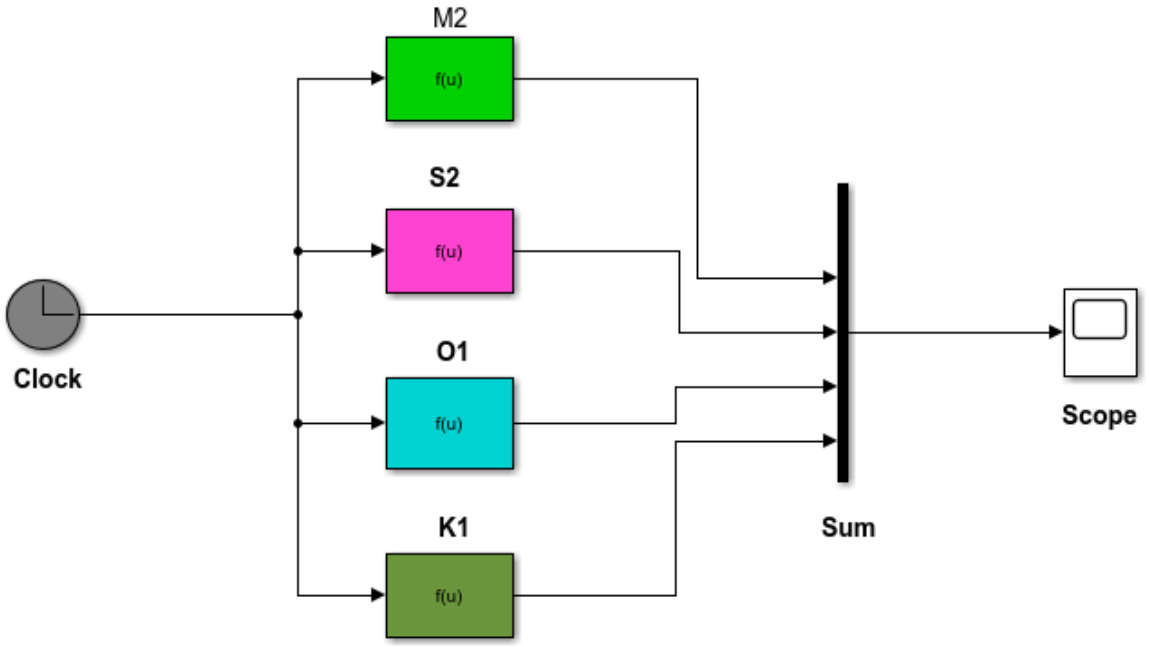

Figure 3.4: MATLAB tidal stream velocity profile

The tidal velocity profile facilitates in establishing the maximum velocity profile for a particular place which then plays a vital role in the design process of tidal turbines to be used. Thus, the installed capacity of a turbine should be rated based on the value of 0.75 x Maximum velocity, the values of the maximum velocity for each site are summarised in table 3.2.

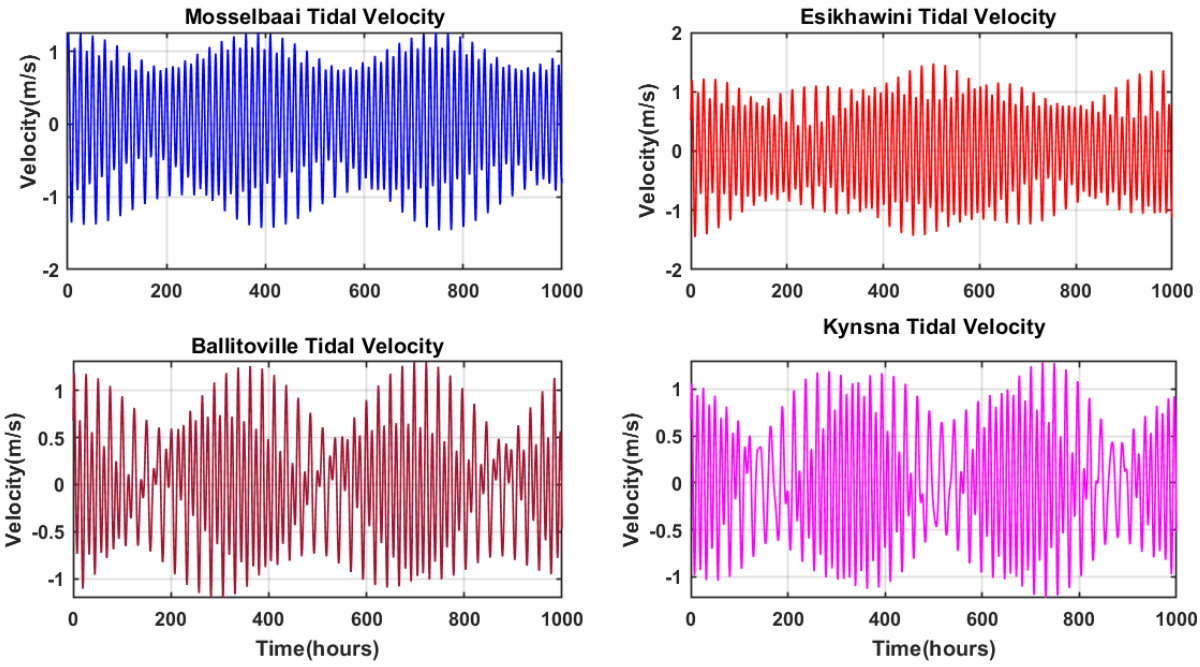

Figure 3.5: Tidal resource in South Africa

Table 3.2: Rating velocity

Plant Location	Max. Velocity (m/s)	Rating Velocity (m/s)
Mosselbaai	1.2595	0.9446
Ballitoville	1.2909	0.9682
East Landon	1.2612	0.9459
Esikhawini	1.4339	1.0784

From the above results and calculations, Esikhawini was selected as the optimum site for this study on the establishment of a tidal Power plant in South Africa

3.4 Analytical Evaluation of Tidal Power

As stated in Chapter two, not all the available power can be extracted from the free tidal stream. A stream tube model, presented in Figure (3.6) can be used analytically to determine the maximum optimal power coefficient $(C_{p(\max)})$. The power coefficient describes how efficiently the turbine can convert tidal energy into useful power. This model describes the work done on the turbine by the kinetic motion of the stream. The turbine is represented by a frictionless actuator disc that separates the upstream and downstream flow. In this stream tube model, in order to determine the amount of power that can be converted from a tidal stream, the following assumptions are made:

- A controlled volume in the stream tube.

- An ambient pressure (P_a) on the surfaces of the far upstream and far downstream.
- There is a velocity continuity through the disk.

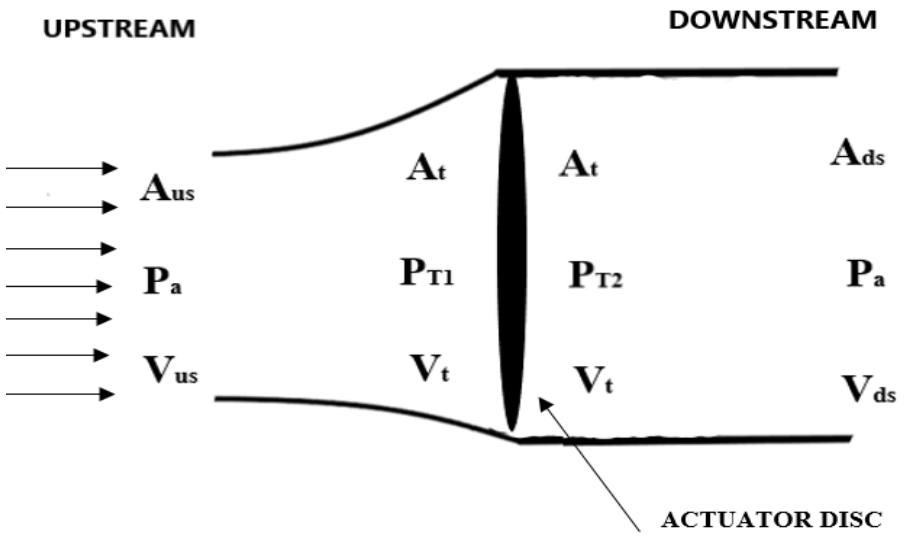

Figure 3.6: Actuator disc model for maximum extractable power

In Figure (3.6), presents the free tidal stream flow, the upstream flow is the tidal current that possesses the extractable tidal power, and the downstream is the tidal stream that has interacted with the turbine. The continuity principle suggests the following:

$$A_{us}V_{us} = A_tV_t = A_{ds}V_{ds} \tag{3.3}$$

Where A_{us}, A_t, A_{ds} are the surface area at the upstream, turbine, downstream, respectively and V_{us}, V_t, V_{ds} are the velocities at the upstream, turbine, downstream, respectively. As the fluid flows from upstream to downstream, a force given in equation (3.5), is exerted on the turbine due to the change in momentum of the stream:

$$F_N = \Delta p = dm(V_{us} - V_{ds}) \tag{3.4}$$

Where dm is the mass flow rate given as:

$$\frac{dm}{dt} = \rho A_{us}V_{us} \tag{3.5}$$

The thrust can be written in terms of pressure difference in the upstream and downstream as:

$$F_N = A_t(p_{T1} - p_{T2}) \tag{3.6}$$

Where p_{T1} is the upstream pressure and p_{T2} is the downstream pressure. Equating (3.5) and (3.7) are equated, and the continuity principle is applied, this yields:

$$(p_{T1} - p_{T2}) = \rho V_t(V_{us} - V_{ds}) \tag{3.7}$$

Bernoulli's principle states that an increase in the fluid velocity occurs simultaneously with the decrease in pressure [83], this principle is applied both upstream and downstream.

Upstream, $$P_a + \frac{1}{2}\rho V_{us}{}^2 = P_{T1} + \frac{1}{2}\rho V_{ds}{}^2 \quad (3.8)$$

Downstream, $$P_a + \frac{1}{2}\rho V_{ds}{}^2 = P_{T2} + \frac{1}{2}\rho V_t{}^2 \quad (3.9)$$

Adding equations (3.9) and (3.10) yields:

$$P_{T1} - P_{T2} = A\frac{1}{2}\rho(V_{us}{}^2 - V_{ds}{}^2) \quad (3.10)$$

Equating equation (3.8) and (3.11) yields:

$$V_t = \frac{1}{2}\left[V_{us} + V_{ds}\right] \quad (3.11)$$

Considering the turbine power coefficient (C_p) which provides a percentage of the amount of power generated from the free stream.

$$C_p = \frac{P_{Gen}}{P_{Ext}} \quad (3.12)$$

Where, $P_{Gen} = F_N V_t$

After mathematical manipulations P_{Gen} is given as:

$$P_{Gen} = \frac{1}{4}\rho A_t V_{us}^3 \left(1 - \frac{V_{ds}^2}{V_{us}^2}\right)\left(1 + \frac{V_{ds}}{V_{us}}\right) \quad (3.13)$$

Let, $x = \frac{V_{ds}}{V_{us}}$

Therefore, $$C_p = \frac{1}{2}\left(1 - x^2\right)\left(1 + x\right) \quad (3.14)$$

For maximum optimal power coefficient, $\frac{dC_p}{dn} = 0$

3.5 Assessment of Tidal Power Resource

If all the kinetic energy available from the tidal stream were to be converted into useful power, the tidal stream speed beyond the turbines would be zero. Practically, the tidal stream velocity beyond the turbine is always moving at a certain velocity that is less than the upstream velocity. If the tidal stream stopped moving at the exit of the turbine, then no fresher tides could get in; it would be blocked. In order to keep the stream moving through

the turbine, there has to be some stream movement, however small, on the other side with some stream velocity greater than zero [22].

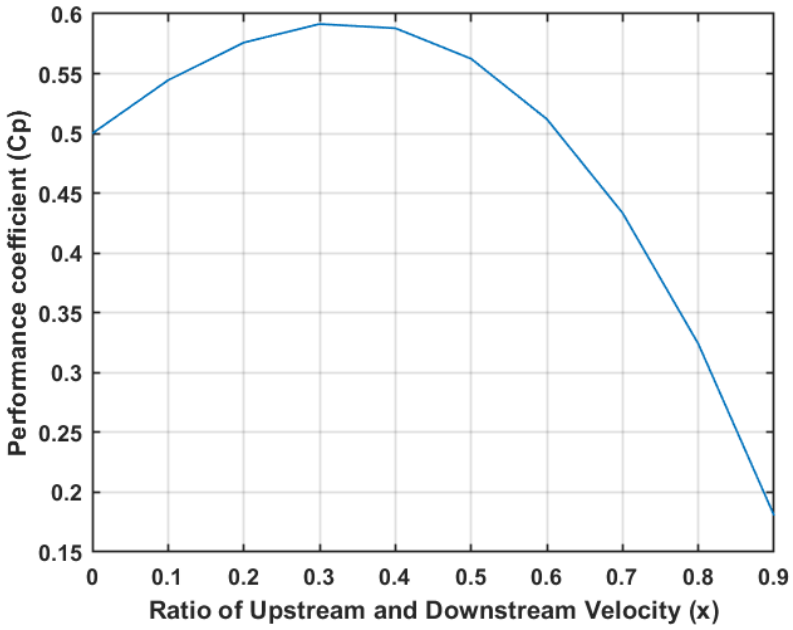

Figure 3.7: Maximum extractable power

Betz's law shows that as the stream flows through a certain area, and as stream velocity slows down from losing energy to extraction from a turbine, the stream flow must distribute to a wider area. As a result, geometry limits any turbine efficiency to a maximum of 59.3% [84, 85] which was illustrated in Figure (3.7). The amount of power generated by the turbine can be determined from the following expression:

$$P = \frac{1}{2} C_p \rho A V^3 \tag{3.15}$$

Where the seawater density in kilograms per cubic meter is ρ , A is the turbine swept area in square meters, and V is the tidal current velocity in meters per second. Figure (3.8) presents a free tidal stream curve for the identified site and the variation in turbine output power as a function of tidal velocity and the turbine performance coefficient.

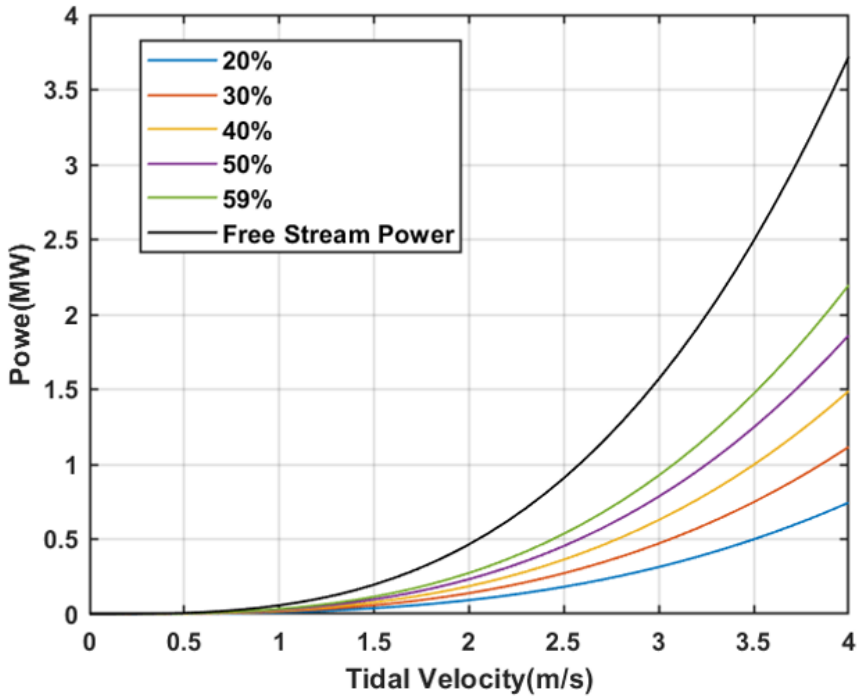

Figure 3.8: Tidal power curve with turbine performance

The black graph presents the maximum available tidal power at Esikhawini; below this curve is the maximum power generated by a turbine with a maximum optimal performance coefficient (59.3%). In reality, there is no turbine that can extract the 59.3%, the possible extractable power at different efficiencies and velocities is illustrated in the above figure. The curves show the amount of power generated by a single turbine, all turbines were assumed to have the same swept area but different performance coefficients. Figure (3.9) illustrates the difference in turbine swept area of an AFWT and CFWT.

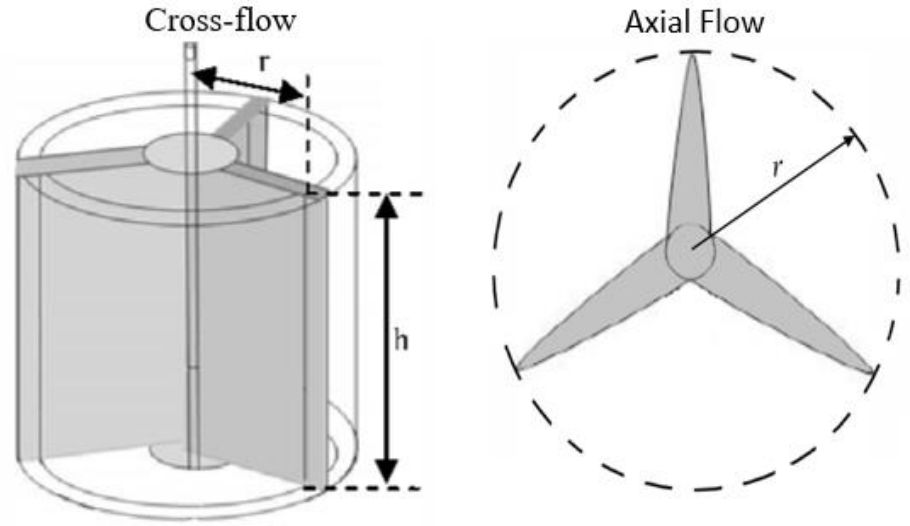

Figure 3.9: Turbine swept area

The cross-sectional area of flow swept by a cross-flow and an axial flow turbine can be determined from equations (3.17) and (3.18), respectively.

$$A = 2Rh \tag{3.16}$$

$$A = \pi R^2 \tag{3.17}$$

Where R is the rotor radius and h is the turbine height. The impact of the turbine configuration is presented in Figure (3.10) where two ideal turbines, an axial and cross-flow were assumed to be deployed at Esikhawini. The radius and turbine performance coefficient were kept constant in both turbines. The turbine output power was assessed from the implementation of equation (3.16).

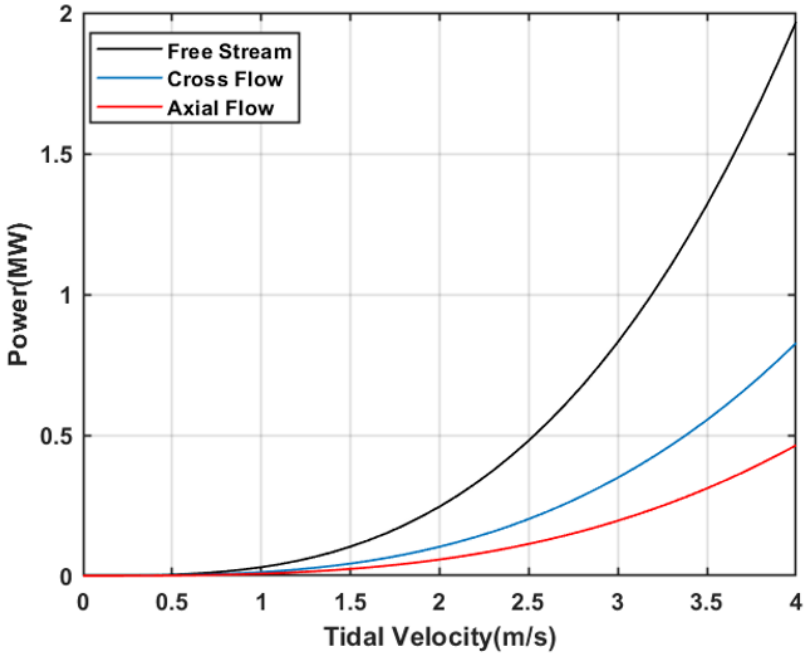

Figure 3.10: Power generated relation with turbine configuration

The cross-flow turbine exhibits superiority compared to the axial flow turbine as more power was generated by the cross-flow turbine. The difference in the turbine output power is correlated to the turbine swept area which was the only variable that was varied in both turbines. Cross-flow turbines may generate more power but there are a few deployed throughout the globe owing to the limited research on cross-flow turbines. The exact amount of power generated from a tidal plant situated at Esikhawini will depend on the selected turbine and the number of turbines deployed. Tidal velocities at Esikhawini are considered low, therefore to ensure that a great amount of power is generated from the site, low-speed tidal turbines with high turbine efficiency should be considered.

3.6 Analysis of Cross Flow Turbines

From the three cross-flow turbines covered in the literature review, the Darrieus and Gorlov turbines were critically analysed for the selection of a tidal turbine. Savonius turbines are not included in this analysis due to low tip speed; low tip speed results in low efficiencies. Another parameter that is considered for turbine selection is the angle of attack (an angle between the relative velocity and the chord), Figure (3.11) shows different angles of attack (α) for different azimuth angles of the cross-flow turbines.

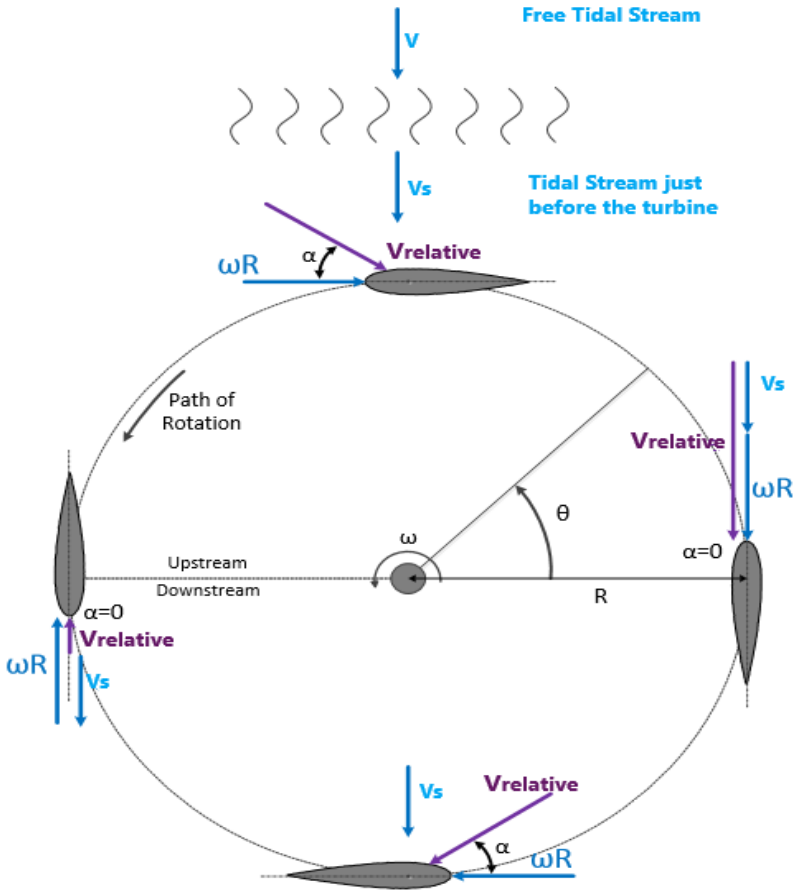

Figure 3.11: Different angles of attack (cross-flow turbines)

The two Darrieus turbines mentioned in the literature are simple, cheap, and do not occupy a lot of space. Both designs suffer from 'torque ripple' as a result of varying angles of attack. In view of the limited research on the hydrodynamics and performance of the Troposkein-bladed turbine, the performance of the straight-bladed turbine is compared to that of a helical turbine. Helical turbines are a modification of the Darrieus turbines resulting in high efficiencies. An experiment conducted in [54] compared the two turbines is given in table 3.3.

Table 3.3: Turbine specifications

Turbine Type	**Darrieus**	**Helical**
Number of Blades	3	3
Height	22.86 cm	22.86 cm
Diameter	21.59 cm	21.59 cm
Hydrofoil	NACA-0020	NACA-0020
Aspect ratio	1.06	1.06
Helical pitch angle	0°	60°

The turbines were printed using a 3D printer (SLA-190), the rotor blades of both turbines were supported by two discs at the end of each blade as illustrated in Figure (3.12). These turbines were tested in water velocities of 0.274 m/s to 1.512 m/s.

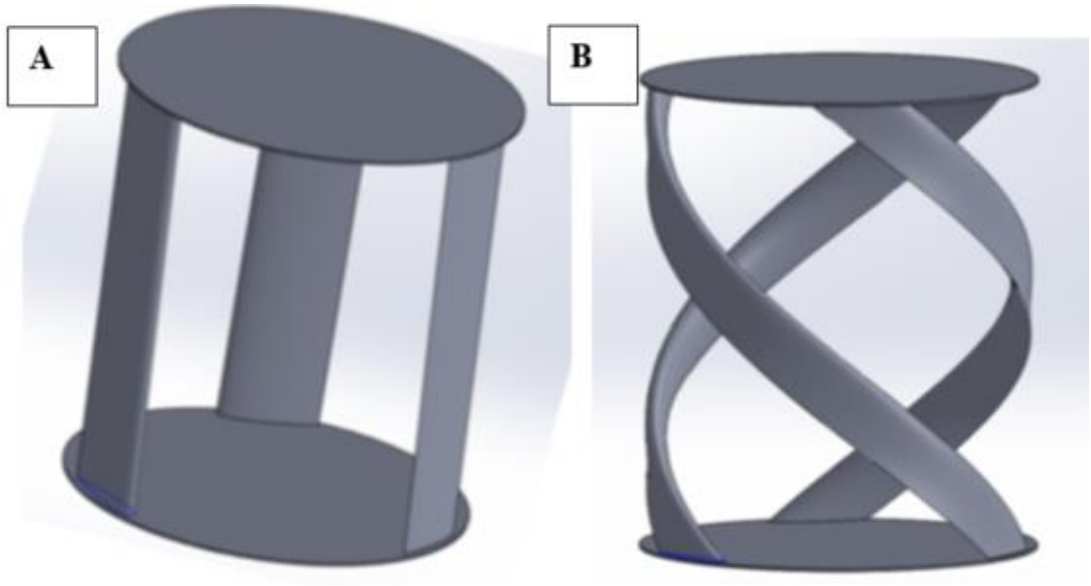

Figure 3.12: A. Darrieus, B.Gorlov Turbine

The experimental results are given in Figure (3.13) below. From the results presented below, the helical turbine exhibits high turbine power with higher efficiencies in low stream speeds compared to the Darrieus turbine. The solidity, aspect ratio, and other turbine design and performance parameters were the same, the only difference was the shape of rotor blades. The helical blades are designed with no circumferential void space, this ensures that at any angular position, a point along the blade is always at an optimal angle of attack [86]. Based on the experimental results presented, the helical turbine was selected for this study.

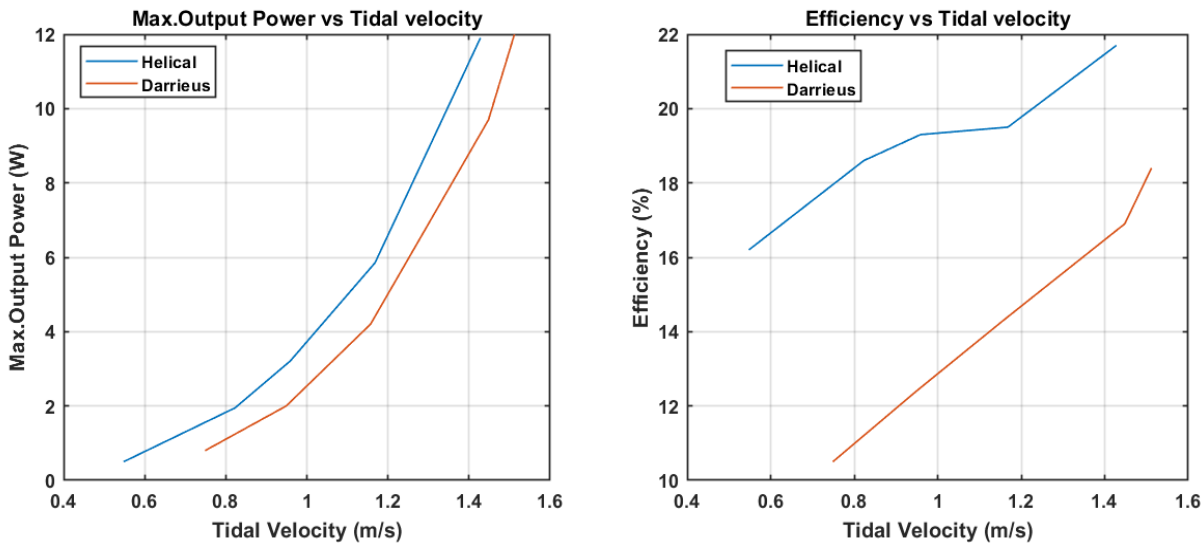

Figure 3.13: Left: Max. output power versus tidal velocity, Right: Efficiency versus tidal velocity [54]

3.7 Turbine Design

Turbine selection is based on the turbine design and performance, this section covers all the important design and performance parameters. When designing a turbine, Bernoulli's equation is used, the principle was explained in the numerical evaluation. Bernoulli's equation consists of three components and can be referred to as first, second, and third components as given in equation (3.19).

$$\begin{matrix} 1^{st} & 2^{rd} & 3^{rd} \\ \downarrow & \downarrow & \downarrow \end{matrix} \qquad z + \frac{p}{\rho} + \frac{V^2}{2g} = const \tag{3.18}$$

This equation describes the fluid flow with the first component representing the fluid elevation, the external pressure due to the water head is defined by the second component, and the third component determines the kinetic energy of the fluid. When designing the traditional turbines which are used in applications such as the tidal barrage and hydropower system, the kinetic energy component is neglected. For the purpose of this study the second component is neglected, this enables the turbine to rotate freely when placed in a stream with minimal resistance to water flow, hence low solidity. Helical turbines rotate at high uniform speeds in slow stream flows, they are unidirectional in reversible fluid currents, and according to the experiment conducted in [54] there are no visible signs of cavitation in water for high rotating speed and the torque developed on the shaft does not fluctuate.

3.7.1 Blade Profile

The concept of helical turbines originated from the idea of improving the performance of Darrieus turbines, the helical turbines possess all the advantages of Darrieus turbines without the disadvantages [54]. This improved performance is correlated to the design of the turbine blades that consists of a hydrofoil profile, which follows a helix path as illustrated in Figure (3.14). When the tidal stream strikes the turbine blades, energy is converted into mechanical power which is then developed on the turbine shaft, and some energy is lost as evaluated in the preceding section.

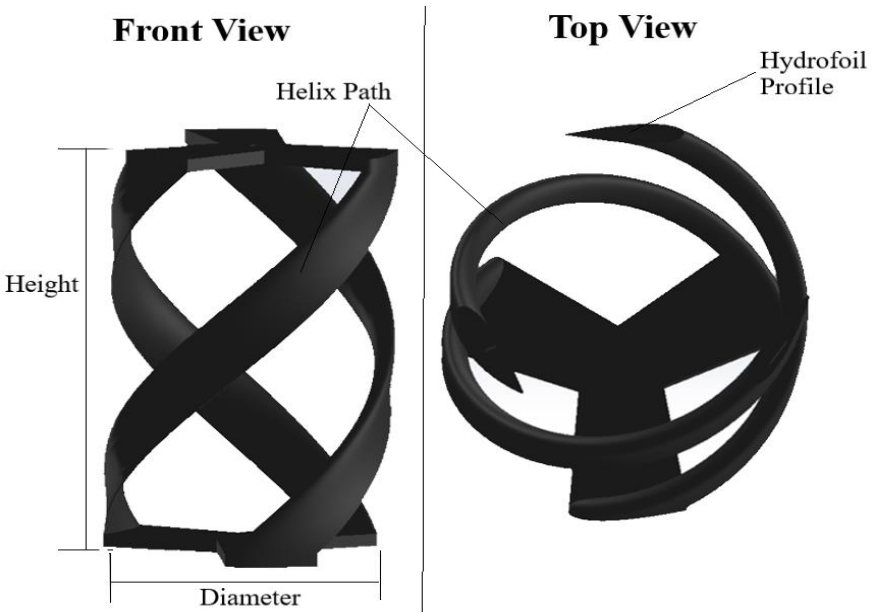

Figure 3.14: Gorlov helical turbine

The blade profile adopted in the design process depends on the type of flow experienced at a site, the Reynolds number (**Re**)determines the stream flow [87]. If the **Re** is less than 2000 the flow is referred to as laminar and if **Re** is greater than 4000, it is a turbulent flow. Equation (3.20) can be used to determine the type of flow at an identified location, Figure (3.15) illustrates the two flows mentioned above.

$$\mathrm{Re} = \frac{\rho V D}{\mu} \tag{3.19}$$

Where ρ is the water density, V is the mean stream velocity, D is the diameter tunnel, and μ is the viscosity of the fluid.

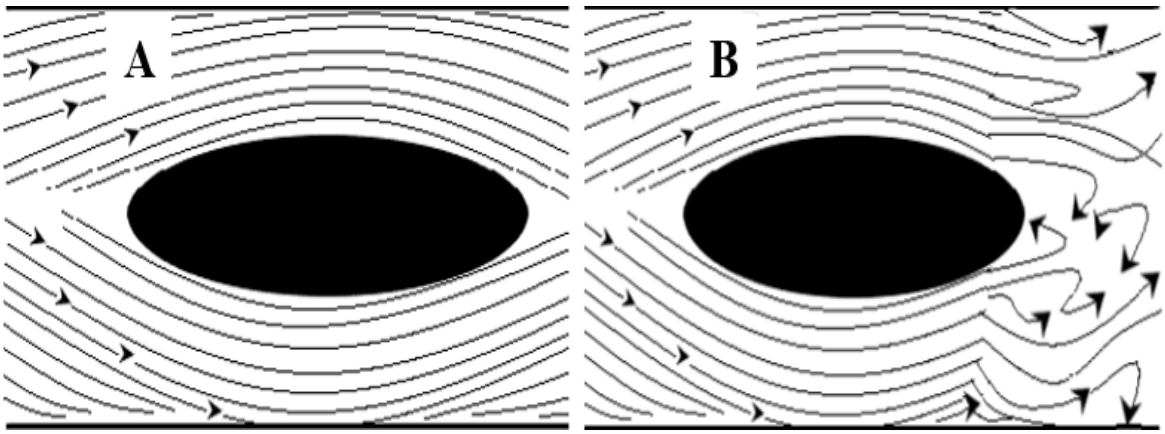

Figure 3.15: A. Laminar flow B. Turbulent flow

Where the flow conditions are unknown it is safe to assume a turbulent flow for the selection of a hydrofoil. A flow analysis over the hydrofoil provides an idea of how the lift and drag forces are induced. In the energy conversion system, as the stream hits the hydrofoil profile of the blade, the stream flow spits as shown in Figure (3.16), the top and bottom flow result in drag and lift forces [73] respectively. According to Bernoulli's principle, the top region is at low pressure due to the increased flow velocity, however, the bottom region experience high pressure as a result of low velocities. When the top flow reaches the end of the hydrofoil, it flows slightly downwards, the slight turn in the fluid flow results in a lift force that is higher than the drag force, thus driving the turbine.

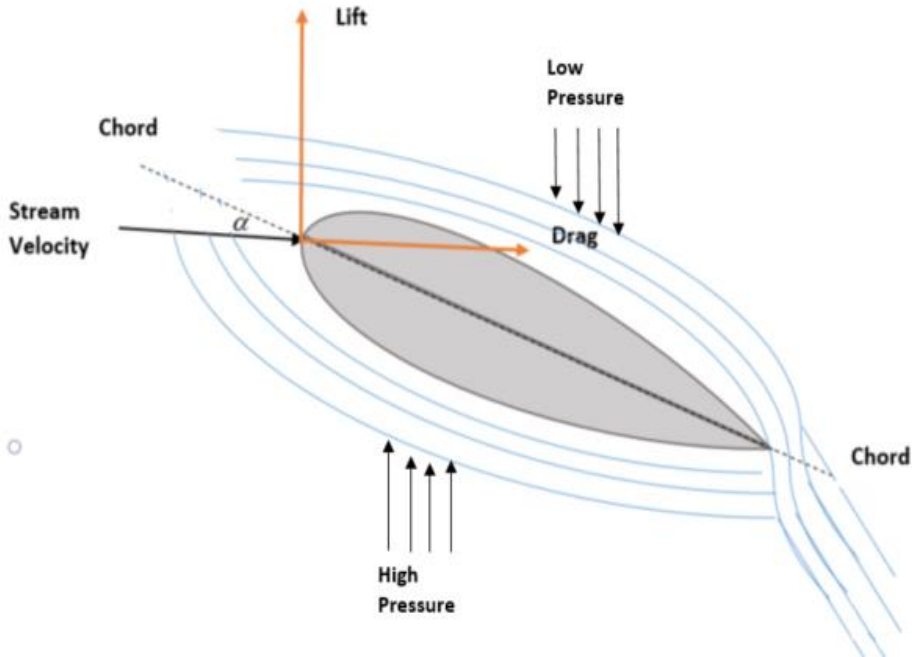

Figure 3.16: Stream flow on hydrofoils

The lift-driven helical turbine requires a hydrofoil with a high lift and low drag coefficient which can be achieved by adjusting the angle of attack (α). If the angle of attack is too high there will be a massive increase in drag force that will result in a reduction of the lift force, this phenomenon is called stall [83]. Two hydrofoils, NACA0018 and NACA0020 were evaluated for the selection of a hydrofoil, both hydrofoils are symmetric and exhibit the shape[88] but they differ in thickness. The lift and drag coefficient data of the two hydrofoils is given in Appendix A for a site with **Re = 250000**. Figure (3.17) is the graphical representation of the data presented. From the figure below it is evident that NACA-0018 is more efficient compared to NACA00202 due to the low drag and high lift in turbulent flows for angles of attack above $4°$. NACA0018 was selected for the helical turbine in this study.

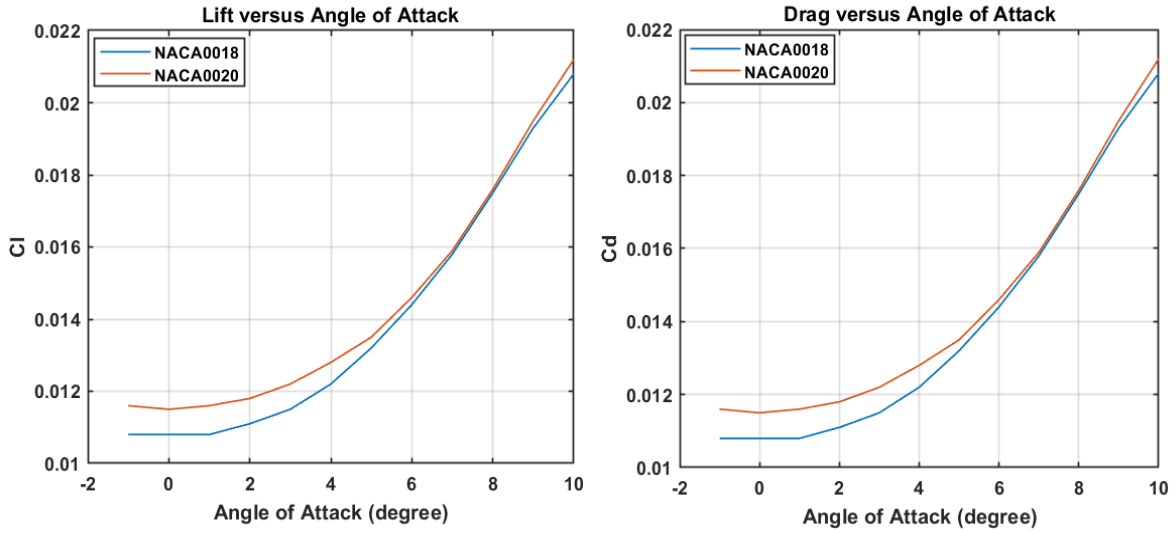

Figure 3.17: Left. Drag versus angle of attack, Right. Lift versus angle of attack

3.7.2 Turbine Parameters

Other than the hydrofoil profile, there are dimensionless performance and design parameters that greatly impact the power generated by the turbine.

3.7.2.1 Performance

The turbine performance depends on the tip speed ratio, efficiency, and Reynolds Number. The tip speed ratio (TSR) describes how fast the turbine blades are rotating relative to the stream velocity given by equation (3.21).

$$\lambda = \frac{\omega R}{V} \tag{3.20}$$

Where λ is the tip speed ratio, ω is the turbine angular velocity, R is the turbine blade radius, and V is the stream velocity. The TSR should not be too high or too low, a very high TSR causes the turbine to form a “wall” that obstructs the fluid flow, thus no power extracted

from the fluid. This can lead to fatigue failure. The turbine performance coefficient is the ratio of the mechanical power (the product of torque developed on the turbine shaft and the angular velocity of the turbine) to the tidal power given in equation (3.22). C_p is also a function of the tip speed ratio and the angle of attack, this will be elaborated upon in the next section.

$$C_p = \frac{T\omega}{0.5\rho V^3} \tag{3.21}$$

Where C_p is the turbine performance coefficient and T is torque developed on the shaft.

3.7.2.2 Design

Design parameters include solidity ratio, the number of blades, aspect ratio, and helical pitch angle (angle of attack). Solidity is the ratio of the solid material to the void space as expressed in (3.23), this describes the circumference occupied by the turbine blades.

$$\sigma' = \frac{Bc}{\pi D} \tag{3.22}$$

Where B is the number of rotor blades, c is the chord length, and D is the turbine diameter. A four and three-bladed turbine with the same solidity may exhibit different turbine efficiency. The solidity of two turbines tested in an experiment documented in [58] remained constant while the number of blades was increased, this resulted in reduced turbine efficiency. The aspect ratio is the ratio of the turbine height to diameter given by equation (3.24).

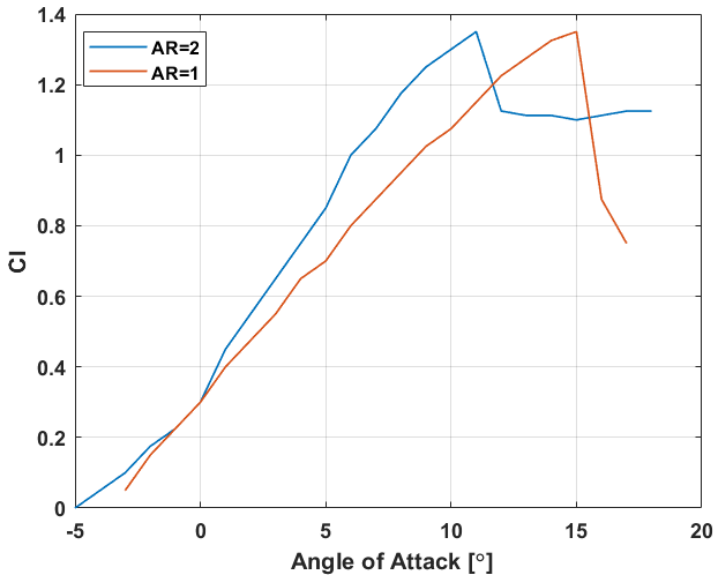

Figure 3.18: The impact of aspect ratio

$$Aspect\ Ratio = \frac{h}{D} \tag{3.23}$$

The aspect ratio affects the turbine performance by either increasing or decreasing the lift coefficient, from Figure (3.18) it is evident that a height aspect ratio increases the lift turbine performance. To obtain a high aspect ratio the turbine high can be increased and according to Gorlov, there is no limit to the helical turbine height. To maintain the high aspect ratio, the turbine diameter, need to be adjusted accordingly. Conversely to the turbine height, there are limits to the turbine diameter, and if ignored this could lead to structural failure.

3.8 Blade Element Momentum Theory (BEMT)

The amount of power generated by the tidal turbine can be analysed by applying the BEMT that is widely used for conducting turbine performance analysis or for designing a completely new turbine [83, 89, 90]. This method is divided into momentum and blade element theory; the momentum theory [91] analyses the axial and angular momentum of the stream whereas the blade element theory suggests that the force exerted on the turbine blade by the stream can be resolved using lift and drag forces.

3.8.1 Momentum Theory

The axial momentum describes the work done on the turbine by the fluid, this was covered in section 3.3. The axial momentum derivative considers the axial induction factor, which describes the reduction in stream velocity. The axial induction factor is given by:

$a = \frac{V_{us} - V_t}{V_{us}}$, Thus,

$$V_t = V_{us}(1-a) \tag{3.24}$$

Substituting equation (3.25) into (3.11) yields:

$$dF_N = A\frac{1}{2}\rho V_{us}^2 4a(1-a) \tag{3.25}$$

3.8.2 Angular Momentum

The stream also exerts a tangential force on the turbine which is defined as a change in angular momentum, the angular momentum can be determined using equation (3.27).

$$L = I\,\omega \tag{3.26}$$

Where I is the moment of inertial and ω is the angular velocity. The expression of the moment of inertial is given by:

$$I = mr^2 \tag{3.27}$$

Where m is the mass rotating at a radius r. The tangential force (torque) can be written as follow:

$$dF_T = \frac{dL}{dt} = \frac{d(mr^2\omega)}{dt} = \frac{dm}{dt} r^2\omega \tag{3.28}$$

Where the volumetric mass is given as:

$$\frac{dm}{dt} = \rho V_t dA \tag{3.29}$$

Where dA is the cross-sectional area and V_t is the velocity just before the turbine. Consider figure 3.19 the cross-sectional area is given by:

$$dA = 2\pi r dr \tag{3.30}$$

Where r is the radius of the ring or blade element and dr is the thickness of the ring.

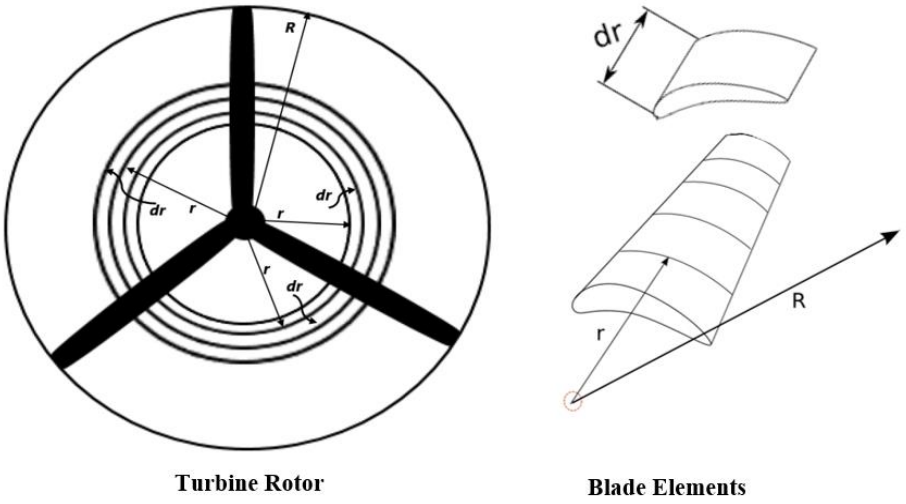

Figure 3.19: Turbine rotor and blade elements

The tangential force can now be given by:

$$dF_T = \rho 2\pi r dr V_t \omega r^2 \tag{3.31}$$

The angular induction factor a' can be expressed in terms of the angular velocity of the wake as given in equation (3.33).

$$a' = \frac{\omega}{2\Omega} \tag{3.32}$$

Therefore,

$$dF_T = 4a'(1-a)\rho V_{us}\Omega\pi r^3 dr \tag{3.33}$$

3.8.3 Blade Element Theory

The blade element theory considers the characteristic of the blade profile to describe the fluid flow [92]. The turbine blades are divided into smaller blade elements or rings that act

independently to surrounding elements. The total power generated by the turbine rotor is a summation of the power generated by each element. Elements are assumed to have no hydrodynamic interactions and the forces on each element are determined by the drag and lift forces. Figure (3.19) shows an example of how the rotor blade can be divided into blade elements, the blade can be sectionalized from a minimum number of ten elements. From the figure, r and dr are radius and thickness of the element respective and R is the radius of the turbine rotor.

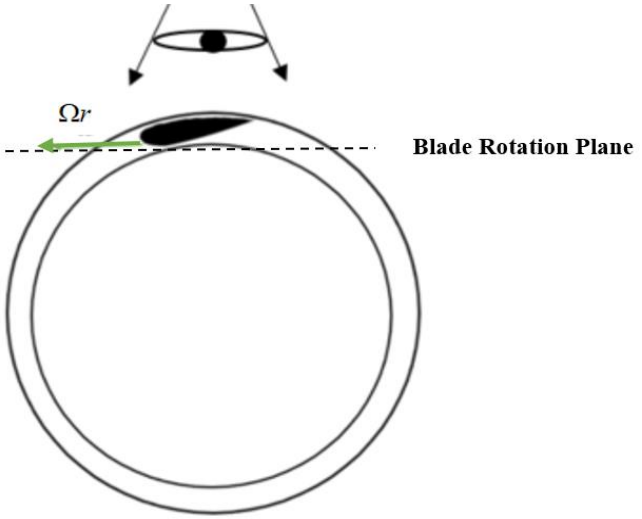

Figure 3.20: Blade element top view

One element is analysed for the purpose of derivation. An element is represented by a hydrofoil on a plane of rotation as illustrated in Figure (3.20). The rotational speed of each element is slightly different and is determined by Ωr, where Ω is the angular velocity of the blade and r is the radius of the element. The governing blade element equations are derived using velocity and force diagrams presented in Figure (3.21) and Figure (3.22), respectively. The hydrofoil is taken as the point of reference for the demonstration of velocities. The rotation of the hydrofoil induces axial and angular velocities denoted as $V_{us}a$ and $\Omega r a'$ respectively with the total induced velocity V_{rel}. In reality, the hydrofoil rotational speed is in the opposite direction as seen in Figure (3.21). This diagram considers the axial $\left(V_{us}(1-a)\right)$ and angular $\left(\Omega r(1+a)\right)$ induced velocities.

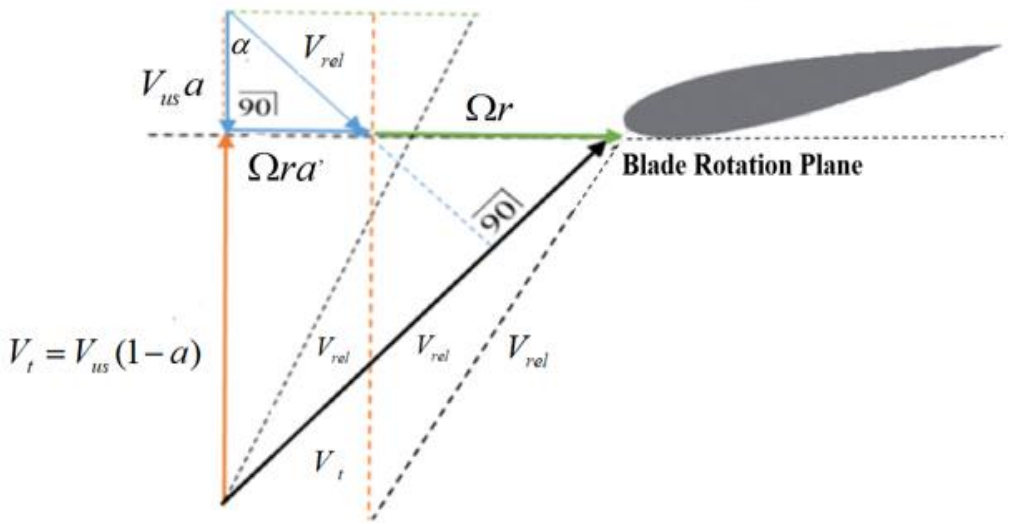

Figure 3.21: Velocity triangles

When the stream hits the hydrofoil, the hydrofoil experiences thrusting (dF_N) and tangential (dF_T) forces. As the stream flows over the hydrofoil it generates lift (dF_L) and drag (dF_d) forces that are perpendicular and parallel to the relative velocity, respectively.

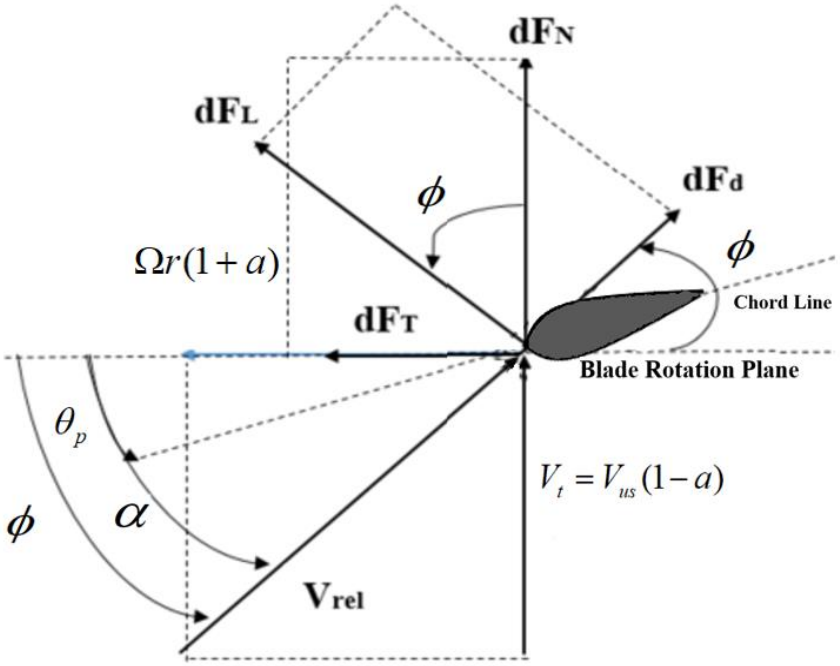

Figure 3.22: The force triangles

The angle between the hydrofoil chord line and the plane of rotation is called a section pitch angle (θ_p) and the angle between the plane and the relative velocity is known as the angle of relative velocity (ϕ). As mentioned in section B the lift and drag coefficients are a function of the angle of attack (α), they are defined as:

$$C_l = \frac{dF_L}{0.5\rho V_{rel}{}^2 cdr} \tag{3.34}$$

$$C_d = \frac{dF_d}{0.5\rho V_{rel}{}^2 cdr} \tag{3.35}$$

Where is the lift coefficient, C_d is the drag coefficient, ρ is the fluid density, V is the stream velocity, c is the chord length, L and D are the lift and drag forces, respectively. The relative velocity can be determined from the expression below:

$$V_{rel} = \frac{V_{us}(1+a)}{\sin\phi} \tag{3.36}$$

Equation (32) is used when solving for the angle of relative velocity (ϕ).

$$\tan\phi = \frac{V_{us}(1+a)}{\Omega r(1-a')} \tag{3.37}$$

The thrust and tangential forces experienced by the hydrofoil can be determined using the following expressions:

$$dF_N = dF_L\cos\phi + dF_d\sin\phi \tag{3.38}$$

$$dF_T = dF_L\sin\phi - dF_d\cos\phi \tag{3.39}$$

Expressing the above force in terms of the lift and drag forces, considering the number of blades yields:

$$dF_N = B\frac{1}{2}\rho V_{rel}^2 cdr(C_l\cos\phi + C_d\sin\phi) \tag{3.40}$$

$$dF_T = B\frac{1}{2}\rho V_{rel}^2 crdr(C_l\sin\phi - C_d\cos\phi) \tag{3.41}$$

3.8.3 BEM Theory

The BEMT combines equate both thrust and tangential equations developed in momentum and blade element theories for the purpose of deriving the turbine performance coefficient. Equating equation (3.26) with equation (3.41) and equation (3.34) with equation (3.42), the following relation was obtained.

$$\left.\begin{aligned} 8a(1-a)V_{us}^2\pi r &= V_{rel}^2 Bc\left[C_l\cos\phi + C_d\sin\phi\right] \\ 8a'(1-a)V_{us}^2\Omega\pi r^2 &= V_{rel}^2 Bc\left[C_l\sin\phi - C_d\cos\phi\right] \end{aligned}\right\} \tag{3.42}$$

Considering the relative velocity (V_{rel}) yields:

$$\frac{a}{(1-a)} = \frac{\sigma}{4} \cdot \frac{\left[C_l \cos\phi + C_d \sin\phi\right]}{\sin^2\phi} \tag{3.43}$$

$$\frac{a'}{(1-a)} = \frac{\sigma}{4} \cdot \frac{\left[C_l \sin\phi - C_d \cos\phi\right]}{\sin\phi\cos\phi} \tag{3.44}$$

There are losses experienced by the turbine at the tip of the rotor blades, these losses were approximated by L. Prandtl [93] as follows:

$$F = \frac{2}{\pi}\cos^{-1}\left(\exp\left(-\frac{B}{2}\frac{R-r}{r\sin\phi}\right)\right) \tag{3.45}$$

Considering the tip losses yields:

$$\frac{a}{(1-a)} = \frac{\sigma}{4F} \cdot \frac{\left[C_l \cos\phi + C_d \sin\phi\right]}{\sin^2\phi} \tag{3.46}$$

$$\frac{a'}{(1-a)} = \frac{\sigma}{4F} \cdot \frac{\left[C_l \sin\phi - C_d \cos\phi\right]}{\sin\phi\cos\phi} \tag{3.47}$$

The power generated by each blade element is given by:

$$dP = \Omega dF_T \tag{3.48}$$

The total power generated by the turbine is the summation of power generated by each element [94], it can be expressed as the integral from the smallest radius to the turbine rotor as given in equation (3.50).

$$P = \int_0^R dPdr = \int_0^R \Omega dTdr \tag{3.49}$$

The turbine efficiency is equal to the power generated by the turbine to the stream power. After algebraic manipulations, the turbine performance coefficient can be given by:

$$C_p = \frac{8}{\lambda^2}\int_{\lambda_r}^{\lambda} F\lambda_r^3 a'(1-a)\left[1-\frac{C_D}{C_L}\tan\phi\right]d\lambda_r \tag{3.50}$$

3.9 Helical Cross-Flow Turbine (BEMT)

The BEMT was initially derived for the purpose of designing and predicting the performance of horizontal axis turbines. The turbine selected for the study is a vertical axis turbine, appropriate alterations are made on the BEMT to satisfy the design of the helical vertical turbine. The momentum model derived in the previous section remains unchanged, due to limited literature on wake rotation of cross-flow turbines. The amount of power generated by the turbine is a function of the forces exerted on the turbine blades. The performance of the blades is determined by two parameters, the stream relative velocity and the angle of attack [95, 96]. The two parameters are functions of the azimuth angle; the expressions of the two

parameters are derived from Figure (3.23). The derivative of the relative velocity and angle of attack corresponds with the blade at azimuth angles between $0°$ to $90°$.

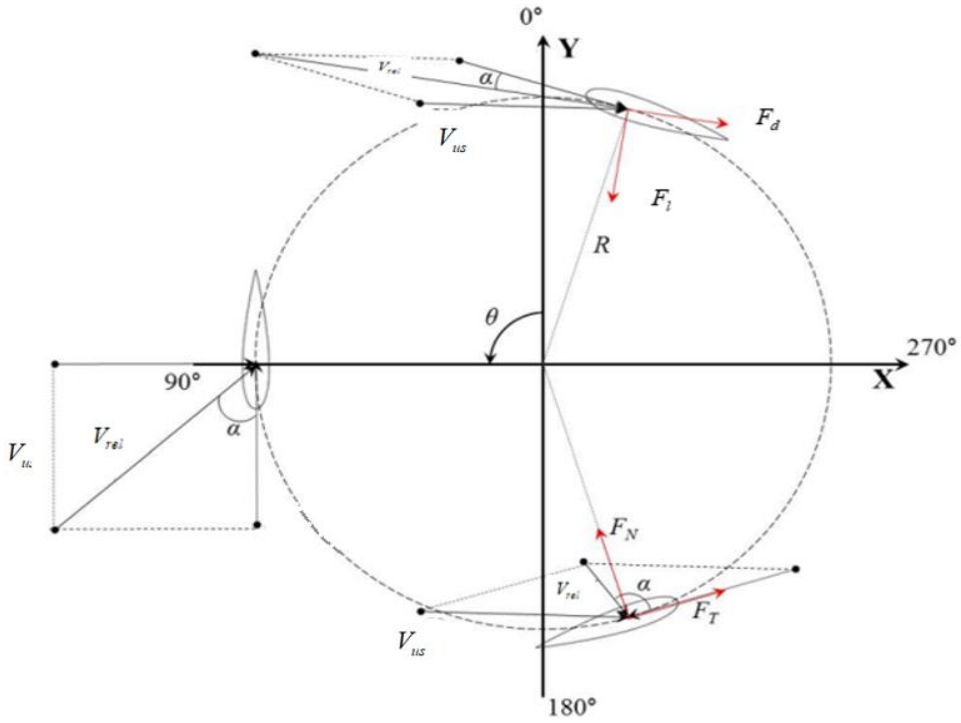

Figure 3.23: Velocities and force on a vertical axis turbine

The relative velocity can be expressed as follows:

$$V_{rel}^2 = (V_{us}\sin\theta)^2 + (V_{us}\cos\theta + \Omega)^2 \tag{3.51}$$

Considering the Pythagorean identity $\sin^2\theta + \cos^2\theta = 1$:

$$V_{rel}^2 = V_{us}^2 + 2V_{us}\Omega\cos\theta + \Omega^2 \tag{3.52}$$

Rearranging the relative velocity in terms of the tip speed ratio:

$$V_{rel} = V_{us}\sqrt{1 + 2\lambda\cos\theta + \lambda^2} \tag{3.53}$$

The angle of attack is given by:

$$\tan\alpha = \frac{V_{us}\sin\theta}{\Omega + V_{us}\cos\theta} \tag{3.54}$$

The angle of attack expressed in terms of the tip speed ratio is:

$$\alpha = \tan^{-1}\left(\frac{\sin\theta}{\lambda + \cos\theta}\right) \tag{3.55}$$

The axial force and tangential force of the turbine blade can be calculated using equation (3.57) and (3.58).

$$F_N = \frac{1}{2}\rho chV_{rel}^2 C_N \tag{3.56}$$

$$F_T = \frac{1}{2}\rho chV_{rel}^2 C_T \tag{3.57}$$

Where the axial coefficient (C_N) and tangential coefficient (C_T) are given as:

$$\left.\begin{aligned} C_N &= C_l \cos\alpha + C_d \sin\alpha \\ C_T &= C_l \sin\alpha - C_d \cos\alpha \end{aligned}\right\} \tag{3.58}$$

The torque developed on the turbine shaft can be determined from the following expression:

$$T(\theta) = \frac{1}{2}\rho chV_{rel}^2 C_T R \tag{3.59}$$

Finally, instantaneous and average power generated by the turbine can be calculated from equations (3.61) and (3.62), respectively.

$$P(\theta) = T(\theta).\Omega \tag{3.60}$$

$$P_{ave} = \frac{N}{2}\pi \int_0^{\pi} P(\theta) d\theta \tag{3.61}$$

The turbine performance coefficient is given by:

$$C_p = \frac{\Omega T(\theta)}{0.5\rho A V_{us}^3} \tag{3.62}$$

3.10 Analytical Performance Analysis of a Helical Turbine

As mentioned in the preceding sections, the angle of attack in helical turbines varies relative to the azimuth angle and the tip speed ratio. South Africa's tidal velocities are moderately low; at low velocities, low tip speed ratios are anticipated. Based on previous literature, the parameters of a turbine suitable for deployment at Esikhawini were calculated. The turbine was designed on SOLIDWORKS and the performance of the turbine was evaluated on MATLAB. A flow simulation was conducted on SOLIDWORKS to analyse the stream velocity over the turbine as presented in Figure (3.24). A linear velocity of 1.4 m/s (maximum stream velocity at Esikhawini) at the inlet of the enclosure was applied. It is clear from the figure below that the velocity increases over the tip of the turbine blades. Based on the flow simulation results, the tip speed ratio was identified as the main parameter that would be investigated in order to obtain an optimum turbine performance coefficient.

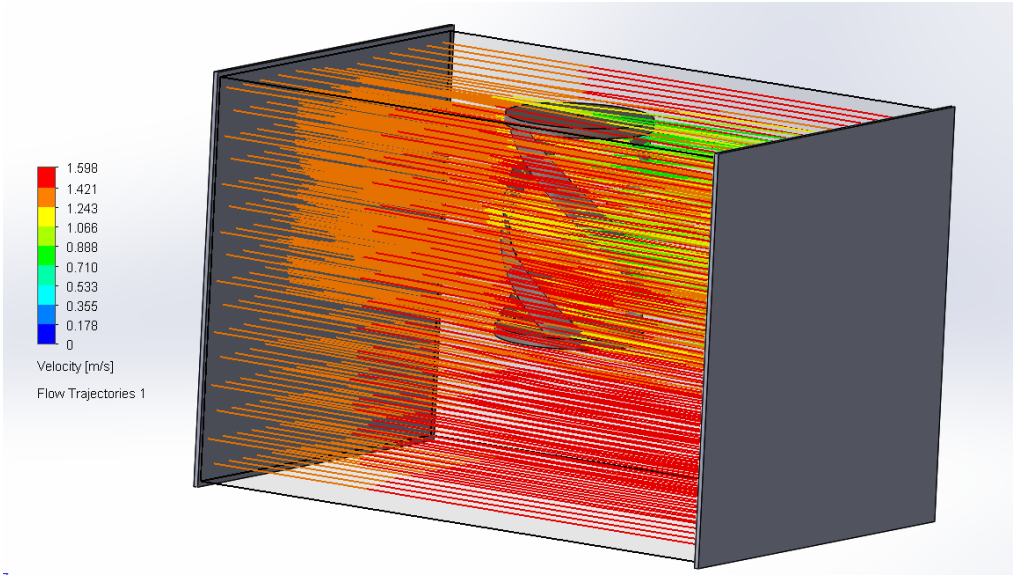

Figure 3.24: The simulation flow over the helical turbine

3.10.1 The Impact of the Tip Speed Ratio (TSR)

It has been established that the power generated by the turbine is a function of the torque and angular velocity. At low South African stream velocities, low angular velocities are anticipated thus a high torque is desired. Torque is a function of the relative velocity and the torque coefficient. To select an optimum TSR for the turbine, the relationship between the TSR and the relative velocity was evaluated. The torque coefficient is a function of the angle of attack, evaluating the relationship of the TSR and the angle of attack would assist is selecting an optimum TSR. Figures (3.25) and (3.26) illustrate the angle of attack and the relative velocity of the turbine as a function of the azimuth angle for different tip speed ratios.

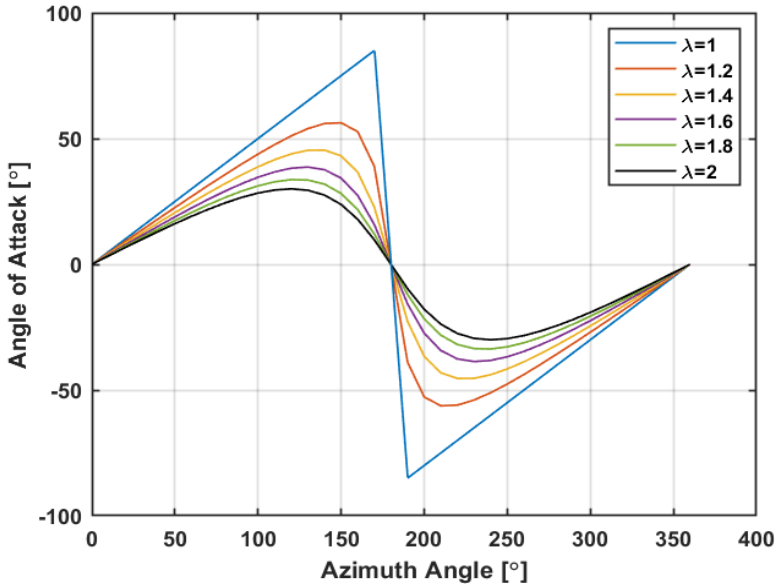

Figure 3.25: Angle of attack for various TSR's at a varying azimuth angle

As the TSR increases, the maximum angle of attack decreases. Low TSRs are then associated with larger ranges of the angle of attack at approximately $\pm 66.5°$. The large range of the angle of attack result in an increased drag force, this reduce*s the lift force that drives the turbine. From the figure below, it can be noted that an increase in TSR conversely increases the relative velocity.

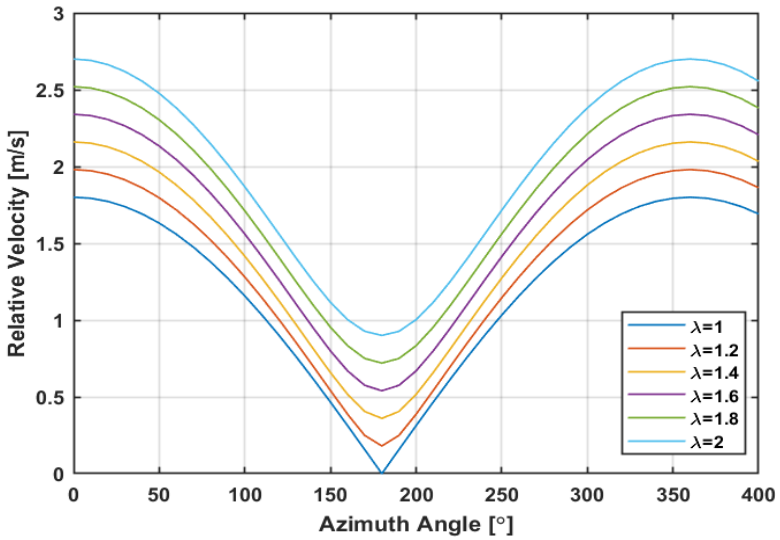

Figure 3.26: Relative velocity as a function of azimuth angles at varying TSR's

Based on the above results and the low stream velocities in South Africa a TSR of 2 was selected for the purpose of simulation and analysis of the designed turbine.

3.10.2 Turbine Performance

An experiment was conducted to verify the accuracy of the model developed. The turbine parameters given in table 3.4 were implemented in a computer simulation on MATLAB to determine the anticipated torque from the experimental results.

Table 3.4: Design turbine parameters

Number of Blades	3
Blade Type	NACA 0018
Solidity	0.3 m
Chord length	0.0348 m
Diameter	0.12 m
Radius	0.06m
Aspect Ratio	1.42
Height	0.17
Swept Area	0.0204
Angle of Inclination	43°
Pitch	0.17
Blade wrap	100%

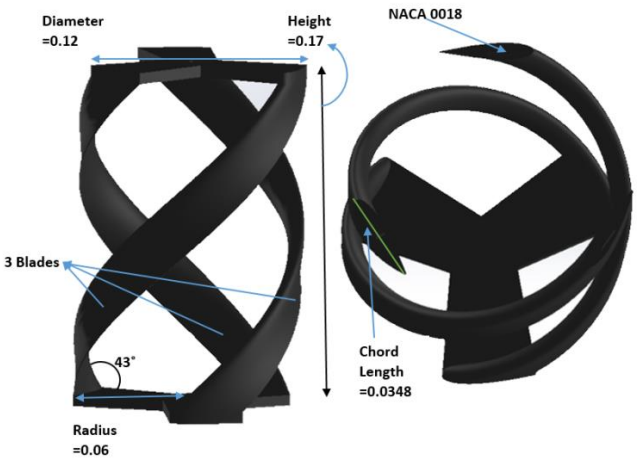

Figures (3.27) and (3.28) illustrate the torque generated by each turbine blade and the summation of the torque generated by each blade (turbine torque) as a function of the turbine azimuth angle, respectively.

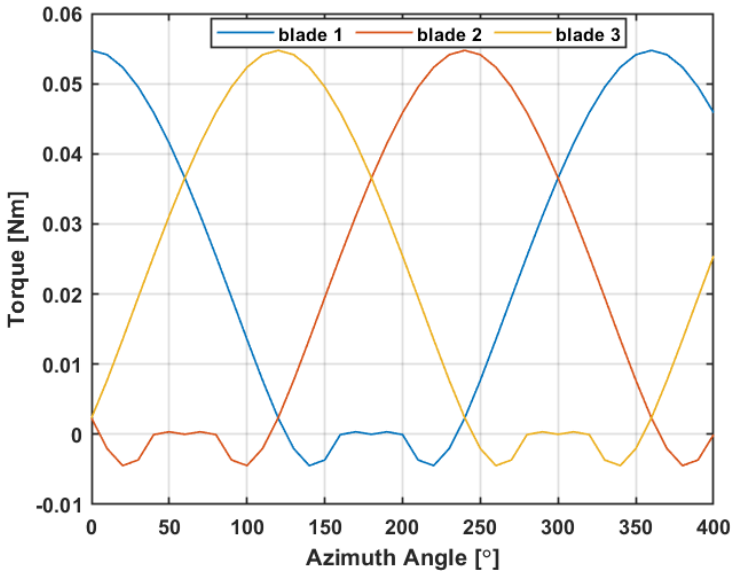

Figure 3.27: Blade torque as a function of the azimuth angle

The fluctuating angles of attack result in 'torque ripples' with the same frequency as the torque produced by each blade. Torque ripples consequently produce fluctuating electric power and the turbine vibration induced by the torque ripple can lead to mechanical failure. According to an experiment document in [97] the helical turbines tested, presented no vibration issues. High TSRs and an increase in the number of turbine blades significantly reduces the torque ripples [64, 98].

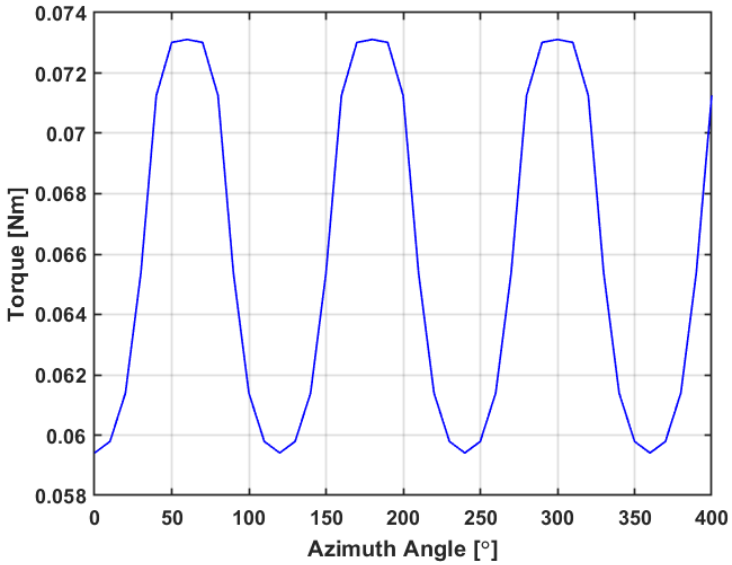

Figure 3.28: Turbine torque as a function of the azimuth angle

The above figure presents the overall torque developed on the turbine shaft. It can be noted that as the turbine reaches its maximum torque, it decreases gradually but it does not dip below zero. This is due to the type of hydrofoil selected. A dip below zero occurs when the chord is aligned with the stream flow resulting in only drag forces and zero lift, thus no power generated.

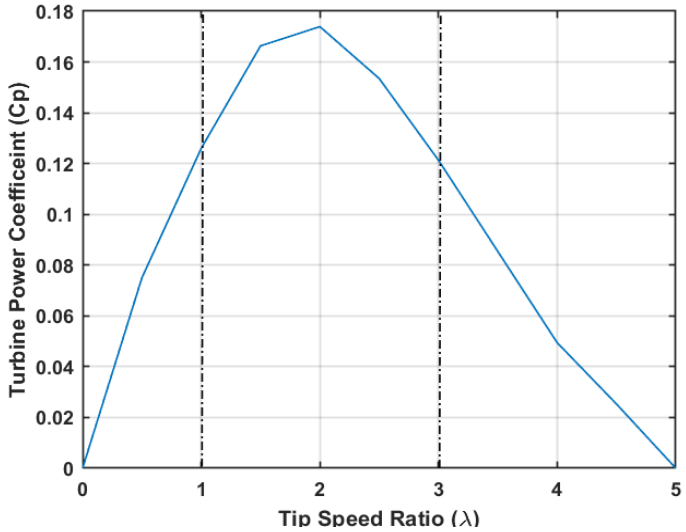

Figure 3.29: Turbine power coefficient as a function of TSR

Figure (3.29) depicts the performance coefficient of the helical turbine with respect to the TSR. The graph is divided into three regions, a dynamic stall region, an operation region, and a drag region. At low TSRs (<1), the turbine rotor spins too slowly and most of the stream passes through the void spaces of the turbine with little or no power generated. The turbine starts rotating and the rapid change in the angle of attack results in large dynamic forces exerted on the turbine, this region is called the dynamic stall region. The region where a maximum optimal (0.173925） TSR is achieved is known as the operation region. This region is between TSRs of 1 and 3 where maximum power generation can be obtained [99]. At high TSRs (>3), the rotor spins too fast, the blades blur and act as a solid wall to the stream, thus less or no power is generated, this region is referred to as the drag region.

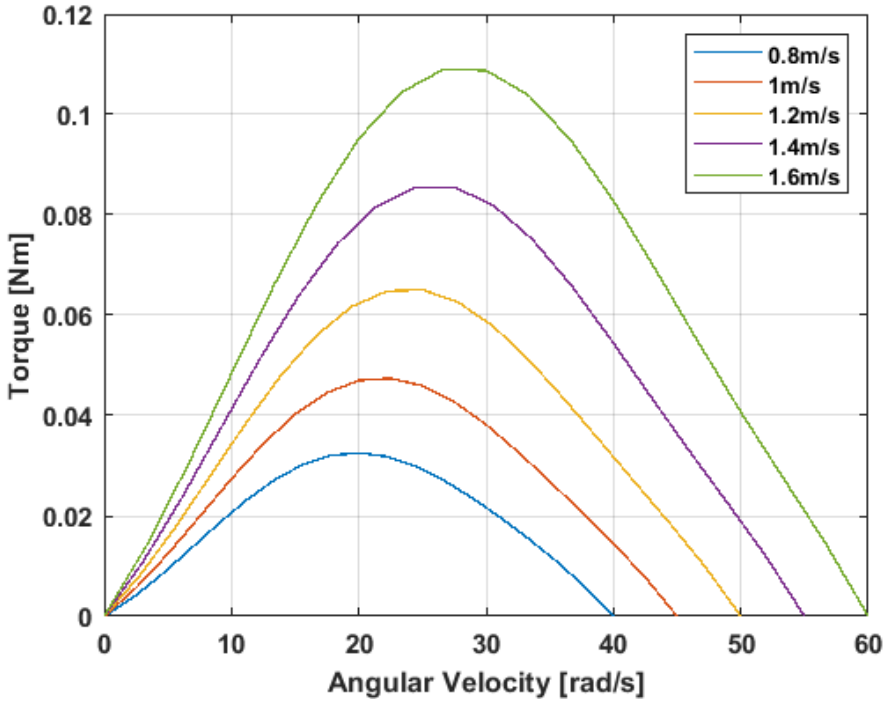

Figure 3.30: The torque-speed curve

The torque-rpm performance curve is illustrated in Figure (3.30), the performance curve was modelled as a function of the torque coefficient and the TSR described in section 3.8. At high stream velocities and low angular velocities, the values of torque developed on the turbine shaft are high and low, respectively. In both high and low stream velocities, as the angular velocity increases, maximum torque is developed at different rotational speeds. Beyond the point of maximum torque, the turbine rotates faster at velocities that are equal to or higher than the stream velocity. The torque slightly falls as minimum or no energy is being extracted by the turbine. The power generated can be evaluated from equation (3.61).

Chapter Four

Experimentation, Results, and Analysis of Results

4.1 General Remarks

The research results, experimentation and results analysis are presented in this chapter so as to validate the analytical model as discussed in chapter 3. The experiment was conducted in a concrete flume, in an indoor testing facility at the University of KwaZulu-Natal. For the experimentations, the testing set-up was done and the detailed explanation for the experimental set-up will be discussed in the next section. The experimental set-up was developed for testing the working of the helical turbine with the aim of highlighting critical issues such as performance, reliability, and efficiency relating to the use of a helical turbine for generating electrical power.

Also presented in this Chapter are results. These results comprise those from the analytical analysis which was implemented in the Matlab/Simulink environments. As explained in Chapter 3, a resource assessment was conducted and an optimum tidal site was identified. Hence, considering the tidal wave characteristics at Esikhawini (optimum site) and the energy conversion system selected in this study, a BEMT model was developed to conduct a performance analysis on the proposed tidal turbine.

The second set of results were obtained from the experimental study. These results were obtained on a single helical turbine configuration. Based on the outcomes of the experimentation, the analysis of a unit turbine configuration was carried out to determine its power output, performance, and efficiency. Considering the efficiency obtained from a unit turbine model, the concepts were then extended to develop the proposed power plant as an array of large-scale turbines (tidal farm). A Sankey diagram was used to illustrate the power conversion process which was used to determine the output power from the turbine, thereby estimating the electrical power that can be generated. Thus, consequently determines the efficiency of the system. Considering the output power of the large-scale unit, a tidal plant was proposed and the installation capacity of the plant was estimated. This proposed configuration was used to ascertain the possibility of the establishment of a tidal plant in South Africa. Finally, the costing of the proposed tidal plant was done in order to determine the cost/benefits of establishing such plants.

4.2 The Concept of the Experimentation

For this study, experimental studies were carried out to validate the model as developed in Chapter 3. To verify the accuracy of the model developed, an experimental model was designed. The helical turbine model was developed which is a newer form of tidal technologies conversion energy device. This device has numerous parameters that are interdependent and this makes its analysis very complex. A small scale model was developed and tested to establish the relationship between relevant design and performance parameters and the experimental set-up is shown in Figure (4.1).

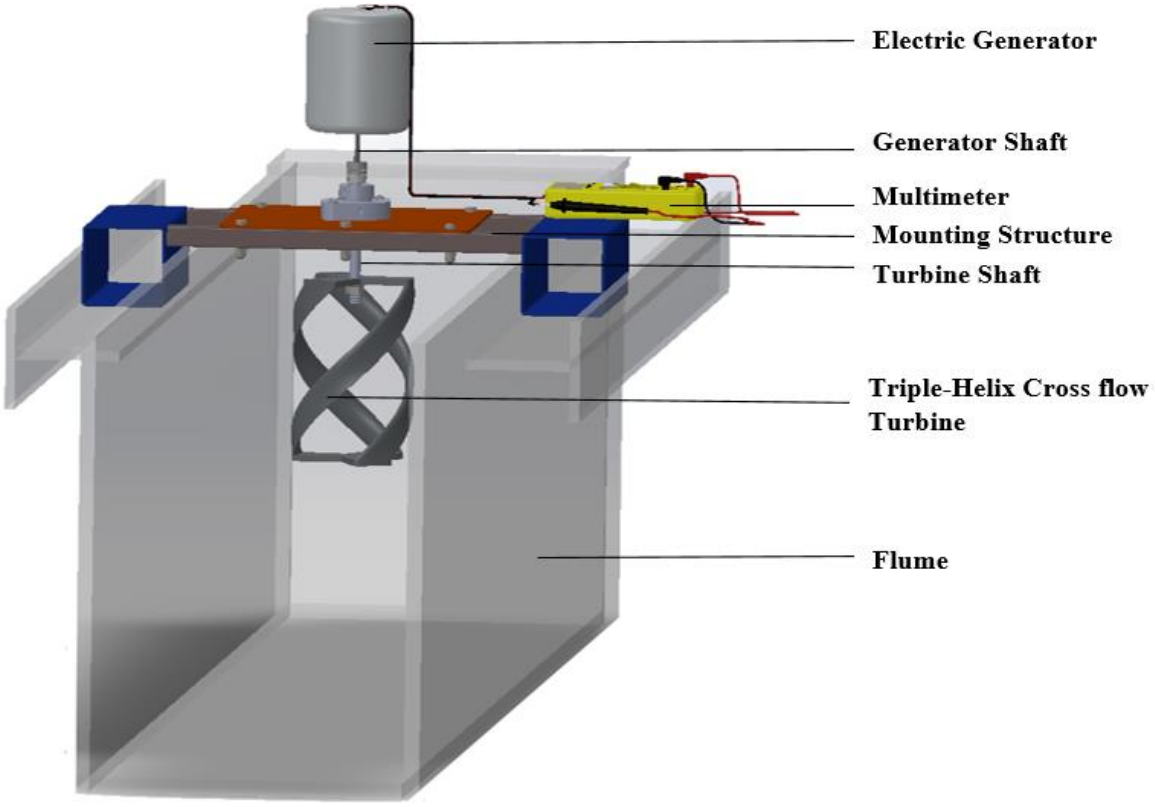

Figure 4.1: Diagram for the experimental set-up

Figure 4.1 illustrates the experimental set-p which comprises a turbine coupled to an electric generator and is mounted on a support structure. The structure is placed across a test flume, allowing the turbine to be deployed in the free stream of the test flume. The aim of this experiment was to conduct testing and analysis on the designed helical turbine in order to ascertain decisions and draw inference on the possible installation of a large-scale tidal power plant in South Africa. The experimental results obtained were used to draw firm conclusions on the following:

1. The amount of power generated from low stream velocities.
2. The performance results of the turbine were analogized to the simulation results to conclude on the accuracy of the analytical model.

3. The performance power coefficient.

4.2.1 Evaluation of Turbine Structural Set-up

Before experimentation is conducted, it is of great concern that the experimental arrangement of the turbine does not overturn when placed on the concrete flume as shown in Figure (4.1). To evaluate the structural integrity of this arrangement, an analytical model was developed and implemented by a graphical user interface (GUI) was developed in MATLAB as shown in Figure (4.2) to carry out this analysis. The mounting of the structure of the turbine is normally placed across the concrete flume. When the structure is mounted on the concrete flume, if it is relatively light in weight, there is a possibility that the experimental arrangement of turbine overturning when testing is being carried on the experimental model. The model developed on MATLAB normally considers the weight of the turbine and the mounting structure and the turbine area. The drag forces on the mounting structure were not considered as the structure was not extended in the stream flow. The tipping moment of the experimental model was evaluated at various stream velocities ranging between 0 – 4 m/s as illustrated in Figure (4.2).

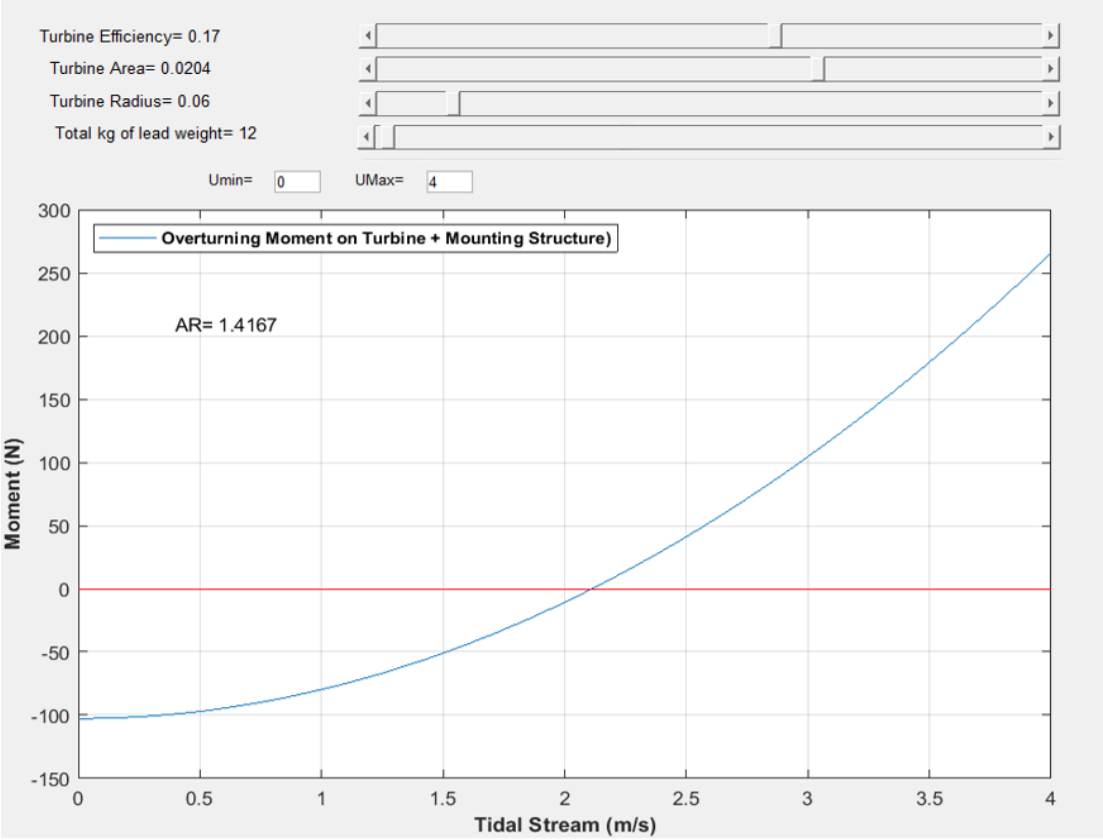

Figure 4.2: Tipping moment of the experimental model.

Negative values of the tipping movement indicate that the model will not overturn whereas positive values imply that the experimental set-up can tip over. From the above results, as shown in the diagram, for this experimental configuration to be mounted on the structure of the contrite flume has a weight below 12 kg and this would tip over at the steam velocities above 2.1 m/s as indicated in the diagram. Hence, considering the stream flow velocity of 1.4 m/s which is equivalent to that estimated at Esikhawini would not tip over. This evaluation serves as the pivotal point in designing the prototype as used in the experiment and a description of the porotype is done in the next section.

4.3 Description of the Prototype Design

For the experimentation, a prototype was developed and then manufactured to carry out the laboratory experiments. This prototype of the helical turbine comprises the following components:

The Helical Blade: The helical blades as shown in Figure (4.3) was developed on the SOLIDWORKS software. It consists of three blades that are 120˚ apart, the spacing consistency was achieved through a 'circular pattern' function. The blades follow a helix path and were produced by the NACA 0018 hydrofoil profile with a chord length of 0.0348m, the data for this hydrofoil profile is presented in Appendix A. The turbine blades are supported by strut arms that are 10mm thick with a 0.06m radius. The strut arms consist of a 6mm hole at the centre which enables a turbine shaft to be extended through the turbine blades.

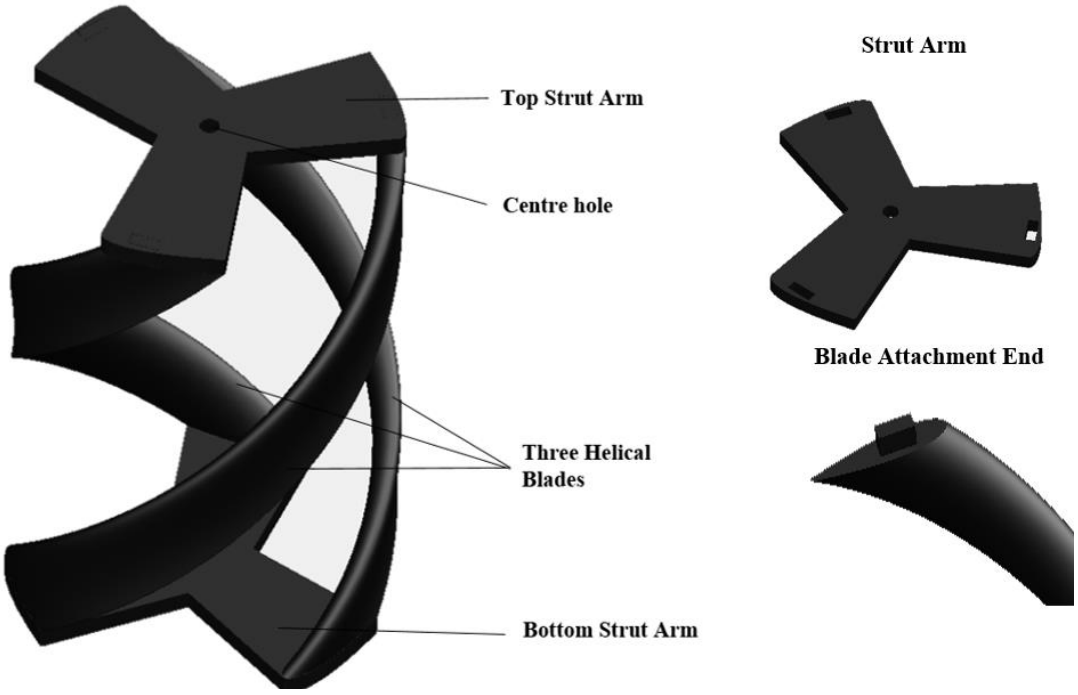

Figure 4.3: The helical turbine blades and strut arm

The lift and drag forces acting on the circular plate blade support were simulated in SOLIDWORKS software and the simulation results are illustrated in Figure (4.4). The rotor blade support was selected based on the assumption that drag forces will be minimized due to the reduction in the surface area. For now, there are no bases to ascertain the effect of the support structure of the turbine blades (strut arms or circular plate) on the helical turbine performance.

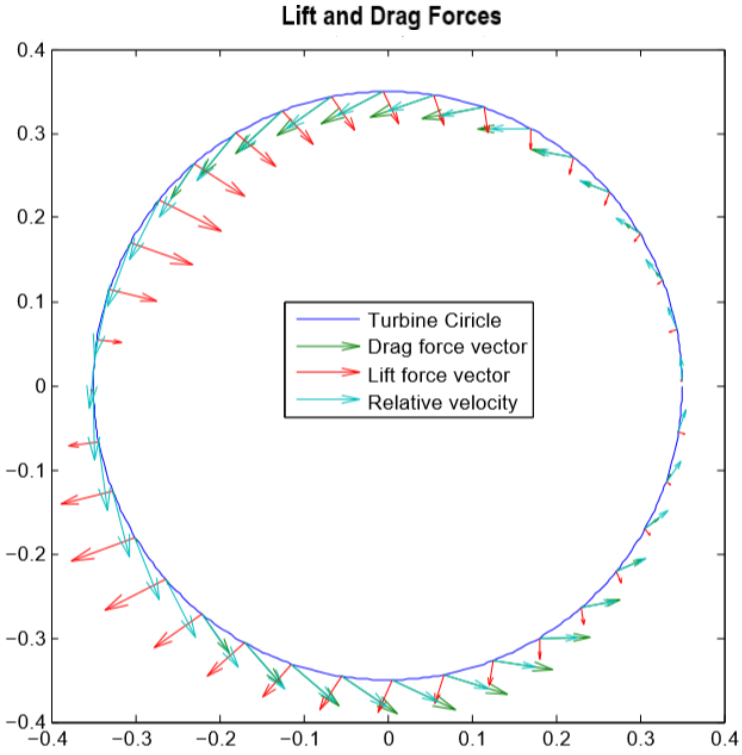

Figure 4.4: Turbine lift and drag forces

The material used in the manufacture of the helical turbine is thermoplastic. The thermoplastic was heated to a certain temperature which allows it to be molded into the desired shape or size and this heating process was done with the 3D printer to produce the turbine as shown in Figure (4.5). There various type of thermoplastic, but the thermoplastic used to produce this helical turbine is the Acrylonitrile Butadiene Styrene (ABS), the properties for this material used to produce the prototype is presented in Appendix B. The material has the advantage of having high tensile strength with a very high stiffness that can make it withstand a high hydrodynamic force when places in the stream flow channel. To manufacture this prototype, the turbine model was developed on the SOLIDWORKS and was converted into STL file format. This file was then exported to be read and printed using the 3D printer, the printed helical turbine is shown in Figure (4.5).

Figure 4.5: The 3D printed helical turbine

The Turbine Shaft: As the water passes the blades causes the turbine blade to rotate, the power extracted by the turbine blades is transferred to the turbine shaft. The shaft is normally held in place by two flange shaft couplers which are connected to each end of the turbine to ensure that the turbine and the shaft rotate as one unit during the conversion of power from kinetic to rotational motion. The effect of the centre shaft configuration was investigated as documented in [58], where three different turbine shaft configurations were tested. As investigated, turbine 1 had no shaft passing through the turbine but attach at both ends of the turbine. Turbine 2 was designed with a shaft with a diameter of 6.4 mm which passes through the turbine. Turbine 3 was also similar to turbine 2 but with a different shaft diameter of 12.7 mm. Based on the experiments conducted on these three difference turbine, the performance curve of all three turbines were almost the same but turbine 1 was unstable during operation. For this study, a 6 mm stainless steel shaft was used as the central shaft which extends centrally through the turbine blades as illustrated in Figure (4.6).

Figure 4.6: The turbine shaft configuration

4.4 Experimental Set-up: Description of Concrete Flume

The experiments for this study were conducted in an indoor testing laboratory. This indoor laboratory is situated at the University of KwaZulu-Natal, Howard College Campus. This laboratory is situated in the Civil Engineering department with a concrete flume as shown in Figure (4.7) was used to conduct the experiment. The rectangular-shaped flume is 26m long, 1.6m wide with a depth of 0.75m. The stream of water in the concrete flume is pumped by a centrifugal pump from a water sump, the water flows through the concrete flume and back to the water sump.The water depth of the flume can be varied for the purpose of testing the turbine at different stream velocities. To determine the stream velocity; a floating obeject was placed on the upstream of the flume and the time taken by the object to travel from upstream to downstream was recorded. This process was repeated ten times to improve its accuracy. From the ten samples, at each depth, the meantime was calculated. With the distance covered and the time calculated, the stream velocity was determined. Table 4.1 presents the flow velocities for various water depths and based on calculations, it was observed that the water velocity increased relative to the water depth as documented in table 4.1. This observation was very important because vary the depth, the required speed can arrive at such 1.2 m/s required for Esikhawini the site chosen for this study.

Table 4.1: Flow velocity data

Depth (m)	Velocity (m/s)
0.05	0.73
0.10	0.78
0.15	0.83
0.20	0.89
0.25	0.97
0.30	1.06
0.35	1.16
0.40	1.29
0.45	1.45
0.50	1.52

Figure 4.7: The concrete flume span layout

4.5 The Experimentation

The helical turbine was tested at varying angles of attack and the various water velocities used for the experimentation are provided in table 4.1. A 0.7 m long central shaft attached to the rotor blades was connected to the mounting structure through an upper and lower plate. Two ball bearings were mounted on the upper and lower plates of the structure to minimize vibrations and allow the rotation of the turbine. The central shaft was coupled directly through a rigid coupler to an electric generator which is a 24V DC permanent magnet motor, for specifications for this generator used refer to Appendix B. The generator was used to

convert the mechanical power in the rotating shaft into electrical power. A multimeter was used to measure the output voltage and current of the generator. The generator was installed on top of the mounting structure to eliminate any dead weight that may be introduced by the generator. The mounting structure did not extend into the flume to eliminate structural turbulence; the structure was placed across the test flume concrete wall for deploying the turbine as illustrated in Figure (4.8).

Figure 4.8: The experimental set-up

To obtain the torque-speed curve the torque coefficient was varied and this was achieved by varying the azimuth angle of the turbine blade, hence for the varying angles of attack, refer to

Figure (4.9). The TSR of the turbine was varied by varying the water velocity. A tachometer and a digital torque meter were used to measure the angular velocity and the torque developed by the turbine shaft. The measured torque and angular velocity were used to evaluate the amount of power generated by the turbine.

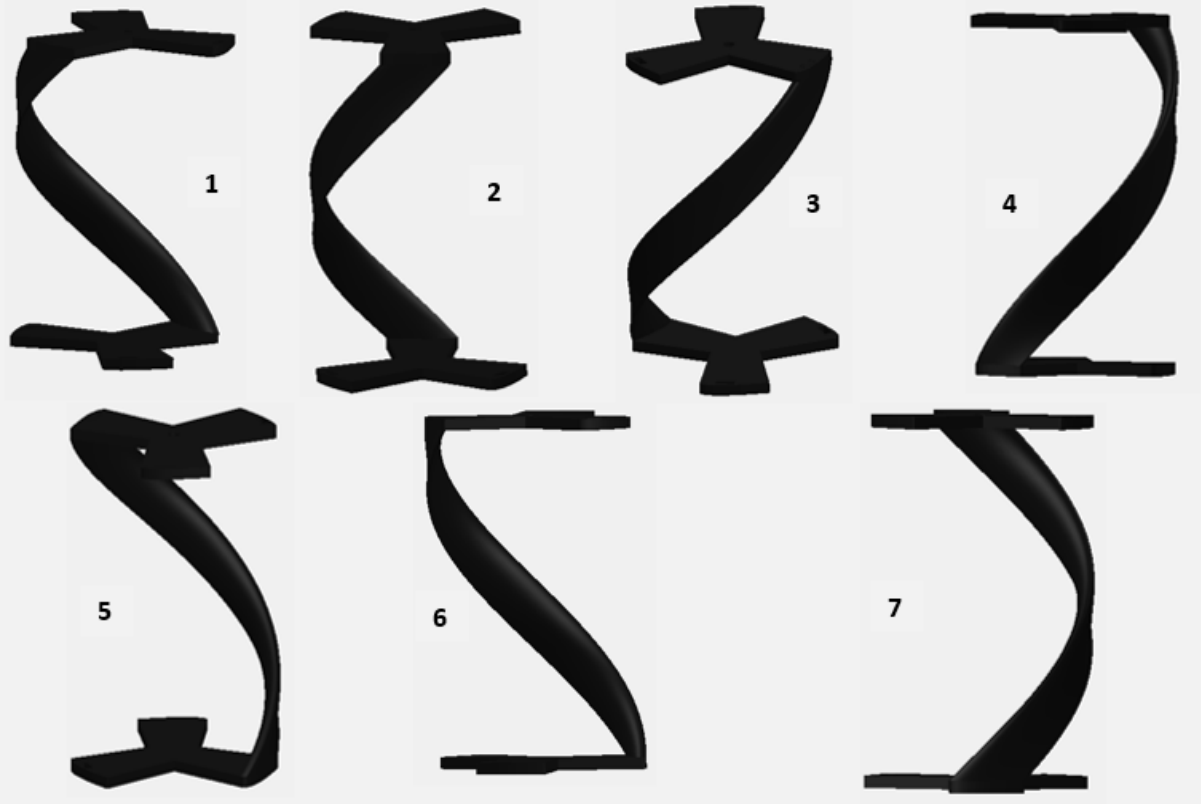

Figure 4.9: Turbine azimuth angles

4.6 Experimental Results and Analysis

As discussed earlier, in the indoor Concrete Flume, a series of tests were carried out to validate results from the analytical modelling. The laboratory experiments conducted on the helical turbine have provided useful data in determining the hydrodynamic properties, performance characteristics, and reliability. A series of dynamic tests were carried out to try and reproduce the phenomenon of fluid dynamics of this turbine which can be compared to real-world scenarios. During the experiments, when the helical turbine was deployed into the flow velocities below 0.8 m/s there was no torque developed on the turbine shaft, thus no power was generated. At a flow velocity of 0.89 m/s, the turbine ramped up from 0 to a maximum recorded rotational speed of 166 rpm. From the above observation, 0.89 m/s was said to be the cut-in speed of the designed turbine. In the experiments various speeds of 0.89 m/s, 1.06 m/s, 1.29 m/s and 1.52 m/s were used. The torque, angular velocity data measure,

and the power calculated from the measured data for the various flow speeds are given in table 4.2.

Table 4.2: Experimental results for angular speed, torque, and power for different speeds.

	0.89 m/s			**1.06 m/s**		
	Angular Velocity (rpm)	**Torque (Nm)**	**Power (W)**	**Angular Velocity (rpm)**	**Torque (Nm)**	**Power (W)**
1	2.59	0.009	0.02	2.94	0.008	0.02
2	5.19	0.15	0.08	4.83	0.012	0.06
3	8.89	0.023	0.21	7.94	0.029	0.23
4	12.59	0.029	0.37	12.68	0.04	0.51
5	17.42	0.036	0.62	23.47	0.047	1.10
6	21.12	0.029	0.61	28.19	0.032	0.90
7	24.83	0.027	0.67	31.67	0.030	0.95
8	28.53	0.024	0.68	35.25	0.027	0.95
9	31.13	0.019	0.59	37.64	0.021	0.79
10	33.69	0.015	0.51	42	0.015	0.63
	1.29 m/s			**1.52 m/s**		
	Angular Velocity (rpm)	**Torque (Nm)**	**Power (W)**	**Angular Velocity (rpm)**	**Torque (Nm)**	**Power (W)**
1	6.81	0.018	0.12	6.12	0.024	0.15
2	9.72	0.033	0.32	9.58	0.043	0.41
3	12.50	0.043	0.54	12.78	0.059	0.75
4	15.28	0.052	0.79	19.15	0.085	1.63
5	22.22	0.063	1.39	28.75	0.097	2.78
6	29.17	0.060	1.75	31.95	0.093	2.97
7	34.72	0.047	1.63	36.85	0.079	2.91
8	40.28	0.031	1.25	41.53	0.062	2.57
9	43.05	0.023	0.99	44.72	0.049	2.19
10	45.83	0.014	0.64	51.11	0.025	1.28

4.6.1 Torque and Power Curve

From the experimental results presented in table 4.2, these experimental results and the results obtained from the BEMT model were compared as shown in Figures (4.10a) to (4.10d). These figures presented indicate that the value of the turbine torque is a function of both the shaft angular velocity and the flow velocities. Thus, high torque values were

recorded at high velocity. Based on these comparisons, with a high degree of agreement, both results can be used to draw conclusions on the performance of the turbine designed.

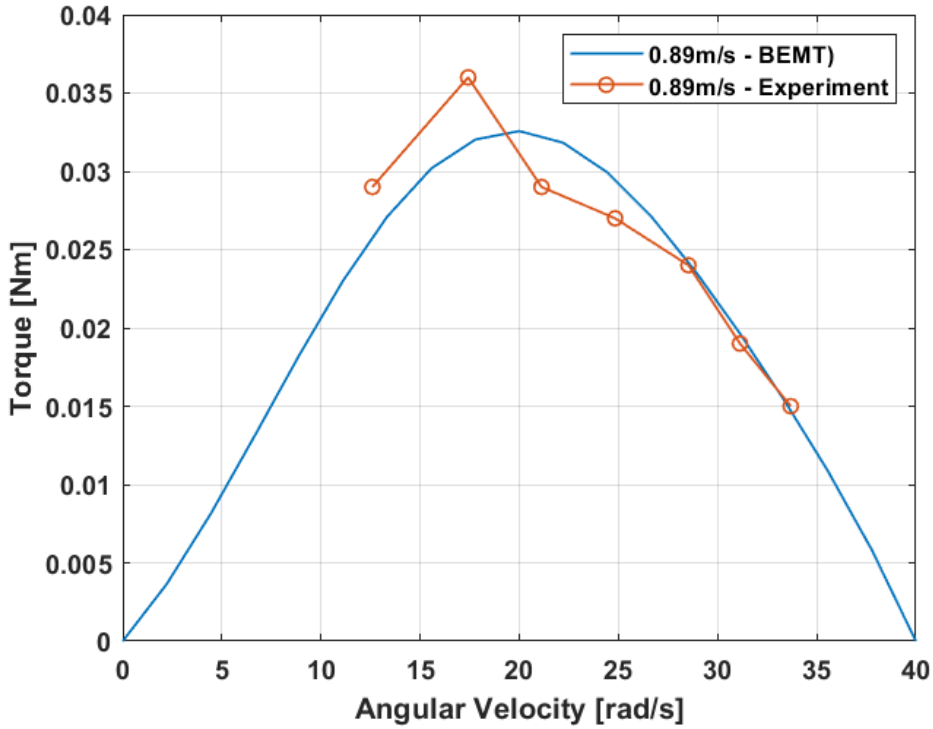

Figure 4.10.a: Turbine torque at 0.89 m/s stream velocity

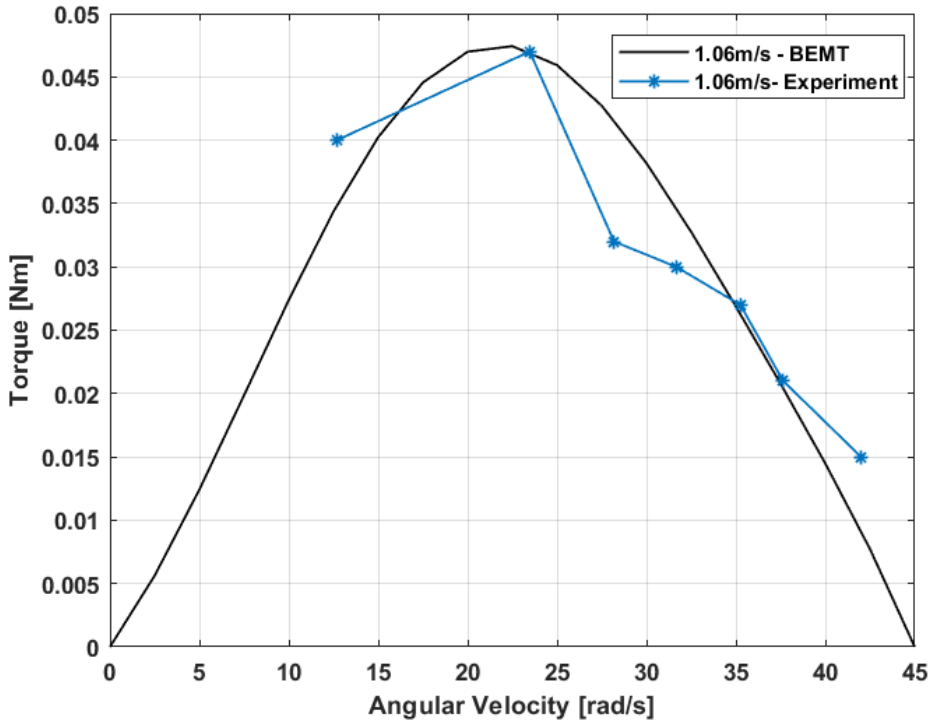

Figure 4.10.b: Turbine torque at 1.06 m/s stream velocity

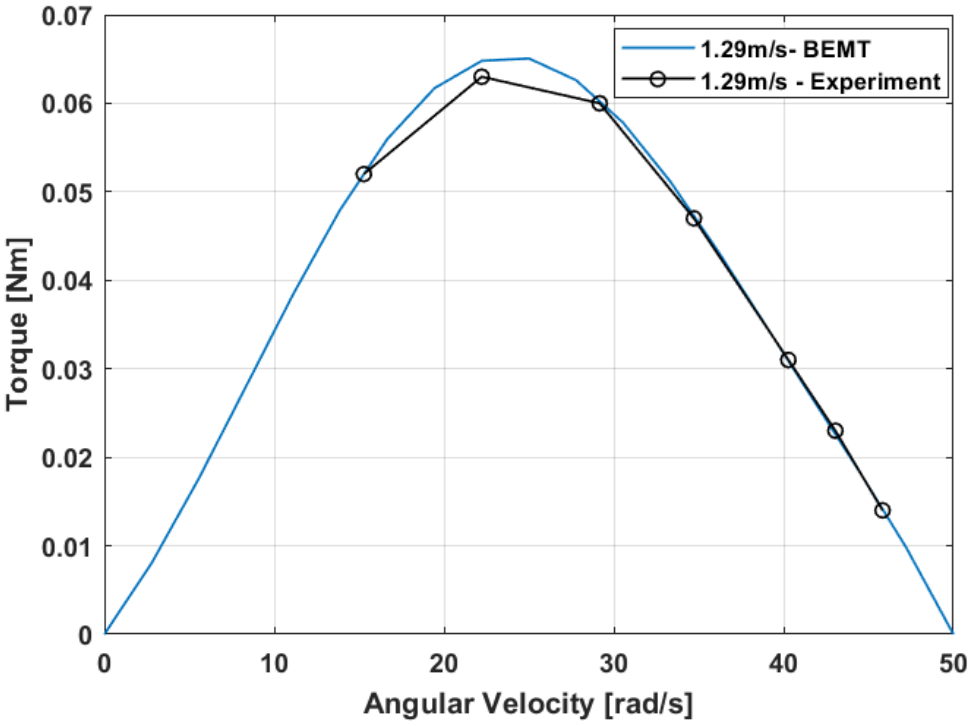

Figure 4.10.c: Turbine torque at 1.29 m/s stream velocity

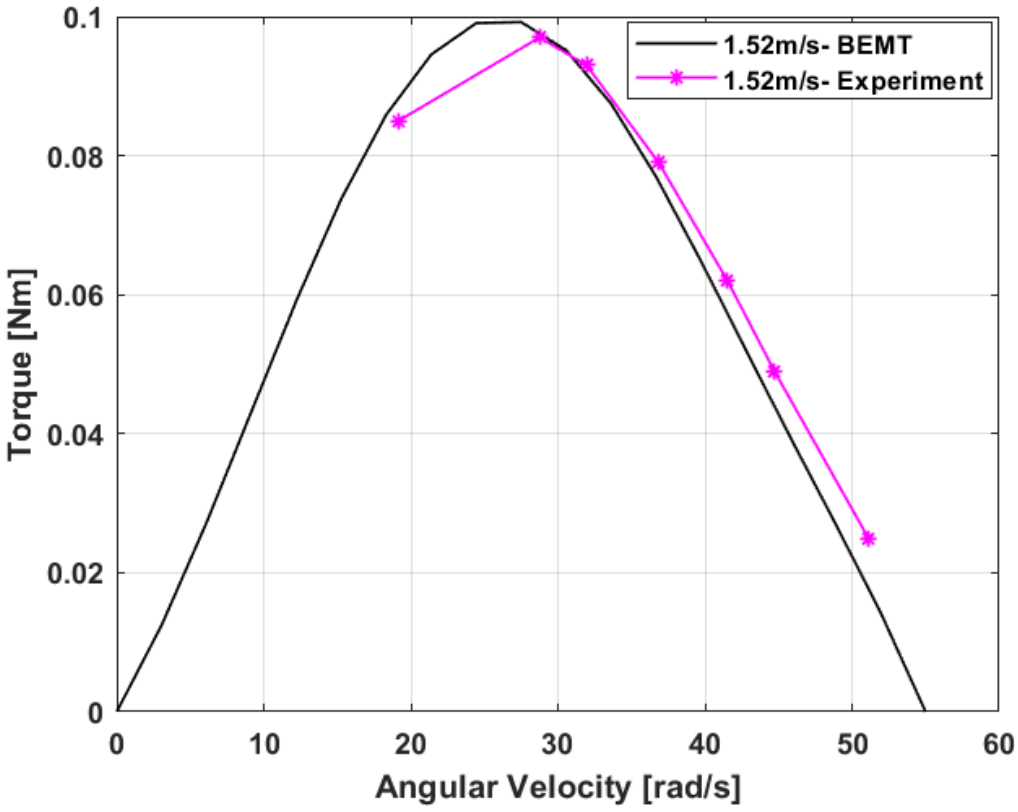

Figure 4.10.d: Turbine torque at 1.52 m/s stream velocity

In a similar manner, using the same results as tabulated in table 4.2, the comparison between the experimental results and the results from the BEMT were compared. Figure (4.11a) to figure (4.11d) was used to present the comparison.

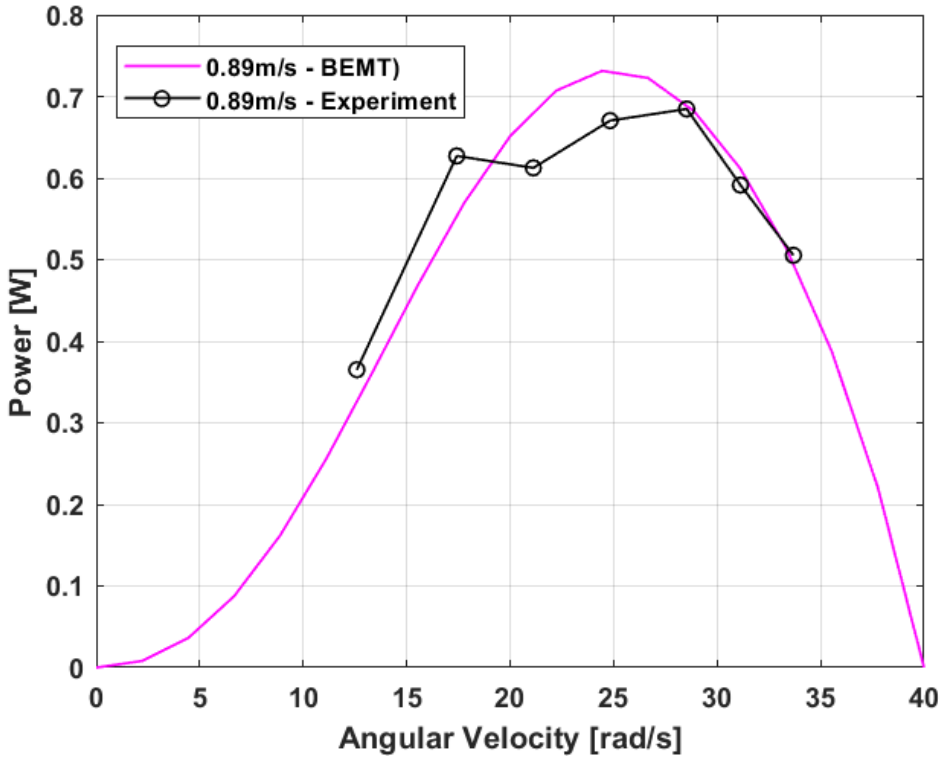

Figure 4.11.a: Turbine power at 0.89 m/s stream velocity

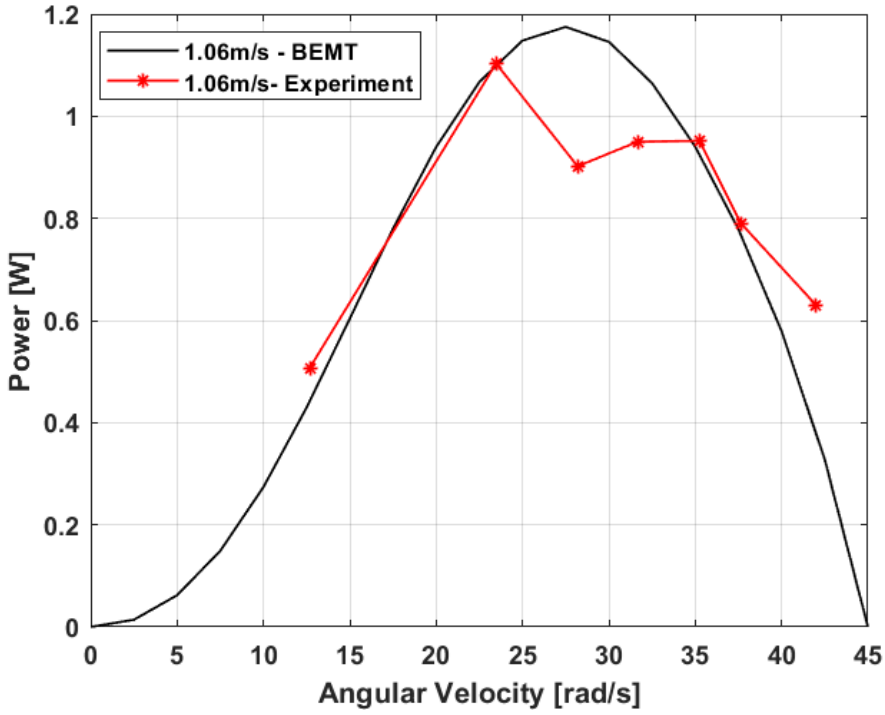

Figure 4.11.b: Turbine power at 1.06 m/s stream velocity

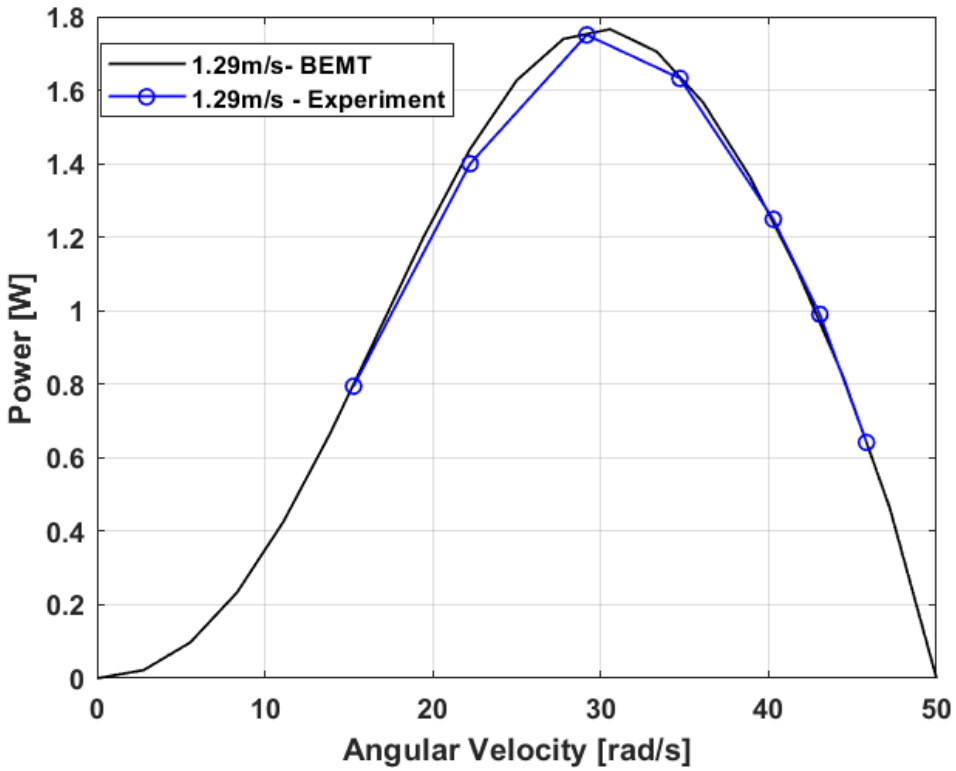

Figure 4.11.c: Turbine power at 1.52 m/s stream velocity

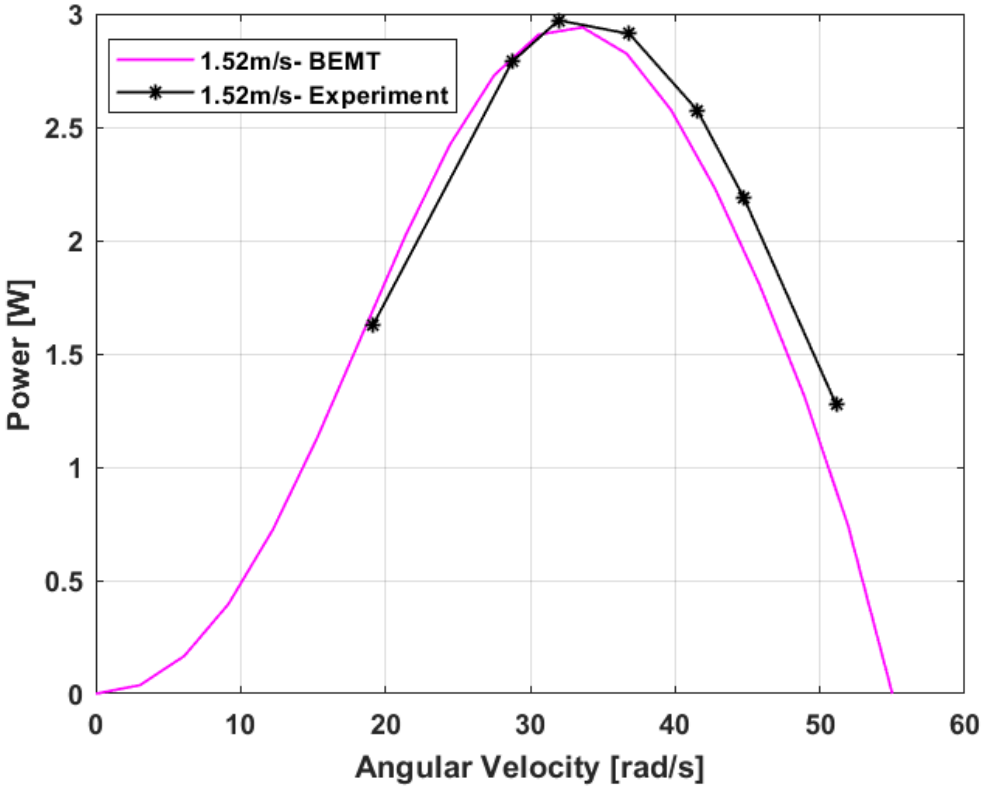

Figure 4.11.d: Turbine power at 1.52 m/s stream velocity

As observed from the figures presented in Figures (4.10) and Figures (4.11), the general trend of both torque and power curves follow the actual performance curves of the turbine with slight deviations. The maximum power of the designed turbine was obtained at a flow velocity of 1.5 m/s which is expected as the power generated is a function of the cube of the velocity. This velocity is higher than what is experienced in South Africa, the turbine performance curve was then estimated using the experimental data obtained at a flow velocity of 1.29 m/s.

4.6.2 Turbine Coefficient Curve

The simulated turbine power coefficient results were compared to the results obtained from the experimental results which were approximated using equation (3.63). As shown in Figure (4.1), there is a significant deviation in the results presented; the simulation model under-predicted the turbine coefficient with the maximum coefficient of 0.17 at a TSR of 2. The actual turbine maximum coefficient obtained was 0.21 at a TSR of 1.3. The accuracy of the simulated power coefficient curve suffers due simplifications of the model developed, however, the trend was useful in understanding the performance of the turbine. The deviation in results may be attributed to the unknown torque coefficient as the turbine blade azimuth angles were not measured. Another contributing factor could be due to the lift and drag forces which are both functions of the angle of attack. As expressed in equation (3.56), the angle of attack is a function of the turbine blade azimuth angle.

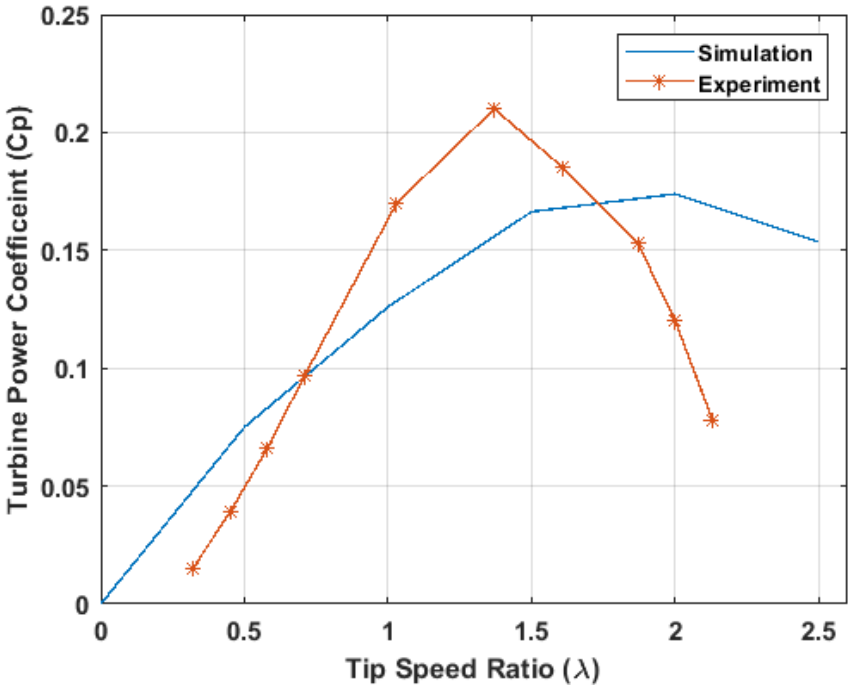

Figure 4.12: Turbine torque and power as a function of TSR and flow Velocity

It can be concluded that for a large-scale model, the BEMT model developed in Chapter 3 can be used to estimate the torque developed on the shaft but the maximum turbine coefficient was assumed to be 0.21 or 21%.

4.7Analysis of a Unit Turbine Configuration

To analyze a tidal power plant, it is imperative to firstly analyze a unit power plant as shown in Figure (4.13), consisting of a unit turbine be extending it the multiple unit plant modules. With the turbine power coefficient obtained from the experiment, the output power for this turbine can be estimated. Considering the possible establishment of a tidal plant, the analyses of a unit tidal plant can be used to develop an operation curve that can be extended any number of turbines employed in a large-scale turbine. This necessary to determine the expected power from any number of turbines the helping in determining the size, performance, and the expected power output.

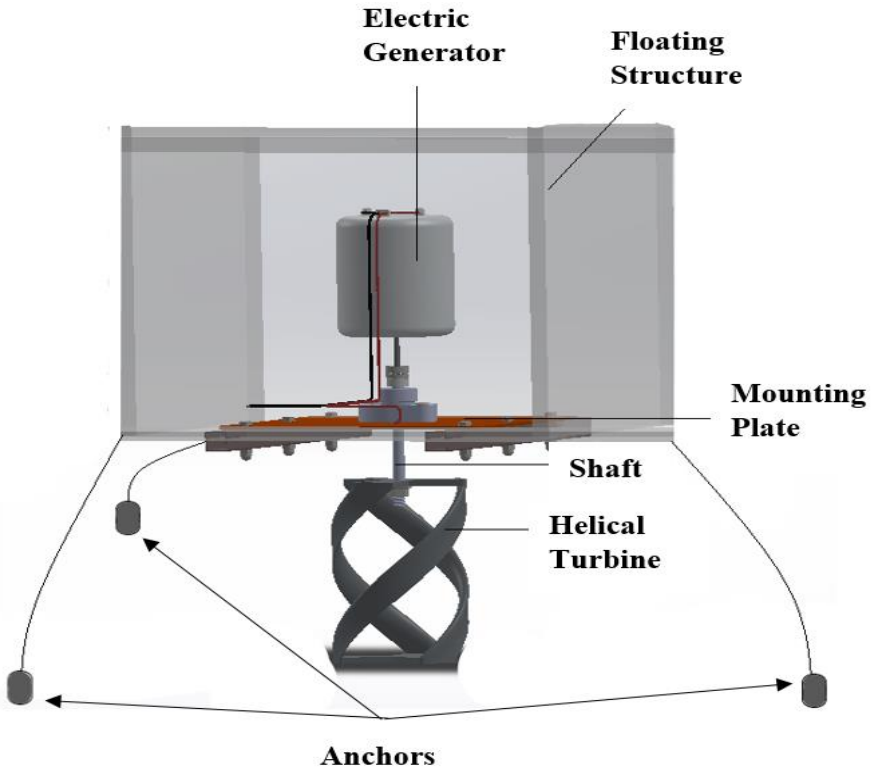

Figure 4.13: The configuration for a unit tidal power plant

Based on the results obtained from numerous experimental results, which serves as inputs variables, a model was developed on the MATLAB environment to evaluate the output power of the unit plant, this model considered the stream velocity at Esikhawini, the power coefficient obtained in the preceding section and the large scale parameters given in table 4.3.The ocean water density was taken as $1025\,kg/m^3$.

Table 4.3 Input Parameters

Radius (r)	3.9 m	Chord length (c)	1.8
Height (h)	10.9 m	Cut in speed (V_{ci})	0.8 m/s
Tip Speed Ratio (λ)	1.3	Rated speed (V_R)	1.4 m/s
Relative velocity (V_{rel})	0.2 m/s	Furling speed (V_f)	3 m/s

The model estimated an out power of 25.1kW as illustrated in Figure (4.14), this is approximately equal to that evaluated by calculation from equation (3.15), thereby verifying the validity of the model. The results presented in the figure show the amount of power available from the free stream at Esikhawini and the actual amount of power extracted by the tidal turbine.

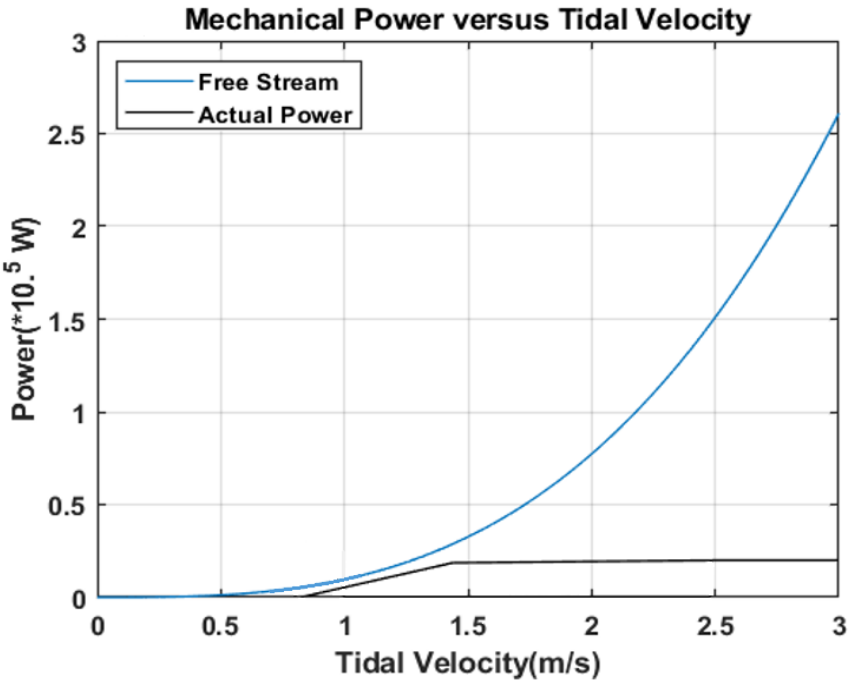

Figure 4.14: Power generated relation from a unit tidal plant

If each turbine is be coupled to an electrical generator with a total efficiency of 0.95. The total electrical power generated from the unit is:

Electrical Power = Mechanical Power × Generator efficiency

$= (25.1kW) \times (0.95)$

$= 23.75kW$

4.7.1 Power Flow Analysis

For the analysis for the unit turbine configuration as shown in Figure (4.13), the then possible to carry out a power flow analysis from the power input at the turbine blade to the output that

is finally converted into electricity. Therefore, the system efficiency of the unit plant as described in the preceding section can be evaluated with an aid of the Sankey diagram as shown in Figure (4.15). The diagram describes the power flow in the system as well as the losses experienced. Generally, the efficiency of a power plant is defined as the ratio of the output power to the input power into the turbine as defined by equation (4.1).

$$Efficiency = \frac{P_{out}}{P_{in}} \tag{4.1}$$

Theoretically, according to the Albert Betz equation, the maximum obtainable turbine efficiency is 59.3 %. The total input power $\left(P_{Str} = \frac{1}{2}\rho AV^3\right)$ of the system is the extractable power from the free tidal stream of 1.4 m/s with a 7.8 m turbine diameter. The total mechanical power $\left(P_T = \frac{1}{2}C_p\rho AV^3\right)$ generated by the turbine is given by the product of the system input power and the turbine efficiency. 79% of the input power was lost due to design limitations and hydrodynamic losses.

Considering the coupling and electric generator efficiency as given in equations (4.2) and (4.3), respectively.

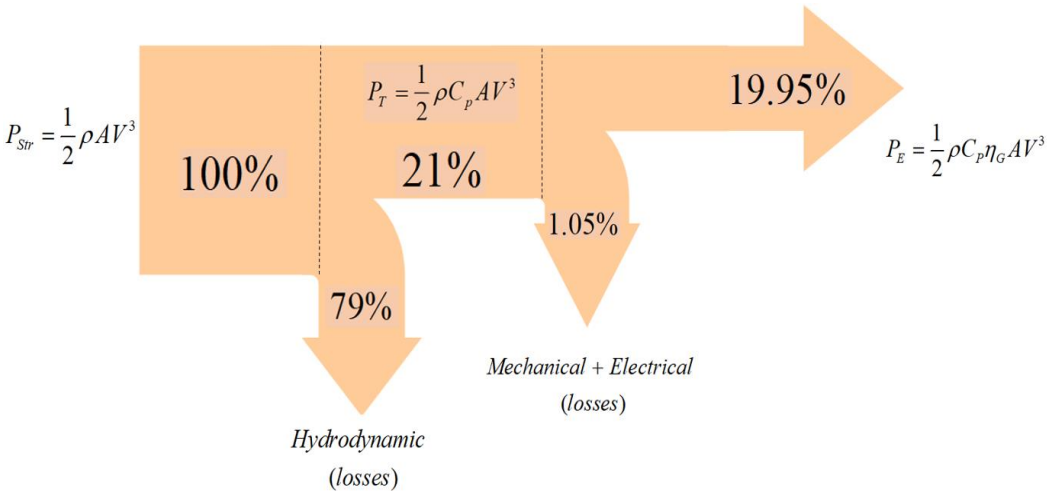

Figure 4.15: Power flow for a unit tidal plant

$$p_s = \frac{P_{shf}}{P_T} \tag{4.2}$$

$$\eta_G = \frac{P_E}{P_{shf}} \tag{4.3}$$

Considering the design and performance parameters of a triple helix turbine as used in this study, an efficiency of 21 % was obtained

Thus, the overall efficiency can be evaluated using equation (4.4).

$$eff = Cp.p_s.\eta_G = \frac{P_{shf}}{P_T} \times \frac{P_T}{P_{Str}} \times \frac{P_E}{P_{shf}} = \frac{P_E}{P_{Str}} \quad (4.4)$$

Thus, the total electrical power $\left(P = \frac{1}{2}\eta_G C_p \rho A V^3 \right)$ generated amounts to 19.95% of the input power which describes the overall efficiency of the system.

4.7.2 Explanation of Tidal Plant Components

For the analysis of the unit tidal plant as discussed, the next step to explain the various components required for the transfer of power from the point of input to where it finally converted to electrical power. Tidal plant components include; tidal turbines, electrical generators, power converters, and system controllers. The basic building block for the tidal plant illustrating from input power to its integration into the national grid is shown in Figure (4.16). The diagram shows a tidal turbine that converts the kinetic energy of tides into mechanical power. The mechanical output power of the turbine developed on the turbine shaft is transferred to the electric generator through the mechanical coupler.

For the helical turbine, its performance is of concern with regards to the grid integration which includes low starting torque, torque oscillations during operation, and off-axis flows. Based on the experiment conducted in this study, the helical turbine demonstrated a good self-starting capability and high starting torque. The operation of the turbine is independent of the direction of the stream, it can also operate at high speeds, and thus, it has high peak efficiency. Generally, the peak operating efficiency of generators is often much higher than that of the tidal turbine which makes torque-speed matching difficult. Hence, the high peak efficiency with the high turbine operation speeds of the helical turbine provides greater compatibility with the electric generators. The rigid mechanical coupler is used to couple the turbine shaft to the electric generator directly. This direct-drive system eliminates the gearbox between the turbine and electric generator, thus reducing maintenance costs and power losses. The mechanical power transferred to the electric generator shaft is converted into electrical power through electromagnetic induction. The 3-phase ac power generated by the turbine is rectified into dc and later converted into ac for grid integration. The success of grid integration is determined by the selection and characterization of system components. This requires a consideration of system components compatibility to meet the requirements of installation and integration. The type of generator suitable for the proposed tidal plant is a permanent magnet synchronous generator. This generator is very efficient it allows for a

direct-drive. For grid integration, a back-to-back converter would be suitable instead of an automatic voltage regulator. A PWM rectifier is placed between the generator and the dc link, and a PWM inverter is connected to the grid. The back-to-back converter regulates the maximum power flow that is finally introduced into the power grid.

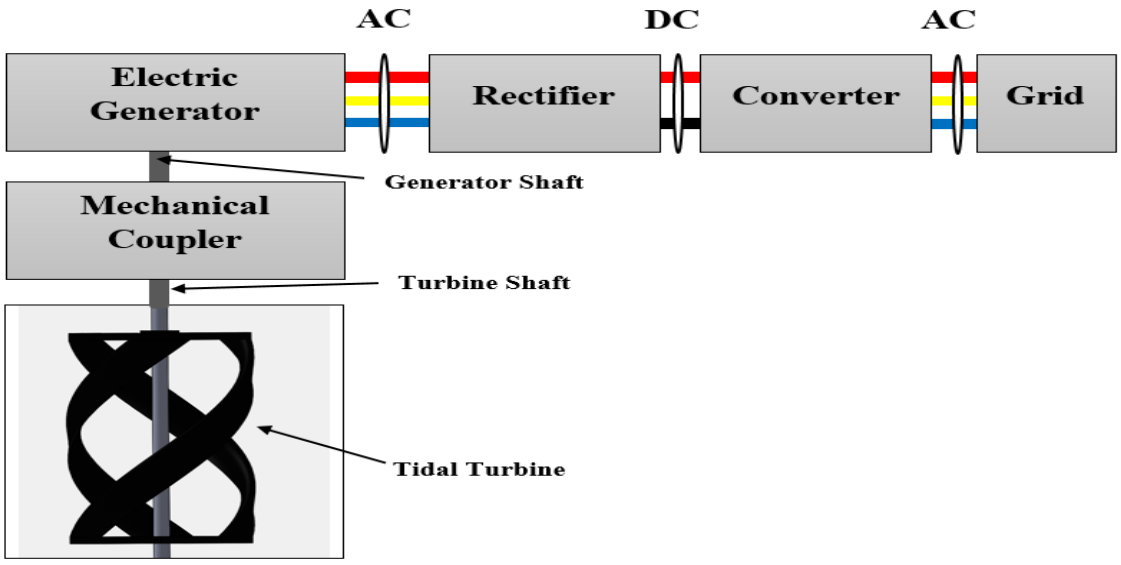

Figure 4.16: The block diagram illustrating the various components of a tidal plant

4.8 Proposed Tidal Power Plant

To achieve the main reason for embarking on this study, a conceptualized tidal power plant was proposed that can be established in South Africa was discussed in this section. Firstly, before going into the discussion of the proposed tidal power, it is necessary to know the factors that can influence the siting of a tidal plant. Before siting a potential tidal power plant, generally, some standards should be met which will then identify the sites that are suitable for the development of tidal energy extraction. The most important variables generally considered are:

1. The local water depth.
2. The nearness to the existing power grid.
3. The environmental impact.
4. Energetic, constant, and persistent resource such as the peak stream velocity

If these factors are met, a site is considered to have solid potential for the development of a tidal power plant. The majority of coastal locations can be rejected by consideration of these factors, but the sites that the developers are interested to extract energy tend to have high peak spring tidal velocities.

The Agulhas Currents which flow along the eastern coast of South Africa with a surface velocity of 2 m/s is the world's second-fastest stream velocity after the Gulf Stream which has

a stream velocity of 2.4 m/s. Innumerable studies have been conducted on establishing a tidal farm in the Gulf stream but there is limited or no literature on exploiting the enormous amount of energy available from the Agulhas currents in South Africa. In this study, the tidal farm which is made up of a number of turbine-generator modules was proposed for estimating the tidal plant capacity that is situated at Esikhawini, along the eastern coast of South Africa. Most importantly, when designing and developing a tidal power plant, special consideration should include minimising the potential effect of siting the plant will have on the environment. The essential parameters that are necessary for designing a tidal power plant, for the proposed power plant, the turbines employed are helical cross-flow turbines; they are mounted on a structure that is 10m below the ocean surface to protect it from any damaging surface conditions. The structure is anchored to the seabed as shown, Figure (4.17). For the proposed plant, the following assumptions are made:

- the stream velocity for tidal resources in South Africa is presented in Figure (3.5),
- there is an adequate water depth,
- The plant is out of the shipping lane but near to the power grid.

The idea is to simplify the power plant, whereby the turbines could be located in a building and be accessible on land or through the building and all the mechanisms pertaining to the rotors could be housed inside a building above sea level. To estimate the installed capacity of a tidal plant, the output power approximated by the unit tidal was considered. A tidal farm with 60 units deployed would generate an output power of 1.4MW. The estimated plant capacity is almost half of the Sol Plaatje hydropower station in Bethlehem, Free State. The advantage of this type of plant is that the plant capacity can be increased by adding more units at the site or by mounting a number of tidal turbines on a common shaft as discussed earlier in the literature review.

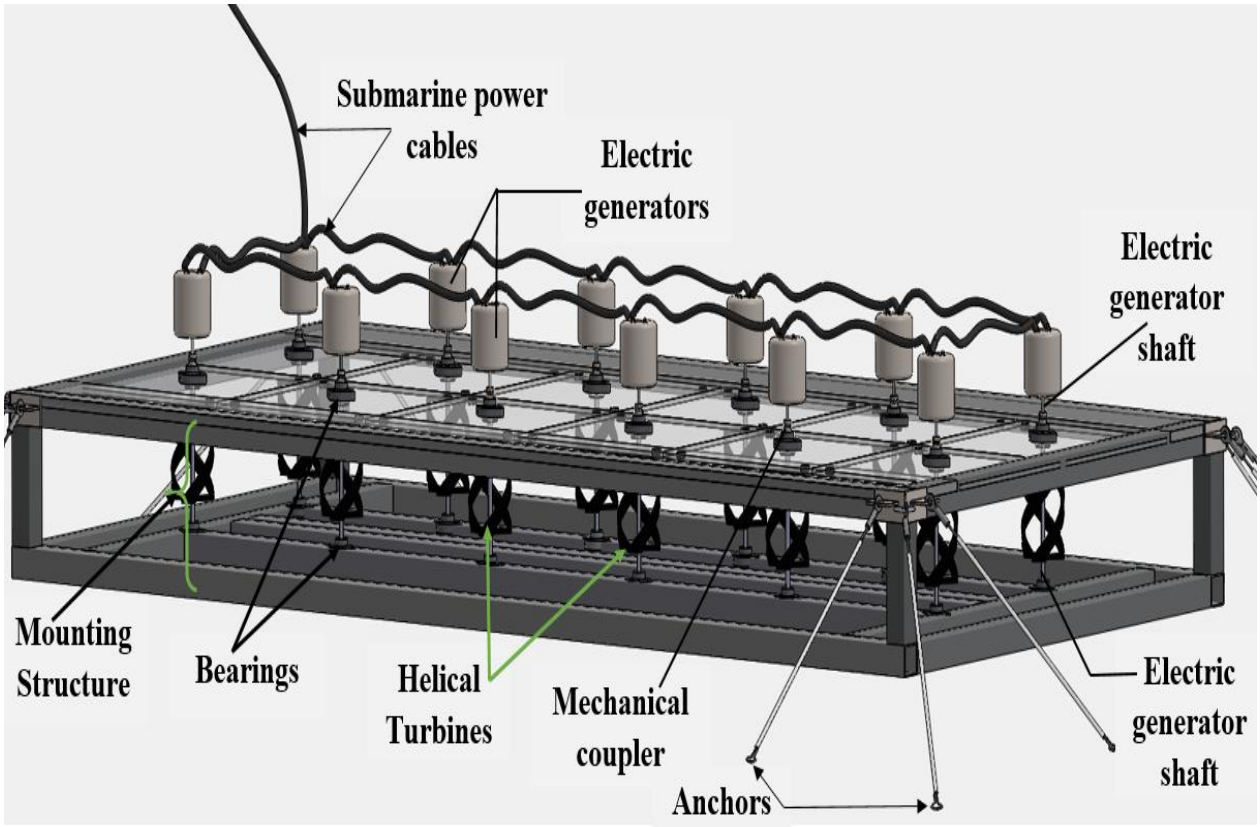

Figure 4.17: Proposed tidal power plant

4.9 Cost Estimation

For the successful completion of this investigation of establishing a tidal power plant in South Africa, it becomes necessary to carry out the cost estimation of siting the plant. Tidal power technologies are still at their developmental stage with the view that there will be an advancement in the future. With reference to the proposed power plant, it is necessary to demonstrate that tidal stream energy extraction is a viable option for clean and renewable energy for South Africa. The costs associated with constructing and maintaining tidal turbines are a function of the site specifically since there is a wide range of conditions that affect how difficult they are to install, and which designs can even be installed in the first place. Current velocities, seabed composition, and available local infrastructure are a few examples of the complicating factors. For these reasons, estimates of the cost for locations for Esikhawini are less valuable than ones that are specifically geared toward the location of interest.

There are a lot of unknown factors with regards to the environmental cost implications, thus the estimation conducted in this section only considers the cost of the plant components.

These include the cost of; the turbines, electric generators, the floating mounting structure which supports both mechanical and electrical components, the anchors which secure the position of the tidal plant, installation, marine transmission cables, and other electrical components. The estimation was conducted based on the analysis of a single unit which can then be extended to any number of units. Costing for a full-scale power plant, the costs per unit go down since it becomes more efficient to install more units and for the proposed power plant the farm is assumed to have 60 turbines. For a single demonstration unit, the costs are summarized in table 4.4.

Table 4.4: Cost estimation of the plant components

	R/kW	R/Turbine	in %
Site anlysis and environmental evaluation	11.5	9 522.8	0.5
Design and Manufacturing	880.9	729 448.5	38.3
Mounting Structure Elements	473.8	392 340.5	20.6
Submarine Cables and Electrical Works Installation	186.3	154 269.8	8.1
Anchors	27.6	22 854.8	1.2
Turbine Installation	552.0	457 095.7	24.0
Waterproofed electric generator	91.9	76 182.6	4.0
Onshore Electric Grid Interconnection	75.9	62 850.7	3.3
Total Installed Cost	2 299.9	1 904 565.39	100

The total costs of the plant can be summarised as follow:

Cost = (1 904 565.39× 60)

= R 114 273 923.4

Thus the unit cost of installed power is:

Unit cost = R 114 273 923.4/ 1 400 kW

= R 81 624.23 per kW

The estimated unit cost is reasonable considering the fact that it is the new technology in the country. The current unit cost of fossil fuel plants is R52 142.87, the unit cost of the proposed plant approximately 56% of the current unit cost of a coal power plant. This amount has been overestimated due to limited literature on cost estimation.

Chapter Five

Conclusions and Recommendations

5.1 Conclusions

Tidal stream technologies are slowly improving on their competitiveness with the increased research and new design adaptations. The information provided in this study serves as a baseline for further investigations on harnessing tidal energy in the country. South Africa has a huge tidal energy potential be the country is bordered by two oceans; the Indian and Atlantic Ocean. The tidal velocity model provided an insight on the stream velocities at different locations, the model may have underestimated or overestimated the tidal resource because of its simplicity. With the availability of bathymetry data and a consideration of other tidal constituents, the accuracy of the model can be improved. However, this model demonstrates the predictability and independence on weather conditions of the energy resource.

After conducting a literature survey on the design and performance of the helical turbine an analytical model was developed, in comparison of the modelling and experimental results, there was a noticeable general trend of both torque and power curves which followed the actual performance curves. There were slight deviations in the experimental results which may be attributed to the unknown torque coefficient, lift and drag forces which are functions of the azimuth angles that were not measured in the experiment. In accounts of the significant deviation in simulated and experimental results of the turbine performance coefficient, when estimating the unit output power, a performance coefficient of 0.21 was assumed which was obtained from the experiment results.

In conclusion, the amount of electrical power generated at a site can be accurately estimated when an optimum tidal turbine and electrical generator have been selected. The selection of these devices is based on the hydrodynamic characteristics, the turbine design, and performance parameters. Extensive research is required in South Africa and prior to establishing a tidal plant, a feasibility study is recommended which will determine the optimum placement, size, and capacity of the tidal turbines. For a desired installed plant capacity, the number of turbines required for deployment can be determined. Based on the analysis, simulation, and experimental results presented above, tidal energy would greatly have a huge impact on the amount of electricity generated in South Africa, if implement.

5.2 Future Work

Research on system component selection, design, and refinement should continue to increase the competitiveness of tidal technologies and for the possible establishment of a tidal plant in South Africa. To improve on the work conducted in the study the following is recommended

- For characterization of tidal potential, Acoustic Doppler Current Profilers should be deployed at a potential site for a minimum period of 30 days for the acquisition of all contributing tidal constituent data. Considering the effects of the bathymetry and the acquired data an improved tidal velocity model can be developed.
- Alternative test location and method of a large-scale model are recommended to improve on the analytical model developed and also determine any performance changes resulting from scaling the turbine.
- From the wind energy industry, it has been demonstrated that it is technically possible to integrate a wind farm into the national grid. A study on tidal farm integration to the national grid is recommended to analyze the system performance.

References

[1] M. O. Onibonoje, N. I. Nwulu, and P. N. Bokoro, "A wireless sensor network system for monitoring environmental factors affecting bulk grains storability," *Journal of Food Process Engineering,* vol. 42, no. 7, p. e13256, 2019.

[2] P. Bokoro and W. Doorsamy, "Reliability analysis of low-voltage metal-oxide surge arresters using accelerated failure time model," *IEEE Transactions on Power Delivery,* vol. 33, no. 6, pp. 3139-3146, 2018.

[3] L. Baker, "Governing electricity in South Africa: wind, coal and power struggles," *Governance of Clean Development Working Paper,* vol. 15, pp. 1-27, 2011.

[4] S. E. B. Elghali, R. Balme, K. Le Saux, M. E. H. Benbouzid, J. F. Charpentier, and F. Hauville, "A simulation model for the evaluation of the electrical power potential harnessed by a marine current turbine," *IEEE Journal of Oceanic Engineering,* vol. 32, no. 4, pp. 786-797, 2007.

[5] A. Uihlein and D. Magagna, "Wave and tidal current energy–A review of the current state of research beyond technology," *Renewable and Sustainable Energy Reviews,* vol. 58, pp. 1070-1081, 2016.

[6] H. Samani and M. Reza Heidary, "Feasibility Study on Renewable Power Plants: Tidal Power Plants," *European Online Journal of Natural and Social Sciences,* vol. 3, no. 3 (s), pp. pp. 66-71, 2014.

[7] L. Mofor, J. Goldsmith, and F. Jones, "Ocean energy: Technology readiness, patents, deployment status and outlook," *Abu Dhabi,* 2014.

[8] T. Montllonch Araquistain, "TIDAL POWER: Economic and Technological Assessment," 2010.

[9] I. Meyer, J. Reinecke, M. Roberts, and J. Van Niekerk, "Assessment of the ocean energy resources off the South African coast," *Centre for Renewable and Sustainable Energy Studies, Faculty of Engineering, University of Stellenbosch,(Stellenbosch South Africa),* 2013.

[10] T. B. Robinson, K. Peters, and B. Brooker, "Coastal invasions: the South African context," in *Biological Invasions in South Africa*: Springer, 2020, pp. 229-247.

[11] D. o. S. i. S. Africa, " Electricity: Coal use inches lower as solar, wind and diesel rise," 2018. [Online]. Available: http://www.statssa.gov.za/?p=11292.

[12] A. Pegels, "Renewable energy in South Africa: Potentials, barriers and options for support," *Energy policy,* vol. 38, no. 9, pp. 4945-4954, 2010.

[13] M. Hendershott, "Lecture 1: Introduction to ocean tides," *2004 Program of Study: Tides,* p. 1, 2005.

[14] E. P. Kvale, "The origin of neap–spring tidal cycles," *Marine geology,* vol. 235, no. 1-4, pp. 5-18, 2006.

[15] P. L. De Boer, A. Oost, and M. Visser, "The diurnal inequality of the tide as a parameter for recognizing tidal influences," *Journal of Sedimentary Research,* vol. 59, no. 6, pp. 912-921, 1989.

[16] O. M. Colangelo, "Assessing the Implications of a Tidal Barrage Power Plant in Hvalfjörður, Iceland," 2019.

[17] N. De Groot, "Tidal power in the Klabat bay, Indonesia: An application of the SEPAM design methodology," 2012.

[18] J. D. Boon, *Secrets of the tide: tide and tidal current analysis and predictions, storm surges and sea level trends*. Elsevier, 2013.

[19] A. Sankaran Iyer, "New methodologies and scenarios for evaluating tidal current energy potential," 2012.

[20] R. G. Dean and R. A. Dalrymple, "Water wave mechanics for engineers and scientists," in *Unknown Host Publication Title*: Prentice-Hall Inc, 1984.

[21] A. K. SONI, V. NOUJAS, and R. KANKARA, "STUDY OF OCEAN WAVE CHARACTERISTICS IN NEARSHORE REGION OF VENGURLA, WEST COAST OF INDIA."

[22] L. P. ONUNDO, "SCHOOL OF ENGINEERING," University of Nairobi, 2017.

[23] M. H. Khan, A. M. Siddiqui, S. S. Sheikh, and S. O. Athar, "State of The Art Tidal Energy Systems: Issues, Challenges, and Possible Solutions," in *2018 International Conference on Power Generation Systems and Renewable Energy Technologies (PGSRET)*, 2018: IEEE, pp. 1-6.

[24] S. J. Kulkarni, "Tidal Energy: A Review," *International Journal of Research,* vol. 2, no. 1, pp. 55-58, 2015.

[25] A. Owen, "Tidal current energy: origins and challenges," in *Future energy*: Elsevier, 2008, pp. 111-128.

[26] E. Baddour, "Energy from waves and tidal currents towards 20yy?," 2004.

[27] A. Etemadi, Y. Emami, O. AsefAfshar, and A. Emdadi, "Electricity generation by the tidal barrages," *Energy Procedia,* vol. 12, pp. 928-935, 2011.

[28] S. M. R. Tousif and S. M. B. Taslim, "Tidal power: an effective method of generating power," *International Journal of Scientific & Engineering Research,* vol. 2, no. 5, pp. 1-5, 2011.

[29] E. S. Fu, Y. Fang, and B. K. Horn, "Power of ocean: Evaluation of blue energy," in *2018 4th International Conference on Universal Village (UV)*, 2018: IEEE, pp. 1-4.

[30] F. O. Rourke, F. Boyle, and A. Reynolds, "Renewable energy resources and technologies applicable to Ireland," *Renewable and Sustainable Energy Reviews,* vol. 13, no. 8, pp. 1975-1984, 2009.

[31] S. Sheth and M. Shahidehpour, "Tidal energy in electric power systems," in *IEEE Power Engineering Society General Meeting, 2005*, 2005: IEEE, pp. 630-635.

[32] G. C. Times, "Renewable Energy: Hydroelectricity." [Online]. Available: http://www.greencitytimes.com/hydroelectricity.

[33] C. Baker, "Tidal power," *Energy Policy,* vol. 19, no. 8, pp. 792-797, 1991.

[34] J. Xia, R. A. Falconer, and B. Lin, "Impact of different operating modes for a Severn Barrage on the tidal power and flood inundation in the Severn Estuary, UK," *Applied Energy,* vol. 87, no. 7, pp. 2374-2391, 2010.

[35] A. Soomro and A. Baharun, "International journal of engineering sciences & research technology suitable powerhouse design for kuching barrage tidal power scheme," *vol,* vol. 6, pp. 154-172, 2017.

[36] S. Waters and G. Aggidis, "Tidal range technologies and state of the art in review," *Renewable and Sustainable Energy Reviews,* vol. 59, pp. 514-529, 2016.

[37] C. Frid *et al.*, "The environmental interactions of tidal and wave energy generation devices," *Environmental Impact Assessment Review,* vol. 32, no. 1, pp. 133-139, 2012.

[38] S. B. Chabane, M. Alamir, M. Fiacchini, R. Riah, T. Kovaltchouk, and S. Bacha, "Electricity grid connection of a tidal farm: An active power control framework constrained to grid code requirements," *IEEE Transactions on sustainable energy,* vol. 9, no. 4, pp. 1948-1956, 2018.

[39] I. Bryden, T. Grinsted, and G. Melville, "Assessing the potential of a simple tidal channel to deliver useful energy," *Applied Ocean Research,* vol. 26, no. 5, pp. 198-204, 2004.

[40] J. King and T. Tryfonas, "Tidal stream power technology-state of the art," in *Oceans 2009-Europe*, 2009: IEEE, pp. 1-8.

[41] M. Z. Zainol, H. N. Z. Rahim, W. Dahalan, A. Abu, M. F. Ghani, and I. Zainol, "Potential Area to Harness the Tidal Energy at West Coast Peninsular Malaysia," in *Applied Mechanics and Materials*, 2015, vol. 785: Trans Tech Publ, pp. 637-641.

[42] J. Callaghan and R. Boud, "Future Marine Energy. Results of the Marine Energy Challenge: Cost competitiveness and growth of wave and tidal stream energy," *Carbon trust,* 2006.

[43] M. Khan, G. Bhuyan, M. Iqbal, and J. Quaicoe, "Hydrokinetic energy conversion systems and assessment of horizontal and vertical axis turbines for river and tidal applications: A technology status review," *Applied energy,* vol. 86, no. 10, pp. 1823-1835, 2009.

[44] M. LEE, "Say “Hello” to the World’s First Large-Scale Tidal Power Farm," 2016. [Online]. Available: https://futurism.com/say-hello-to-the-worlds-first-large-scale-tidal-power-farm.

[45] S. Lain, L. T. Contreras, and O. López, "A review on computational fluid dynamics modeling and simulation of horizontal axis hydrokinetic turbines," *Journal of the Brazilian Society of Mechanical Sciences and Engineering,* vol. 41, no. 9, p. 375, 2019.
[46] K. Lee and L. Seng, "Simulation studies on the electrical power potential harnessed by tidal current turbines," *Journal of Energy and Environment,* vol. 1, no. 1, 2013.
[47] N. Sveinsson, "Profitability Assessment for a Tidal Power Plant at the Mouth of Hvammsfjörður, Iceland," 2011.
[48] S. D'Alessandro, T. Bailey, S. Chuah, and J. Vince, "Submission to the House Standing Committee on Industry, Science and Resources on Innovative solutions to Australia's waste management and recycling industries," 2020.
[49] L. Krause, "South Korea Coast Tidal Energy Project," 2008. [Online]. Available: https://mendocoastcurrent.wordpress.com/2008/03/17/south-korea-coast-tidal-energy-project/.
[50] O. Keysan, A. S. McDonald, and M. Mueller, "A direct drive permanent magnet generator design for a tidal current turbine (SeaGen)," in *2011 IEEE International Electric Machines & Drives Conference (IEMDC)*, 2011: IEEE, pp. 224-229.
[51] S. K. S. Kushwaha, "DYNAMIC ANALYSIS OF MARINE CURRENT FARM CONNECTED TO GRID," 2015.
[52] E. H. Schumann, "Sea level variability in South African estuaries," *South African Journal of Science,* vol. 109, no. 3-4, pp. 01-07, 2013.
[53] A. M. Gorlov, "Helical turbine assembly operable under multidirectional fluid flow for power and propulsion systems," ed: Google Patents, 1997.
[54] E. G. Frankel and U. W. Kitzinger, "Macro-engineering and the Earth: World Projects for the Year 2000 and Beyond; a Festschrift in Honour of Frank Davidson," ed: Horwood, 1998.
[55] K. Gaywala, H. Shah, and P. Patel, "Performance Prediction of a Straight-Bladed Darrieus Water Turbine using Multiple Stream Tube Model," *SSRG International Journal of Mechanical Engineering,* vol. 4, no. 6, pp. 41-45, 2017.
[56] P. Fleming and S. Probert, "The evolution of wind-turbines: An historical review," *Applied energy,* vol. 18, no. 3, pp. 163-177, 1984.
[57] J.-L. Cornet, "Evaluation of the unsteady effects for a class of wind turbines," California Institute of Technology, 1984.
[58] A. L. Niblick, "Experimental and analytical study of helical cross-flow turbines for a tidal micropower generation system," 2012.
[59] A. J. Johnston, "Analytical and numerical modeling of performance characteristics of cross-flow hydrokinetic turbines," 2011.
[60] M. Kamoji, S. Kedare, and S. Prabhu, "Performance tests on helical Savonius rotors," *Renewable Energy,* vol. 34, no. 3, pp. 521-529, 2009.
[61] M. Zemamou, M. Aggour, and A. Toumi, "Review of savonius wind turbine design and performance," *Energy Procedia,* vol. 141, pp. 383-388, 2017.
[62] M. D'Ambrosio and M. Medaglia, "Vertical axis wind turbines: History, technology and applications," ed, 2010.
[63] U. Saha and M. J. Rajkumar, "On the performance analysis of Savonius rotor with twisted blades," *Renewable energy,* vol. 31, no. 11, pp. 1776-1788, 2006.
[64] I. Paraschivoiu, *Wind turbine design: with emphasis on Darrieus concept*. Presses inter Polytechnique, 2002.
[65] J.-H. Lee, Y.-T. Lee, and H.-C. Lim, "Effect of twist angle on the performance of Savonius wind turbine," *Renewable Energy,* vol. 89, pp. 231-244, 2016.
[66] P. Bachant and M. Wosnik, "Experimental investigation of helical cross-flow axis hydrokinetic turbines, including effects of waves and turbulence," in *Fluids Engineering Division Summer Meeting*, 2011, vol. 44403, pp. 1895-1906.

[67] P. Bachant and M. Wosnik, "Performance measurements of cylindrical-and spherical-helical cross-flow marine hydrokinetic turbines, with estimates of exergy efficiency," *Renewable Energy,* vol. 74, pp. 318-325, 2015.
[68] A. Rolan, A. Luna, G. Vazquez, D. Aguilar, and G. Azevedo, "Modeling of a variable speed wind turbine with a permanent magnet synchronous generator," in *2009 IEEE international symposium on industrial electronics*, 2009: IEEE, pp. 734-739.
[69] J. Ukonsaari and N. Bennstedt, "Wind turbine gearboxes: Maintenance effect on present and future gearboxes for wind turbines," report 2016: 279. Tech. Rep, 2016.
[70] K. Touimi, M. Benbouzid, and P. Tavner, "Tidal stream turbines: With or without a Gearbox?," *Ocean Engineering,* vol. 170, pp. 74-88, 2018.
[71] J. Coy, D. Townsend, and E. Zaretsky, "Gearing. NASA RP-1152," AVSCOM TR 84-C, 1985.
[72] S. Chapman, *Electric machinery fundamentals*. Tata McGraw-Hill Education, 2005.
[73] M. Benbouzid *et al.*, "Concepts, modeling and control of tidal turbines," ed: John Wiley & Sons, 2012.
[74] R. K. S. Babainejad, "Analysis of Transient Voltage Stability of a Variable Speed Wind Turbine with Doubly Fed Induction Generator Affected by Different Electrical Parameters of Induction Generator," *Trends in Applied Sciences Research,* pp. 5: 267-278., doi: 10.3923/tasr.2010.267.278.
[75] Y. Errami, M. Ouassaid, and M. Maaroufi, "Control of a PMSG based wind energy generation system for power maximization and grid fault conditions," *Energy Procedia,* vol. 42, pp. 220-229, 2013.
[76] J. Xia, R. A. Falconer, B. Lin, and G. Tan, "Estimation of annual energy output from a tidal barrage using two different methods," *Applied Energy,* vol. 93, pp. 327-336, 2012.
[77] A. Boretti, "Trends in tidal power development," in *E3S Web of Conferences*, 2020, vol. 173: EDP Sciences, p. 01003.
[78] A. M. Gorlov, "Helical turbines for the gulf stream: conceptual approach to design of a large-scale floating power farm," *Marine Technology and Sname News,* vol. 35, no. 3, p. 175, 1998.
[79] F. L. Rashid, A. H. Mohamad, and A. Hashim, "Power Production using Tidal Energy," *British Journal of Science,* vol. 3, no. 2, 2012.
[80] C. Okoli, R. Uhunmwangho, and H. Nwogu, "A simulation model for tidal energy extraction in Nigeria using tidal current turbine," in *2017 IEEE PES PowerAfrica*, 2017: IEEE, pp. 500-505.
[81] S. Searson, "Extreme sea levels around the coast of Southern Africa," University of Cape Town, 1995.
[82] A. Williams, M. Nthontho, S. Chowdhury, and S. Chowdhury, "Modelling South African Agulhas marine current profile data for electricity generation," in *2012 IEEE International Conference on Power System Technology (POWERCON)*, 2012: IEEE, pp. 1-7.
[83] G. Ingram, "Wind turbine blade analysis using the blade element momentum method. Version 1.1," *School of Engineering, Durham University, UK,* 2005.
[84] M. B. Soultanzadeh, "Isfahan Wind Turbine Modeling," *Majlesi Journal of Energy Management,* vol. 2, no. 4, 2013.
[85] D. A. Krawczyk, "BUILDINGS."
[86] A. O. Aluko, "Modelling and performance analysis of doubly fed induction generator wind farm," 2018.
[87] P. Gunai, S. ShardulGumaste, S. Gathe, and A. Das, "Design, Analysis and Improvisation of Helical Cross Flow Hydro Kinetic Turbine," *International Journal of Advanced Engineering Research and Science,* vol. 3, no. 9, p. 236832.
[88] E. E. Nwe and A. K. Latt, "Design and Performance of Vertical Axis Helical Cross-Flow Turbine Blade for Micropower Generation," *International Journal of New Technology and Research,* vol. 4, no. 6, 2018.

[89] I. Masters, J. Chapman, M. Willis, and J. Orme, "A robust blade element momentum theory model for tidal stream turbines including tip and hub loss corrections," *Journal of Marine Engineering & Technology,* vol. 10, no. 1, pp. 25-35, 2011.

[90] R. Bontempo and M. Manna, "The axial momentum theory as applied to wind turbines: some exact solutions of the flow through a rotor with radially variable load," *Energy Conversion and Management,* vol. 143, pp. 33-48, 2017.

[91] R. Bontempo and M. Manna, "Analysis and evaluation of the momentum theory errors as applied to propellers," *AIAA Journal,* vol. 54, no. 12, pp. 3840-3848, 2016.

[92] M. K. Rwigema, "Propeller blade element momentum theory with vortex wake deflection," in *27th International congress of the aeronautical sciences*, 2010, vol. 2010, p. 2.3.

[93] F. Mahmuddin, "Rotor blade performance analysis with blade element momentum theory," *Energy Procedia,* vol. 105, pp. 1123-1129, 2017.

[94] M. Moghin and H. Motawej, "Comparison Aerodynamic Performance and Power Fluctuation Between Darrieus Straight-BIaded and Gorlov Vertical Axis Wind Turbines," *Journal of Applied Fluid Mechanics,* vol. 13, no. 5, 2020.

[95] D. Han, Y. G. Heo, N. J. Choi, S. H. Nam, K. H. Choi, and K. C. Kim, "Design, fabrication, and performance test of a 100-w helical-blade vertical-axis wind turbine at low tip-speed ratio," *Energies,* vol. 11, no. 6, p. 1517, 2018.

[96] A. Johnston and M. Wosnik, "Analytical and Numerical Modeling of Performance Characteristics of Cross-Flow Axis Hydrokinetic Turbines," in *Fluids Engineering Division Summer Meeting*, 2011, vol. 44403, pp. 1907-1918.

[97] A. Gorlov, "Development of the helical reaction hydraulic turbine. Final technical report, July 1, 1996--June 30, 1998," Northeastern Univ., Boston, MA (United States), 1998.

[98] P. Kozak, "Effects of unsteady aerodynamics on vertical-axis wind turbine performance," Illinois Institute of Technology, 2014.

[99] A. Sagharichi, M. J. Maghrebi, and A. ArabGolarcheh, "Variable pitch blades: An approach for improving performance of Darrieus wind turbine," *Journal of Renewable and Sustainable Energy,* vol. 8, no. 5, p. 053305, 2016.

Appendix A

Hydrofoil Data

Table A1: The lift and drag coefficients of the two hydrofoils

Angle of Attack	NACA0020		NACA0018	
	Lift (C*l*)	Drag (C*d*)	Lift (C*l*)	Drag (C*d*)
- 1.00	-0.1030	0.0116	-0.1042	0.0108
0.00	0.0000	0.0115	0.0000	0.0108
+1.00	0.1031	0.0116	0.1043	0.0108
+2.00	0.2056	0.0118	0.2075	0.0111
+3.00	0.3075	0.0122	0.3135	0.0115
+4.00	0.4090	0.0128	0.4181	0.0122
+5.00	0.5097	0.0135	0.526	0.0132
+6.00	0.6103	0.0146	0.6455	0.0144
+7.00	0.7244	0.0159	0.7778	0.0158
+8.00	0.8508	0.0176	0.9038	0.0175
+9.00	0.9694	0.0195	1.0092	0.0193
+10.00	1.0294	0.0212	1.0025	0.0208

Hydrofoil Profile (NACA 0020)

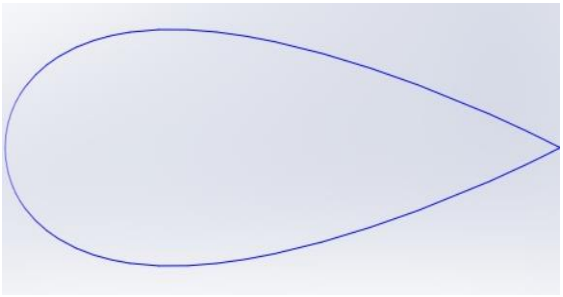

Hydrofoil Profile (NACA 0018)

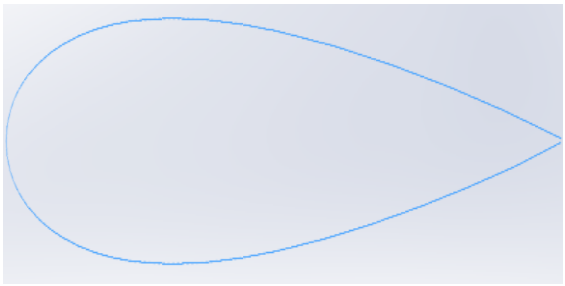

NACA 0018 Database

X	Y	Z
1.000000	-0.000000	0
0.999561	0.000106	0
0.998246	000424	0
0.996057	0.000953	0
0.992998	0.001689	0
0.989074	0.002628	0
0.984292	0.003767	0
0.978660	0.005099	0
0.972188	0.006618	0
0.964888	0.008316	0
0.956773	0.010186	0
0.947856	0.012219	0
0.938153	0.014405	0
0.927682	0.016735	0
0.916461	0.019198	0
0.904508	0.021785	0
0.891847	0.024484	0
0.878498	0.027285	0
0.864484	0.030176	0
0.849832	0.033147	0
0.834565	0.036186	0
0.818712	0.039282	0
0.802300	0.042423	0
0.785357	0.045599	0
0.767913	0.048798	0
0.750000	0.052007	0
0.731648	0.055217	0
0.712890	0.058413	0
0.693758	0.061586	0
0.674286	0.064723	0
0.654508	0.067810	0
0.634460	0.070837	0
0.614175	0.073789	0
0.593691	0.076654	0
0.573042	0.079418	0
0.552264	0.082068	0
0.531395	0.084590	0
0.510471	0.086970	0
0.489529	0.089194	0
0.468605	0.091249	0
0.447736	0.093120	0
0.426958	0.094794	0
0.406309	0.096258	0
0.385825	0.097498	0
0.365540	0.098503	0
0.345492	0.099261	0
0.325714	0.099762	0
0.306242	0.099995	0
0.287110	0.099952	0
0.268352	0.099627	0
0.250000	0.099012	0
0.232087	0.098105	0

```
  0.214643    0.096900  0
  0.197700    0.095398  0
  0.181288    0.093598  0
  0.165435    0.091502  0
  0.150168    0.089113  0
  0.135516    0.086437 0
  0.121502    0.083478  0
  0.108153    0.080246  0
  0.095492    0.076748  0
  0.083539    0.072995  0
  0.072318    0.068996  0
  0.061847    0.064764  0
  0.052144    0.060311  0
  0.043227    0.055648  0
  0.035112    0.050788  0
  0.027812    0.045743  0
  0.021340    0.040526  0
  0.015708    0.035147  0
  0.010926    0.029616  0
  0.007002    0.023945  0
  0.003943    0.018140  0
  0.001754    0.012211  0
  0.000439    0.006162  0
  0.000000    0.000000  0
  0.000439   -0.006162  0
  0.001754   -0.012211  0
  0.003943   -0.018140  0
  0.007002   -0.023945  0
  0.010926   -0.029616  0
  0.015708   -0.035147  0
  0.021340   -0.040526  0
  0.027812   -0.045743  0
  0.035112   -0.050788  0
  0.043227   -0.055648  0
  0.052144   -0.060311  0
  0.061847   -0.064764  0
  0.072318   -0.068996  0
  0.083539   -0.072995  0
  0.095492   -0.076748  0
  0.108153   -0.080246  0
  0.121502   -0.083478  0
  0.135516   -0.086437  0
  0.150168   -0.089113  0
  0.165435   -0.091502  0
  0.181288   -0.093598  0
  0.197700   -0.095398  0
  0.214643   -0.096900  0
  0.232087   -0.098105  0
  0.250000   -0.099012  0
  0.268352   -0.099627  0
  0.287110   -0.099952  0
  0.306242   -0.099995  0
  0.325714   -0.099762  0
  0.345492   -0.099261  0
  0.365540   -0.098503  0
```

```
  0.385825   -0.097498  0
  0.406309   -0.096258  0
  0.426958   -0.094794  0
  0.447736   -0.093120  0
  0.468605   -0.091249  0
  0.489529   -0.089194  0
  0.510471   -0.086970  0
  0.531395   -0.084590  0
  0.552264   -0.082068  0
  0.573042   -0.079418  0
  0.593691   -0.076654  0
  0.614175   -0.073789  0
  0.634460   -0.070837  0
  0.654508   -0.067810  0
  0.674286   -0.064723  0
  0.693758   -0.061586  0
  0.712890   -0.058413  0
  0.731648   -0.055217  0
  0.750000   -0.052007  0
  0.767913   -0.048798  0
  0.785357   -0.045599  0
  0.802300   -0.042423  0
  0.818712   -0.039282  0
  0.834565   -0.036186  0
  0.849832   -0.033147  0
  0.864484   -0.030176  0
  0.878498  -0.027285  0
  0.891847   -0.024484  0
  0.904508   -0.021785  0
  0.916461   -0.019198  0
  0.927682   -0.016735  0
  0.938153   -0.014405  0
  0.947856   -0.012219  0
  0.956773   -0.010186  0
  0.964888   -0.008316  0
  0.972188   -0.006618  0
  0.978660   -0.005099  0
  0.984292   -0.003767  0
  0.989074   -0.002628  0
  0.992998   -0.001689  0
  0.996057   -0.000953  0
```

Appendix B

Experimental Component Specifications

Turbine Material

The turbine material used for the prototype developed in this study is ABS, material properties are given in table B.1.

Table B.1: ABS Thermoplastic Properties

Properties	**PLA**	**ABS**
Tensile Strength	37 MPa	27 MPa
Elongation	6%	3.5-50%
Density	1.3	1-1.4g/cm^3
Biodegradable	Yes	No
Glass transition temperature	60˚C	105˚C

Electric Motor

The specifications of the motor used in the experiment are given in table B.2.

Table B.2: DC motor

Voltage (V)	3-24V	
Continuous Current (A)	4000 rpm	
Commutation	Brush	

Bearings and Coupler

Two stainless steel ball bearings were pressed onto the mounting structure to allow easy installation and smooth rotation of the turbine shaft. A rigid aluminium coupling was used to couple the turbine shaft to the electric motor.

Figure B.1: Bearings and Coupler

Measuring Instruments

The measuring instruments that were used to collect the experimental data ae given in the figure below.

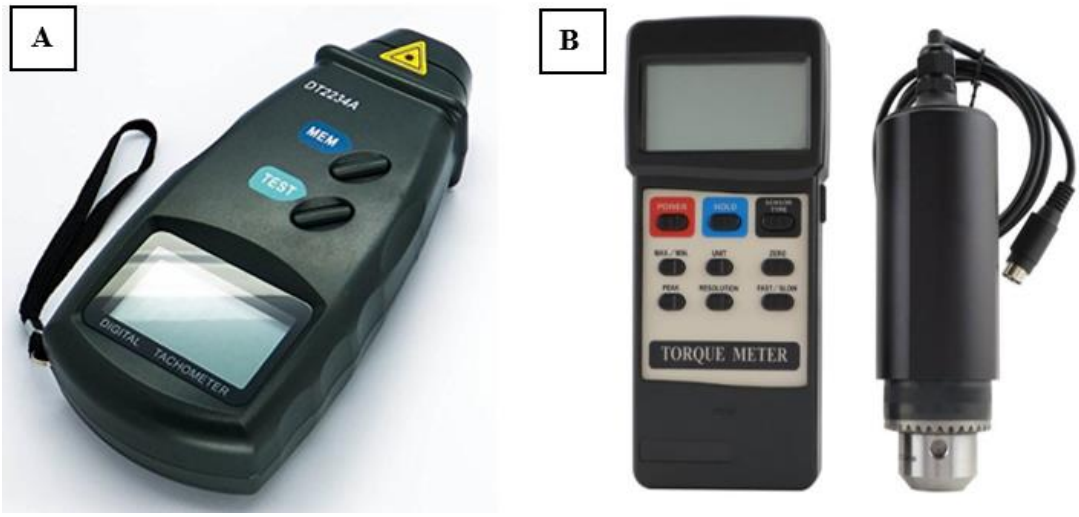

Figure B.2: A. Tachometer B. Digital Torque Meter